GEOLOGICAL SURVEY OF CANADA
BULLETIN 400

THE GAS-BEARING DEVONIAN MANETOE FACIES, YUKON AND NORTHWEST TERRITORIES

D. W. Morrow
G.L. Cumming
K.L. Aulstead

1990

Energy, Mines and Resources Canada
Énergie, Mines et Ressources Canada

Canada

THE ENERGY OF OUR RESOURCES

THE POWER OF OUR IDEAS

GEOLOGICAL SURVEY OF CANADA
BULLETIN 400

THE GAS-BEARING DEVONIAN MANETOE FACIES, YUKON AND NORTHWEST TERRITORIES

D.W. Morrow
G.L. Cumming
K.L. Aulstead

1990

Available in Canada through
authorized bookstore agents and other bookstores
or by mail from

Canadian Government Publishing Centre
Supply and Services Canada
Ottawa, Canada K1A 0S9

and from

Geological Survey of Canada offices:

601 Booth Street
Ottawa, Canada K1A 0E8

3303-33rd Street N.W.
Calgary, Alberta T2L 2A7

A deposit copy of this publication is also available
for reference in public libraries across Canada

Cat. No. M42-400E
ISBN 0-660-13722-4

Price subject to change without notice

Critical readers

A.W. Norris
B.C. Richards

Editor

N.C. Ollerenshaw

Cartography

Drafting as submitted by author

Authors' addresses

D.W. Morrow
Institute of Sedimentary and Petroleum Geology
Geological Survey of Canada
3303-33rd Street N.W.
Calgary, Alberta, Canada T2L 2A7

G.L. Cumming
Department of Physics
Institute of Earth and Planetary Physics
University of Alberta
Edmonton, Alberta, Canada T6G 2J1

K.L. Aulstead
Shell Canada Limited
3655-36th Street N.W.
P.O. Box 2506
Calgary, Alberta, Canada T2P 3S6

Original manuscript submitted: 85.04.18
Revised manuscript submitted: 89.02.01
Approved for publication: 89.07.14

PREFACE

The Manetoe Facies of Yukon and the Northwest Territories belongs to a type of dolomite that occurs in only a few places throughout the world. These white, coarsely crystalline masses of dolomite commonly host large lead-zinc deposits. The Manetoe appears to be unique in being the host for large gas accumulations and for its unparalleled lateral extent. Analysis, based on a wide array of data types and analytical methods, indicates that the Manetoe Facies is the result of two distinct geological events: the creation of a laterally persistent cavern system by solution, followed by the precipitation of dolomite in these caverns from geothermally heated, hypersaline, residual marine brines, originating from underlying Elk Point Basin strata.

Conclusions of immediate importance to hydrocarbon exploration include the documentation of a probable thermal event of anomalously high heat flow in the Late Devonian, and the deduction that hydrocarbons moved downward into Manetoe reservoirs during the late Paleozoic. This study also identifies and emphasizes the need to investigate the source rock potential of the sedimentary sequence overlying Devonian carbonates in this and adjoining regions, in order to fully characterize the hydrocarbon potential of these strata.

Elkanah A. Babcock
Assistant Deputy Minister
Geological Commission of Canada

PRÉFACE

Le faciès Manetoe, au Yukon et dans les Territoires du Nord-Ouest, fait partie d'un type de dolomie que l'on ne trouve qu'à quelques endroits dans le monde. Ces massifs de dolomie blanche à grains grossiers renferment souvent d'immenses gisements de plomb-zinc. Les faciès Manetoe a comme caractéristique particulière de receler de vastes accumulations de gaz et de présenter une extension latérale non parallèle. Son analyse, basée sur une vaste gamme de données et de méthodes analytiques, indique que le faciès Manetoe est le résultat de deux événements géologiques distincts: la création par dissolution d'un réseau de cavernes latéralement persistant, suivie de la précipitation dans ces cavernes de la dolomie à partir de saumures marines résiduelles hypersalines, réchauffées géothermiquement, et issues des couches sous-jacentes du bassin d'Elk Point.

Les conclusions d'importance immédiate pour l'exploration des hydrocarbures sont notamment celles partout sur la possibilité d'un écoulement thermique anormalement élevé pendant la fin du Dévonien et du déplacement des hydrocarbures vers les roches réservoirs de Manetoe sous-jacentes pendant la fin du Paléozoïque. La présente étude souligne en outre le besoin d'analyser le potentiel comme roche mère de la séquence sédimentaire des carbonates dévoniens sus-jacents dans cette région et les régions voisines, afin de caractériser tout le potentiel en hydrocarbures de ces couches.

Elkanah A. Babcock
Sous-ministre adjoint
Commission géologique du Canada

CONTENTS

1 Abstract/Résumé
3 Summary/Sommaire
5 Introduction
5 Methods, and sources of data
8 Regional stratigraphy of the Manetoe Facies
8 Geological setting, distribution, and configuration of the Manetoe Facies
13 Relationship between the Manetoe and Presqu'île facies
13 Manetoe cavern fillings and associated dolomitization
16 Diagenetic sequence and petrography
19 Paleontological thermal maturation indicators
22 Fluid-inclusion data
22 Inclusions in dolomite
23 Inclusions in calcite
23 Inclusions in quartz
25 Stable-isotope data and chemistry
29 Strontium isotope data
30 Lead isotope data and interpretation
34 Origin of the Manetoe dolomite
39 Emplacement of hydrocarbons, and post-dolomitization diagenesis
41 Summary and conclusions
41 References
49 Appendix 1 – Isotopic and mineralogical data – outcrop sections
50 Appendix 2 – Isotopic and mineralogical data – subsurface sections
52 Appendix 3 – Major and minor element composition – surface sections
53 Appendix 4 – Carbon and oxygen isotope content of selected dolomite samples from the Manetoe Facies
54 Appendix 5 – Carbon and oxygen isotope content of selected limestones and calcite cements associated with the Manetoe Facies

Illustrations

Figures

6 1. Distribution of the Manetoe Facies within the southern Mackenzie Mountains
7 2. Generalized map of Manetoe Facies distribution
7 3. Schematic cross-section, showing the distribution of the Manetoe and Presqu'île facies
10 4. Locations of surface and well sections of the Manetoe facies
11 5. Cross-section of Devonian shelf sequence stratigraphy
12 6. Schematic three-dimensional reconstruction of the combined Manetoe and Presqu'île facies
14 7. Outcrop photographs of the Manetoe Facies at Nahanni Butte
15 8. Outcrop photographs of the Manetoe Facies at First Canyon
17 9. Subsidence and diagenetic history of strata containing the Manetoe Facies
18 10. Diagenetic textures of the Manetoe Facies
19 11. Microcrystalline quartz and chalcedony at the top of the Nahanni Formation
19 12. Thermal maturation values plotted in terms of stratigraphic position
20 13. Location map for conodont and palynomorph samples
22 14. Frequency plot of homogenization temperatures for fluid inclusions in Manetoe dolomite
24 15. Comparison of fluid-inclusion homogenization temperatures
25 16. Frequency plot of homogenization temperatures for fluid inclusions in calcite cements
26 17. Frequency plot of homogenization temperatures for fluid inclusions in quartz cements
27 18. Plot of oxygen and carbon isotope data for dolomite and calcite of the Manetoe Facies
28 19. Relationship between the temperature of precipitation of dolomite and the $\delta^{18}O‰$ content of the precipitate

29 20. Strontium isotope content of dolomite, calcite cement, and unaltered limestone
32 21. Lead isotope data
35 22. Schematic reconstruction of a paleoaquifer system
37 23. Possible origins for Manetoe dolomite
38 24. Structure contour map of the upper surface of the Nahanni Formation
40 25. Schematic summary of events leading to the emplacement of hydrocarbons

Tables

9 1. Regional thicknesses of the Manetoe Facies and associated formations
16 2. Names and locations of wells from which Manetoe dolomite core has been sampled for fluid inclusion, chemical, or isotopic analyses
21 3. Paleontological thermal maturation data – conodont Colour Alteration Index (CAI)
21 4. Paleontological thermal maturation data – palynomorph Thermal Alteration Index (TAI)
23 5. Summary of freezing data for fluid inclusions in dolomite cements from the Manetoe Facies
23 6. Summary of freezing data for fluid inclusions in calcite cements from the Manetoe Facies
24 7. Summary of freezing data for fluid inclusions in quartz from the Manetoe Facies
26 8. Summary and comparison of stable isotope data from white, void-filling dolomite and grey, replacement dolomite
29 9. Iron, manganese, and strontium content (ppm) in Manetoe Facies dolomite–summary statistics
31 10. Strontium isotope ($^{87}Sr/^{86}Sr$) content of selected samples of Manetoe dolomite and associated limestone
31 11. Zinc-lead deposits, host carbonates, and associated shales
33 12. Lead isotope analyses of galena from carbonate-hosted zinc-lead deposits in the northern Cordillera
34 13. Regression analysis of isotopic groups

THE GAS-BEARING DEVONIAN MANETOE FACIES, YUKON AND NORTHWEST TERRITORIES

Abstract

The white sparry dolomite of the Manetoe Facies is the northwestward continuation of the well known Presqu'île Facies at Pine Point in the Northwest Territories. The Manetoe Facies extends for 38 000 km^2 (15 000 mi^2) in the subsurface of the northern interior plains and is exposed along the southern Mackenzie Mountains. It is a diagenetic facies of dolomitized breccia that replaces large parts of the Lower to Middle Devonian carbonate strata of the Mackenzie Shelf sequence. This facies forms the reservoir for the Pointed Mountain, Kotaneelee, and Beaver River gas fields, which are Canada's northernmost producing fields.

Dolomite of the Manetoe Facies may have filled a pre-existing cavern system that was excavated by fresh groundwater during widespread subaerial exposure of the Elk Point Basin in Middle Devonian time. Dolomite crystals contain hypersaline fluid inclusions that indicate precipitation at high temperature (150 to 200°C). This is consistent with their low $\delta^{18}O$ values of about $-12‰$. Dolomite precipitation and dolomitization probably occurred as the result of the circulation of heated residual brines that had risen from depths of several kilometres, from Elk Point Basin strata, during a Late Devonian thermal event. Paleontological maturation indicators suggest that strata beneath the Upper Devonian have undergone a much greater degree of thermal maturation than supra-Devonian strata.

Late Paleozoic burial of the Devonian carbonates was accompanied by the maturation and expulsion of hydrocarbons from the overlying siliciclastic rocks into the Manetoe Facies, at those places where vertical extensions of the facies bring it into direct contact with the siliciclastics. Migration of hydrocarbons was accompanied and followed by calcite and quartz cementation and partial silicification of the Manetoe Facies. Emplacement of galena and sphalerite veinlets in early Mesozoic time, as indicated by lead isotope determinations, precludes the possibility of a Tertiary origin for the Manetoe dolomite. Deep burial of Manetoe hydrocarbons in Mesozoic to Tertiary time caused the generation of dry gas in the Manetoe Facies.

Résumé

La dolomie blanche à gros grains du faciès Manetoe est le prolongement nord-ouest du faciès bien connu Presqu'île, à Pine Point dans les Territoires du Nord-Ouest. Le faciès Manetoe s'étend sur 38 000 km^2 (15 000 mi^2) dans le sous-sol des plaines intérieures septentrionales et affleurent le long du sud des monts Mackenzie. C'est un faciès diagénétique de brèche dolomitisée qui remplace de grandes parties des couches carbonatées du Dévonien inférieur à moyen de la séquence de la plate-forme de Mackenzie. Ce faciès forme la roche réservoir des champs gaxifières Pointed Moutain, Kotaneelee et Beaver River, qui sont les champs les plus au nord exploités au Canada.

La dolomie du faciès Manetoe a pu remplir un réseau de cavernes formées par l'eau douce souterraine durant une vaste exposition sub-aérienne du bassin d'Elk Point pendant le Dévonien moyen. Les cristaux de dolomie contiennent des inclusions de fluide hypersalin indiquant une précipitation à haute température (de 150 à 200°C). Ces données sont corroborées par leur faible valeur $\delta^{18}O$ d'environ $-12‰$. La précipitation de la dolomie et la dolomitisation ont probablement été causées par la circulation de saumures résiduelles chaudes qui ont remonté des profondeurs de plusieurs kilomètres, à partir des couches du bassin d'Elk Point, au cours d'un événement thermique du Dévonien supérieur. Les indicateurs de maturation paléontologique indiquent que les couches sous-jacentes au Dévonien supérieur ont subi une maturation thermique beaucoup plus importante que les couches sus-jacentes.

L'enfouissement au Paléozoïque supérieur des carbonates dévoniens a été accompagné par la maturation et l'expulsion d'hydrocarbures des roches silicoclastiques sus-jacentes vers le faciès Manetoe, là où des prolongements verticaux du faciès le mettent en contact direct avec les roches silicoclastiques. La migration des hydrocarbures a été accompagnée et suivie d'une cémentation de la calcite et du quartz et d'une silification partielle du faciès Manetoe. La mise en place de veinules de galène et de sphalérite au début du Mésozoïque, indiquée par des datations des isotopes du plomb, exclut la possibilité que la dolomie de Manetoe soit d'origine tertiaire. L'enfouissement profond des hydrocarbures de Manetoe du Mésozoïque au Tertiaire a causé la formation de gas sec dans le faciès Manetoe.

Summary

The white, coarsely crystalline, sparry dolomite of the Manetoe Facies extends for 38 000 km^2 (15 000 mi^2) in Middle Devonian carbonate strata of the southern Mackenzie Mountains and the subsurface of the Interior Plains and lowlands east and south of the Mackenzie Mountains. The Manetoe Facies and the better known Presqu'île Facies of the Pine Point District are probably coextensive – a conclusion based on stratigraphic correlation and on the fact that their oxygen and carbon compositions are coextensive and plot along the same collinear trend. The Manetoe, like the Presqu'île, is a diagenetic facies of dolomitized breccia and developed primarily as a stratiform body within the Landry Formation and the upper part of the Arnica Formation. Locally, large vertical developments of the Manetoe extend upward into the Headless and Nahanni formations above the Landry. Some of the larger Manetoe Facies masses that extend above and below the stratigraphic level of the Landry Formation contain Canada's northernmost producing gas fields: the Pointed Mountain, Kotaneelee, and Beaver River fields.

Dolomite of the Manetoe Facies was probably precipitated in a pre-existing cavern system. These caverns may have been excavated during the period of exposure of the Elk Point Basin that preceded deposition of the overlying Watt Mountain Formation, and during deposition of the fluvial and deltaic sediments of that formation. Homogenization temperatures, ranging from about 150 to 200°C for hypersaline aqueous fluid inclusions in dolomite crystals, indicate precipitation at high temperature. This is consistent with the low average $\delta^{18}O$ value of about $-12‰$ for these dolomites if the inclusion brines were derived from the evaporation of Devonian seawater. Dolomite precipitation and dolomitization probably occurred as the result of the circulation of geothermally heated residual brines, from the Elk Point Basin, that had risen from depths of several kilometres during a Late Devonian thermal event. The modern Salton Sea geothermal system of southern California is similar to this hypothesized ancient geothermal system of brine recirculation. The existence of a Late Devonian thermal event is indicated by a comparison of thermal maturation indicators above and below the Nahanni Formation. Sub-Nahanni conodonts have Colour Alteration Index values (CAI values) of 5.0, whereas conodonts from Mississippian strata only 2000 m above the Nahanni have CAI values of only 1.0 to 1.5. The high strontium isotope ($^{87}Sr/^{86}Sr$) values for Manetoe dolomite are consistent with the values to be expected, based on the suggestions of previous workers that the interaction of Elk Point residual brines caused the albitization of feldspar in underlying Precambrian crustal rocks.

The development of thick deposits of fine grained siliciclastic sediments over the Devonian Mackenzie Shelf carbonates, in late Paleozoic time, led to the thermal maturation of organic material in the siliciclastic rocks and the generation of hydrocarbons. Progressive burial caused the expulsion of hydrocarbons downward into the Manetoe Facies at those places where the Manetoe Facies extends vertically upward to the top of the Nahanni Formation, immediately beneath the siliciclastic rocks. Migration of hydrocarbons was accompanied and followed by calcite and quartz cementation and silicification of the occurrences of Manetoe Facies beneath the upper Nahanni contact. The correlation of fluid-inclusion homogenization temperatures for quartz and calcite with their present depths of burial, indicates that cementation of the Manetoe Facies by these minerals occurred under the influence of a normal geothermal gradient. Mineralization, in the form of veinlets of galena and sphalerite, was the last diagenetic event, apart from the development of stylolites, to affect the Manetoe Facies. Lead isotope age determinations, in conjunction with other data, suggest an early Mesozoic age for lead-zinc mineralization. This precludes a post-Mesozoic age for the Manetoe dolomitization event. Extreme burial depths during the Tertiary led to the generation of dry gas in Manetoe reservoirs.

Sommaire

La dolomie blanche à grain grossier du faciès Manetoe s'étend sur 38 000 km² (15 000 mi²) dans des couches carbonatées du Dévonien moyen dans le sud des monts Mackenzie et le sous-sol des plaines intérieures et des basses-terres à l'est et au sud des monts Mackenzie. Le faciès Manetoe et le faciès mieux connu Presqu'île, dans le district de Pine Point, sont probablement de même étendue – cette conclusion est basée sur une corrélation stratigraphique et sur le fait que leur composition en oxygène et en carbone sont équivalentes et leur reconstitution sur graphique correspond à la même direction colinéaire. Le faciès Manetoe, comme le faciès Presqu'île, est un faciès diagénétique de brèche dolomitisée, constitué principalement d'un massif stratiforme au sein de la formation de Landry et la partie supérieure de la formation d'Arnica. Par endroits, de larges prolongements verticaux du faciès Manetoe pénètrent vers le haut dans les formations de Headless et de Nahanni au-dessus de la formation de Landry. Certains des plus grands amas du faciès Manetoe qui s'étendent au-dessus et au-dessous du niveau stratigraphique de la formation de Landry renferment les champs gazifères les plus au nord exploités au Canada: Pointed Mountain, Kotaneelee et Beaver River.

La dolomie du faciès Manetoe a probablement précipité dans un réseau de cavernes formées antérieurement. Les cavernes pourrait avoir été formées durant l'exposition du bassin d'Elk Point qui a précédé la sédimentation de la formation de Watt Mountain sus-jacente et durant le dépôt des sédiments fluviaux et deltaïques de cette formation. Les températures d'homogénéisation, variant entre 150° environ à 200°C pour les inclusions de fluide aqueux hypersalin contenues dans les cristaux de dolomie, indiquent une précipitation à haute température. Ces données corroborent la faible valeur moyenne $\delta^{18}O$ d'environ $-12‰$ de ces dolomies, si les saumures des inclusions ont été le résultat de l'évaporation d'eau de mer dévonienne. La précipitation de la dolomie et la dolomitisation ont probablement eu lieu par suite de la circulation de saumures résiduelles chauffées géothermiquement provenant du bassin d'Elk Point après avoir remonté plusieurs kilomètres de profondeur au cours d'un événement thermique du Dévonien supérieur. Le système géothermique de la Salton Sea actuelle, dans le sud de la Californie, est semblable à cet ancien système géothermique de recirculation de saumures. L'existence d'un événement thermique du Dévonien supérieur est indiquée par une comparaison des indicateurs de maturation thermique au-dessus et au-dessous de la formation de Nahanni. La valeur de l'indice d'altération des couleurs des conodontes sous la formation de Nahanni est de 5,0 tandis que celle des conodontes des couches mississippiennes qui ne se trouvent qu'à 2000 m au-dessus de la formation de Nahanni n'est que de 1,0 à 1,5. Les valeurs élevées $^{87}Sr/^{86}Sr$ de la dolomie de Manetoe sont conformes aux prévisions basées sur l'hypothèse d'anciens chercheurs selon laquelle l'interaction des saumures résiduelles d'Elk Point aurait causé l'albitisation des feldpath dans les roches de croûte précambrienne sous-jacentes.

L'accumulation, pendant la fin du Paléozoïque, d'épais dépôts de sédiments silicoclastiques à grain fin au-dessus des carbonates dévoniens de la plate-forme de Mackenzie a causé la maturation thermique des matières organiques dans les roches silicoclastiques et la formation d'hydrocarbures. L'enfouissement progressif a provoqué l'expulsion des hydrocarbures vers le faciès Manetoe sous-jacent, là où le faciès Manetoe s'étend verticalement vers le haut jusqu'au sommet de la formation de Nahanni, juste au-dessous des roches silicoclastiques. La migration des hydrocarbures a été accompagnée et suivie de la cémentation de la calcite et du quartz et de la silification des manifestations du faciès Manetoe au-dessous du contact supérieur de la formation de Nahanni. La corrélation des températures d'homogénéisation des inclusions de fluide en ce qui concerne le quartz et la calcite avec leur profondeur d'enfouissement actuelle, indiquent que la cémentation du faciès Manetoe par ces minéraux a eu lieu sous l'influence d'un gradient géothermique normal. La minéralisation, sous la forme de veinules de galène et de sphalérite, a été le dernier événement diagénétique, mis à part la formation de stylolites, ayant affecté le faciès Manetoe. Les datations par les isotopes du plomb combinées à d'autres données indiquent que la minéralisation de plomb-zinc remonterait au début du Mésozoïque. Cette conclusion exclut la possibilité d'un âge post-mésozoïque pour la dolomitisation du faciès Manetoe. Des profondeurs d'enfouissement très grandes au cours du Tertiaire est à l'origine de la formation de gaz sec dans les roches réservoirs de Manetoe.

INTRODUCTION

The Manetoe Facies is an extremely widespread, white, "sparry" dolomite of diagenetic origin, developed in Devonian strata of northern Canada, north of 60°N latitude (Figs. 1, 2). It developed within Lower and Middle Devonian strata of the Mackenzie Shelf carbonate sequence that accumulated north and west of the Elk Point Basin of Western Canada (Fig. 3). This shelf sequence is part of the westward thickening miogeoclinal wedge of shallow water deposits that form the east side of the Cordilleran Geosyncline. Mackenzie Shelf carbonate sequences outcrop extensively in the Mackenzie Mountains (Fig. 1).

In the subsurface southeast of the Mackenzie Mountains the Manetoe Facies contains three large gas fields: the Beaver River, Kotaneelee, and Pointed Mountain fields (Figs. 3, 4). These fields have in place gas reserves of about 2.4 trillion cubic feet (T.E. Hage, pers. comm., 1988). Production problems have been encountered, however, and the original recoverable reserve estimates of some of these fields have been revised downward to several hundred billion cubic feet each (Snowdon, 1977). Exploration for similar gas reservoirs elsewhere in the Manetoe Facies has continued to be a part of the exploration strategy of most companies involved in resource exploration in this area.

In spite of the economic importance of the Manetoe Facies and its similarity to other deposits of white, sparry, megacrystalline dolomite that contain economic deposits of lead-zinc and hydrocarbons, this facies has not been the object of systematic geological investigations until recently (e.g., Morrow et al., 1986; Aulstead, 1987). Previous data concerning this distinctive facies were published as parts of broad regional studies dealing with the structure, stratigraphy and tectonic history of the Mackenzie Mountains and adjacent Interior Plains region. Douglas and Norris (1960, 1961), in the process of regional mapping at a scale of 1:250 000, first identified the Manetoe Facies dolomite as a distinctive map unit and stratigraphic marker in the southern Mackenzie Mountains and named it the Manetoe Formation (Douglas and Norris, 1961). The Manetoe Formation was regarded primarily as a depositional entity, a bioclastic and reef facies above the Arnica Formation and beneath the Headless and Nahanni formations (e.g., Brady and Wissner, 1961; Law, 1971; de Wit et al., 1973). The distinctive, megacrystalline, white, sparry dolomite of the Manetoe was assumed to be coextensive with Manetoe reefal strata and, therefore, exploration strategy was biased toward the search for the Manetoe Reef edge. For example, the Manetoe Facies is particularly thick along the carbonate shelf edge surrounding the Funeral Formation shales in the Virginia Falls map area (95 G, Fig. 4) and, for this reason, some authors (Law, 1971; Noble and Ferguson, 1971) applied the name "Manetoe Barrier Reef" to the Manetoe Facies bordering the Funeral shales. A major reinterpretation of the Manetoe Formation and its significance as a map unit was advanced by Williams (1981b) and by Morrow and Cook (1987). In these publications, the Manetoe is identified as a facies rather than a formation, consistent with the diagenetic rather than depositional origin of the constituent dolomite.

Recognition of the diagenetic character of the Manetoe Facies has led to a reappraisal of its origin. The origin of the Manetoe Facies is important both from the standpoint of petroleum exploration and also because of the similarity of the facies to other megacrystalline, white, sparry dolomites, such as those associated with Mississippi Valley Type lead-zinc deposits. Consequently, this paper is devoted to a more complete characterization, documentation and interpretation of the Manetoe Facies and its diagenetic minerals (such as quartz and calcite), and to the interpretation of the origin of its hydrocarbons.

METHODS, AND SOURCES OF DATA

Most data for this study were gathered from 44 field sections (Fig. 4; Table 1) and from field mapping in the southern Mackenzie Mountains during the summers of 1975, 1976, and 1980 (Morrow and Cook, 1987). Additional data were obtained from well sections in the Interior Plains east of the Mackenzie Mountains (Fig. 4; Table 2), and from previously published studies of Devonian strata in both the Interior Plains and Mackenzie Mountains. Approximately 180 samples of Manetoe Facies dolomite and its host strata were collected from surface sections, and all available cores from boreholes in the Pointed Mountain and Kotaneelee gas fields were examined petrographically.

Many samples were analyzed for their mineralogical composition, their major and minor element content, and their carbon, oxygen, and strontium isotope content – in order to compare dolomites of the Manetoe Facies with descriptions of other, similar dolomites. The isotopic compositions of leads from samples of galena associated with the Manetoe Facies also were determined – in order to provide additional constraints on the interpretation of the origin of the Manetoe Facies, as well as information concerning the origin of the galena mineralization itself. Fluid-inclusion microthermometry was applied to selected dolomite, calcite and quartz cements associated with the Manetoe Facies (see Aulstead, 1987). Additional background data, concerning the thermal maturity of both the Mackenzie Shelf sequence that encloses the Manetoe Facies, and the overlying Upper Devonian and Mississippian siliciclastic rocks, were obtained from conodont Colour Alteration Index (CAI) and palynomorph Thermal Alteration Index (TAI) measurements.

Most samples of the Manetoe Facies analyzed by chemical means contained both void-filling, white, megacrystalline,

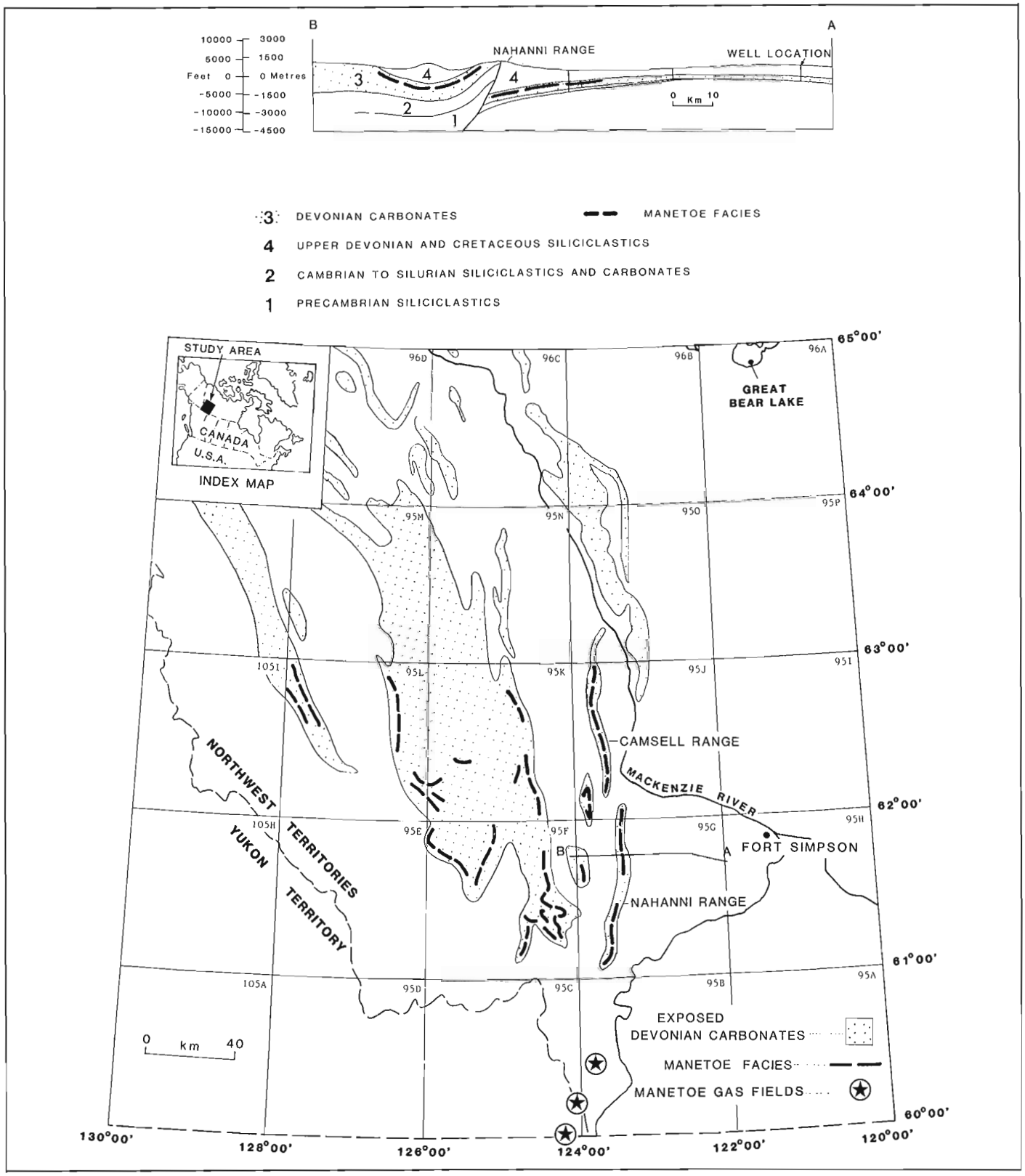

Figure 1. *Distribution of the Manetoe Facies within the predominantly Devonian carbonate strata of the southern Mackenzie Mountains. The northern limit of exposure for the Manetoe Facies is at about latitude 63°N. Cross-section B-A shows the pronounced westward thickening of Devonian strata.*

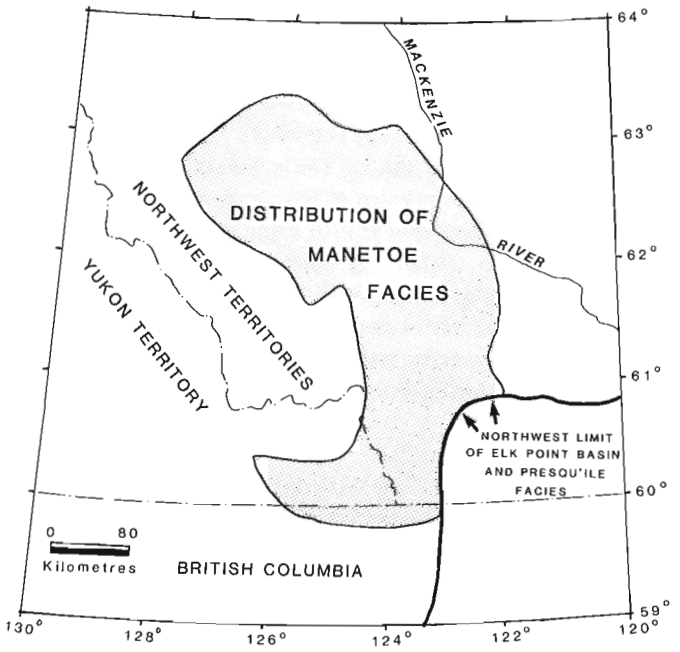

Figure 2. *Generalized map of Manetoe Facies distribution (outcrop and subsurface). The facies extends northward and westward from the edge of the Presqu'île Barrier at the northern end of Elk Point Basin.*

sparry dolomite, and fine to medium crystalline, grey, replacement dolomite in which primary textural features were still preserved (Appendices 1-3). These two types of dolomite were separated by physical means and were converted to powders by grinding separately in a swing mill. Other components analyzed separately included limestone samples from sequences that contain parts of the Manetoe Facies (such as Landry Formation strata), and the megacrystalline, white, sparry calcite associated with white dolomite.

X-ray diffraction powder patterns, using a Philips PR4920/00 X-ray diffraction unit, provided semiquantitative data concerning the mineralogy of bulk samples. The mole per cent $CaCO_3$ content of all dolomite samples was derived from X-ray diffractometer data, according to the methods of Goldsmith and Graf (1958a,b) and Lumsden and Chimahusky (1980), except that the exact position of the dolomite 10.4 reflection was obtained by its separation from the 111 peak (28.466° for CuKα radiation) of a Philips silicon goniometer alignment slug. The uncertainty of this measurement was estimated to be ±0.001 nm. Also, the degree of cation order of the dolomites was estimated following the method of Patterson (1972), in which the sum of the 10.1, 01.5 and 02.1 peak intensities are divided by the intensity of the 11.3 reflection. Larger values for this parameter represent a greater degree of cation ordering. This ordering ratio is subject to a rather high uncertainty of about 10 per cent of the mean, owing to the difficulty in locating some of these low intensity peaks. Duplicate runs were made on five samples and triplicate runs on two samples. In most sample replicate runs the locations of the dolomite d_{104} peaks were identical to those in the original runs and the cation order ratios displayed a range of less than 10 per cent of the mean.

The amounts of major, minor, and trace elements (Appendix 3) were determined by X-ray fluorescence analysis of 59 powdered samples from surface sections. The powders of these samples were mixed with lithium tetraborate, lithium fluoride and ammonium nitrate, and fused to a bead at a temperature of 1000°C on a Claisse Fluxer. The resultant lithium tetraborate beads were analyzed by X-ray fluorescence (XRF) on a Philips PW 1212/80 XRF analyzer. Results were processed according to the methods of Trail and Lachance (1965), and Heinrich and Foscolos (1984).

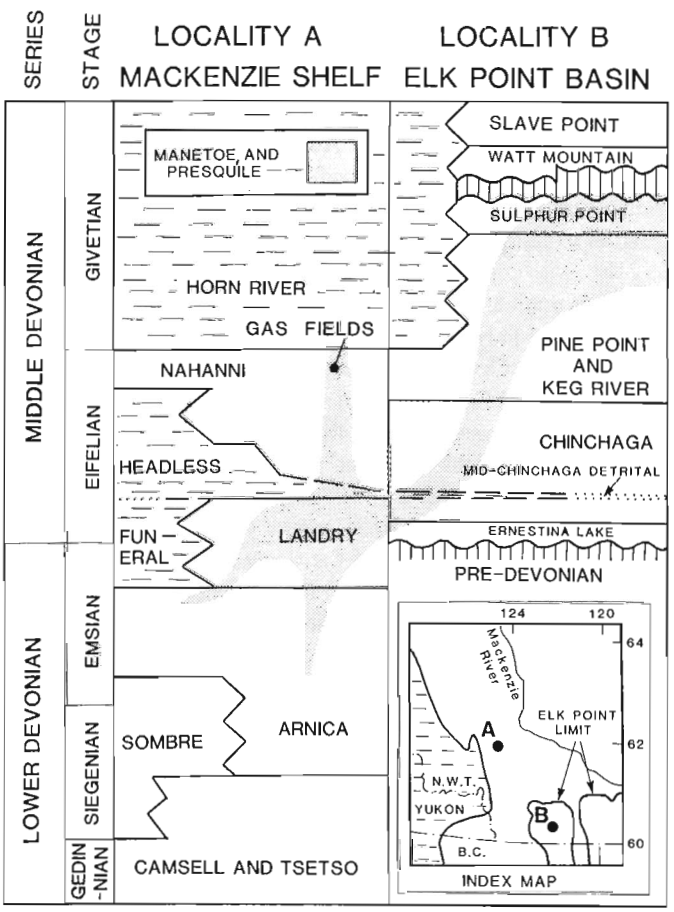

Figure 3. *Schematic cross-section, showing the distribution of the Manetoe and Presqu'île facies within the Lower to Middle Devonian sequence of the Mackenzie Shelf (Locality A) and Elk Point Basin (Locality B). The index map (inset) shows the locations.*

Oxygen and carbon isotope abundances for most samples reported in Appendices 1 and 2 were determined by analysis of sample powders using a direct combustion technique involving $SnCl_2$; a method first employed in the Soviet Union (Borshchevskiy et al., 1974; Borshchevskiy et al., 1980). In this method, mixtures of $SnCl_2$ and carbonate sample powders in evacuated pyrex ampoules are decomposed at 300°C and the evolved CO_2 is analyzed isotopically. All isotopic analyses were performed on a mass spectrometer constructed around components of a Micromass 602. Results are reported as per mil (‰) deviations (i.e., $\delta^{18}O$ and $\delta^{13}C$) from carbonate of the Pee Dee Belemnite (PDB). The results obtained using this method were compared with those derived by the traditional method of acid digestion (McCrea, 1950) for six previously analyzed samples, and an additional six samples were processed by the acid digestion technique. The variation in the carbon and oxygen isotope concentrations determined by these two methods is less than ±1.0 ‰ for the six samples (Appendix 1). The average variation between determinations by these two methods is no greater than the variation between the duplicate analyses of sample C-060989-1.

All stable isotope analyses were performed at the stable isotope laboratory in the Department of Physics at the University of Calgary, Calgary, Alberta, under the supervision of R. Krouse. The carbon and oxygen isotope contents reported in Appendix 4 were obtained solely by the acid digestion technique.

Paleontological thermal maturation data (Tables 3, 4) for conodonts and palynomorphs were supplied by T. Uyeno and J. Utting of the Geological Survey of Canada. Determination of conodont Colour Alteration Index values (CAI values), required for the assessment of the degree of thermal maturation of conodonts, followed the procedures of Epstein et al. (1977) and Rejebian et al. (1987). Determination of palynomorph Thermal Alteration Index values (TAI values), required for the assessment of the degree of thermal maturation of pollen and spores, followed the procedures of Correia (1969) and Hunt (1979), as modified by Utting (1987).

The fluid inclusion data reported here are from Aulstead (1987). Temperatures of homogenization (Th) and initial (Te) and final (Tm) melting (Tables 5-7) were obtained from approximately 200 two-phase aqueous inclusions in dolomite crystals from the Manetoe Facies, and nearly 100 fluid inclusions in calcite and quartz associated with the Manetoe Facies. Homogenization temperatures, particularly of aqueous inclusions, are estimates of the solution temperatures at the time the inclusions formed, whereas the initial and final melting temperatures provide information regarding the salinity and solution composition of the inclusions (Aulstead and Spencer, 1985). Homogenization temperature is the elevated temperature at which the shrinkage cavity of vapour in a fluid inclusion at room temperature disappears, so that the inclusion is filled with a uniform fluid phase. Phase transitions within inclusions were observed and measured using a heating-cooling stage and attached microscope. A Fluid Inc.-modified USGS heating-cooling stage was used for microthermometry of fluid inclusions in cleavage fragments and doubly polished thick sections (100 μm thick). The behaviour of fluid inclusions as they are broken open to the atmosphere (i.e., opened to atmospheric pressure) was also examined using the crushing stage (Roedder, 1970). The shrinkage or expansion of the vapour bubble under atmospheric pressure permits the differentiation of normal shrinkage bubbles from bubbles that have formed by other means; such as the entrapment of vapour bubbles formed during boiling in inclusions (Aulstead and Spencer, 1985).

Strontium isotope ($^{87}Sr/^{88}Sr$) data were obtained for 14 samples of Manetoe Facies dolomite and associated carbonates (Table 7). Samples were dissolved in hydrochloric or nitric acid and strontium was separated from other elements by means of ion exchange columns. Isotope ratios were measured by comparison with standard $SrCO_3$ (NBS SRM 987) for which a ratio of 0.71014 is assumed. Measurements were made using a second-order, double focusing, Nier-Johnson-type mass spectrometer.

Strontium analyses were performed at the Research Department of the Mobil Research and Development Corporation at Dallas, Texas, U.S.A., under the supervision of R.B. Koepnick.

Eighteen galena samples, from strata that are geographically or stratigraphically related to the Manetoe Facies, were analyzed for lead isotopes. The results of these analyses, in conjunction with other published determinations (e.g., Godwin et al., 1981, 1982; Morrow and Cumming, 1982), were used to interpret the history of lead-zinc mineralization in lower Paleozoic strata that contain the Manetoe Facies.

In individual lead analyses, samples weighing a few milligrams were dissolved in HCl and purified, using an HBr-HCl anion exchange column. Approximately 1 μgm of Pb was placed on an Re filament with silica gel/phosphoric acid and the sample was analyzed on a Micromass MM30 mass spectrometer. Measuring precision was better than 0.2 ‰ per mass unit difference at 2 sigma error limits.

REGIONAL STRATIGRAPHY OF THE MANETOE FACIES

Geological setting, distribution, and configuration of the Manetoe Facies

The Manetoe Facies is developed almost entirely within strata of the Arnica, Landry, Headless and Nahanni formations

(Table 1; Fig. 3), over an area of about 15 000 square miles (38 000 square kilometres), northwest of the Presqu'île Barrier Complex (Fig. 4). The facies has been mapped as a formation in five map areas (Fig. 1); by Gabrielse et al. (1973), Douglas (1974), and Douglas and Norris (1977a,b,c). In addition, the Manetoe Facies was found to occur in the southern parts of the Wrigley Lake and Dahadinni map areas (NTS 95 M and 95 N; Fig. 1).

In the western parts of the Virginia Falls and Glacier Lake map areas (NTS 95 F and 95 L), coarsely crystalline white dolomites, developed in the carbonates immediately beneath the shales of the Funeral Formation, were mapped previously as parts of the Grizzly Bear and Natla formations (Gabrielse et al., 1973; Douglas and Norris, 1977c). These dolomites are included herein as part of the Manetoe Facies, because of their close geographic and stratigraphic proximity to the main mass of the Manetoe Facies farther east.

In general, the western limit of the Manetoe Facies is a short distance west of the eastern limit of the Funeral Formation (Fig. 4).

Continuity of the Manetoe Facies dolomite in the subsurface east and southeast of the southern Mackenzie Mountains (Fig. 5) has been demonstrated by Law (1971) and Williams

TABLE 1

Regional thicknesses (in metres) of the Manetoe Facies and associated formations

SECTION	SECTION NAME	SOMBRE (D = Detrital) member)	ARNICA (BR = Bear Rock) (B = Basinal member)	FUNERAL (N = Natla)	LANDRY (G = Grizzly Bear)	HEADLESS	NAHANNI	MANETOE FACIES[1]
1	Nahanni Butte		135.5+			7.5	195.5	213.5(A, H and N)
2	Grainer River		344.0+		30.0	49.5	130.0+	118.0(A, L and H)
3	Red Rock Pass		613.5		46.0	3.0	204.0+	30.5(A, L and H)
4	First Canyon	104.0+	625.5		54.0	30.0	24.0+	85.0(A and L)
5	Ram Plateau 1			354.6+		213.0	234.0	
6	Sundog Creek		217.5+		79.0	82.0	42.0+	43.5(A and H)
7	Ram River 2		94.5+	154.0		71.5	38.0+	94.5(A)
8	West Ram Plateau 2		201.0+		(?)	28.5+		151.5(A and L?)
9	West Ram Plateau 1		3.8+(B)		96.0+			
10	South Ram Plateau		5.0+		100.0	15.0		60.0(A and H)
11	Meilleur River		27.5+	(?)		65.5	241.0+	
12	Second Canyon 1	276.0	872.0	25.0(?)		95.0?	28.5	61.5(A)
13	Second Canyon 2		111.0+	159.0		72.0+		
14	Prairie Creek 3	313.0+	433.0+					41.0+(A)
15	South Tundra		1378.5					
16	West Tundra 1		305.0(B)	150.0		207.5	306.0+	
17	Tundra Ridge	1101.5	2.5+	466.0		177.0	231.0+	
18	West Headless		93.0(B)	6.0+				
19	Prairie Creek 4		334.0(B)	368.5	22.0	250.0	79.5+	
20	Manetoe Range 2	556.5			187.5	238.5+		102.0(L)
21	South Manetoe 1	350.0(D)	139.5+		6.4+			
22	Manetoe Range 1	686.5			60.0	18.0	45.0	78.0(H and L)
23	South Manetoe 2	269.0		90.0+				
24	Arnica Ridge 3		11.0	668.0		76.0	215.0+	
25	Arnica Ridge 2	1069.5		20.0+	40.0			
26	Arnica Ridge 1	918.5	111.5+					31.5(A)
27	Cathedral Mountain	1086.0	13.5+	244.0		122.0	12.0	Present at top of Sombre
28	Trench Creek	286.0	143.0	257.0	229.0			
29	Pastel Creek	592.5	250.0		20.0+			60.0(A and L)
30	Iverson Lake		251.0		10.0	5.0+		251.0(A)
31	MTA-79-10[2]	1037.5	121.5+					
32	MTA-79-16	443.5		20.0+				
33	MTA-79-4	547.0	210.0		46.5(G)			
34	MTA-79-3	598.0	311.0		163.0			40.5(L)
35	MTA-79-9	165.0	50.5		160.5	33.0+		4.5(A)
36	MTA-79-14	508.5		148.5	89.0(G)	93.0		20.0(G)
37	MTA-79-26	175.0	157.0	207(N)				
38	MTA-79-23	511.5	62.0	10.0+ 192.0(N)				57.0(N)
39	MTA-79-2		103.5		156.5	75.5	68.5+	20.0(A)
40	MTA-79-1	208.0	254.5		248.5			18.0(L)
41	MTA-79-7	142.5+	85.5+		176.5			10.0(A)
42	MTA-79-15		925.0		139.5	205.5	96.0	15.0(A)
43	MTA-79-5	244.5	94.5		217.0			15.0(A)
44	MTA-79-8		143.0(BR)		10.5	109.5		

[1]Manetoe Facies developed in the Arnica (A), Landry (L), Grizzly Bear (G), Headless (H), or Nahanni (N).
[2]Field numbers of unpublished sections (31-44).

(1981b). The southeastern limit of the Manetoe Facies is defined arbitrarily as the northern boundary of the Upper Elk Point subgroup (Fig. 5). Southward across this boundary the coarsely crystalline dolomite of the Manetoe Facies passes into the coarsely crystalline dolomite of the Presqu'île Facies (Law, 1971; Skall, 1975) with no apparent physical separation. In other words, this boundary was created by the exigencies of stratigraphic nomenclature and is not a true physical boundary.

The eastern and northeastern limits of the Manetoe Facies coincide approximately with the western limit of the Bear Rock Formation and Chinchaga Formation evaporites (Fig. 4).

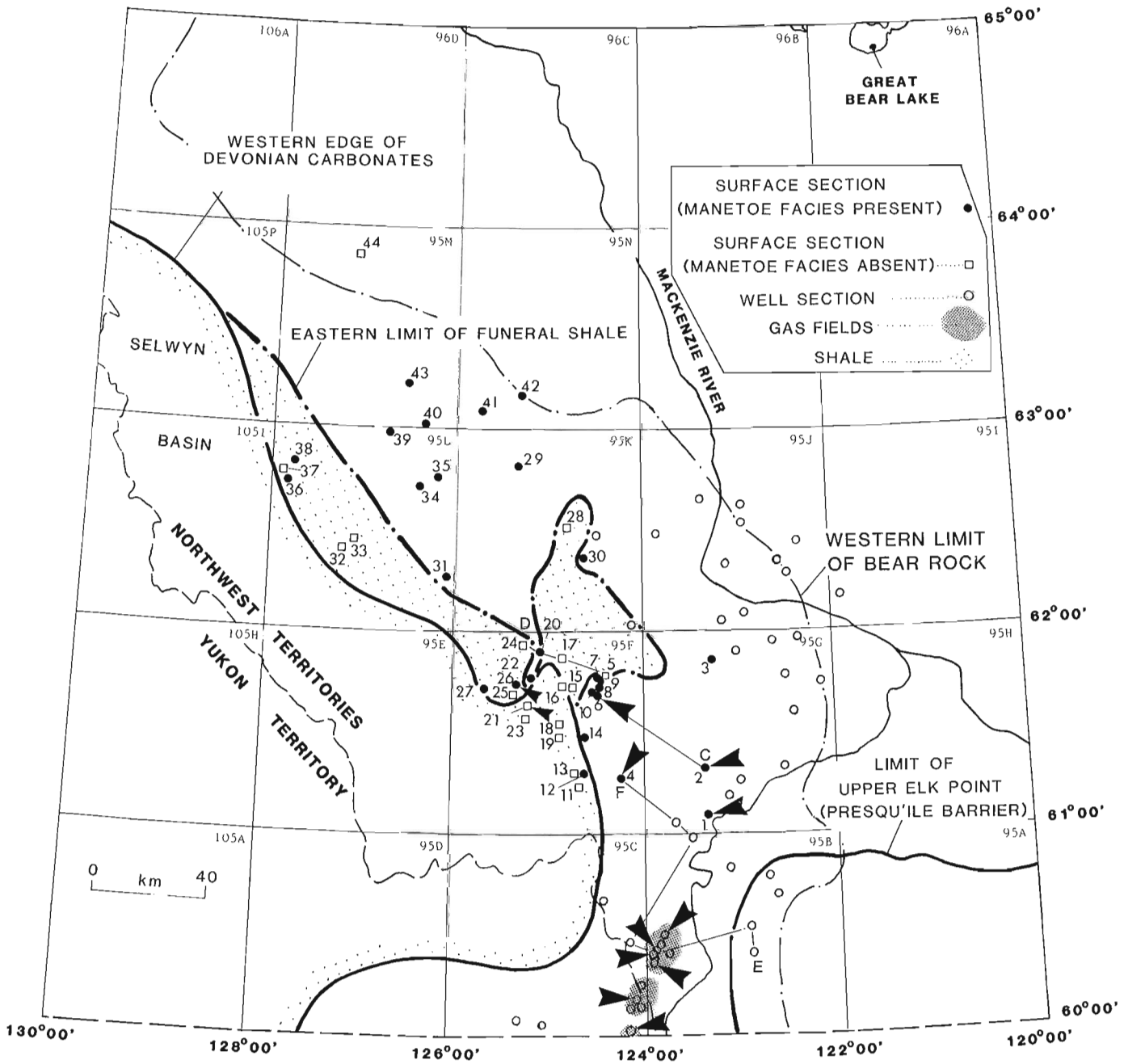

Figure 4. *Locations of surface and well sections of the Manetoe Facies, related to formation boundaries. Arrows indicate sample localities from which chemical and isotope data were obtained (Appendices 1-3). The cross-section corresponding to the line of section E-F is shown in Figure 5.*

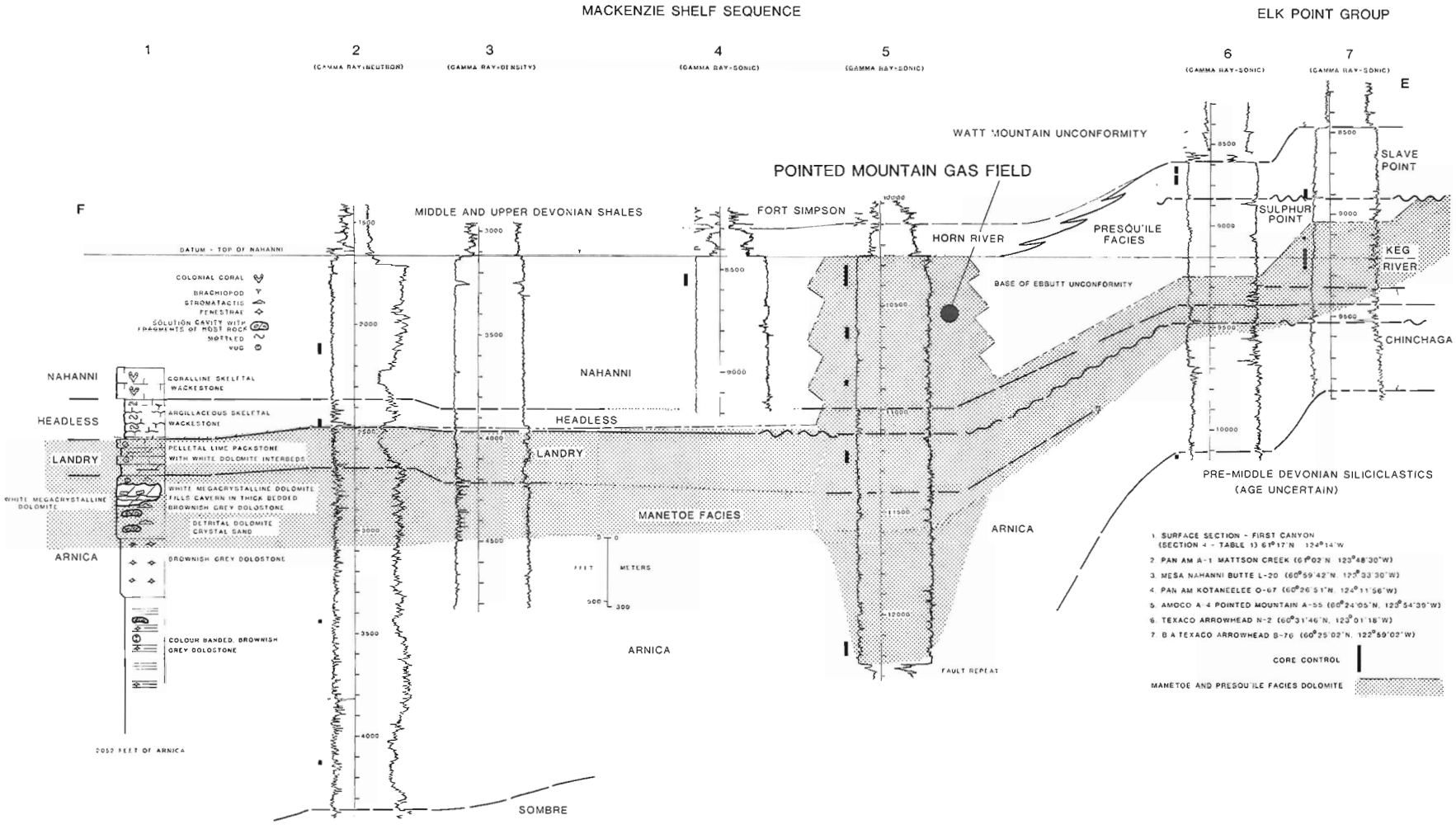

Figure 5. *Cross-section of Devonian shelf sequence stratigraphy, from the edge of the Elk Point Group northwestward (right to left) across the Mackenzie Shelf. (See line of section E-F on Figure 4.) The diagenetic Manetoe Facies developed preferentially in limestone of the Landry Formation, and in the vuggy, stromatactis-bearing dolostone of the uppermost part of the Arnica Formation. The facies is mainly restricted to strata beneath the shaly limestone of the Headless Formation.*

In a northwest direction, parallel to the trend of the Mackenzie shelf edge, the Manetoe Facies ends at about latitude 63°30′N, within the Wrigley Lake map area (NTS 95 M; Fig. 4). This northwestern boundary does not coincide with any documented sedimentary facies change.

The Manetoe Facies has an approximately tabular configuration beneath the argillaceous strata of the Headless Formation (Figs. 5, 6). It can be subdivided into three distinct regional components, based on variations in shape from southeast to northwest (Fig. 6). The upper contact of the Manetoe tends to be abrupt but its lower contact is less well defined. This is largely because the upper surface of the Manetoe occurs within limestones of the Headless and Nahanni formations, whereas the lower contact commonly occurs within dolostone of the Landry Formation.

In the southeast, near the Elk Point limit (i.e., the Presqu'île Barrier Complex), large masses of Manetoe dolomite extend vertically for varying distances above the level of the Headless Formation, toward the top of the Nahanni Formation (Figs. 5, 6). The Beaver River, Pointed Mountain and Kotaneelee gas fields occur within some of these vertical developments, where the dolomite bodies are in contact with the overlying Devonian shales. The region of vertical developments lies largely in the subsurface and the locations of individual vertical developments are inferred from lateral facies changes from well to well within the Nahanni Formation (Fig. 5). However, some vertical developments are exposed along the Nahanni Range, particularly near the type section of the Nahanni Formation at Nahanni Butte (Section 1 in Table 1). The thickness of the Manetoe in this region varies considerably, from a minimum of a few hundred feet, to a maximum of more than 500 m (1600 ft) in the Pointed Mountain and Kotaneelee gas fields (Fig. 5). A similar thickness variation was also observed along the Nahanni Range (e.g., compare Sections 1 to 3 in Table 1).

Farther northwest in the Mackenzie Mountains the Manetoe Facies is confined largely beneath the Headless Formation and maintains a fairly constant thickness of about 50 to 100 m (e.g., Sections 3, 4, 6, 7, and 10 in Table 1). The continuity of the Manetoe Facies to the northwest is

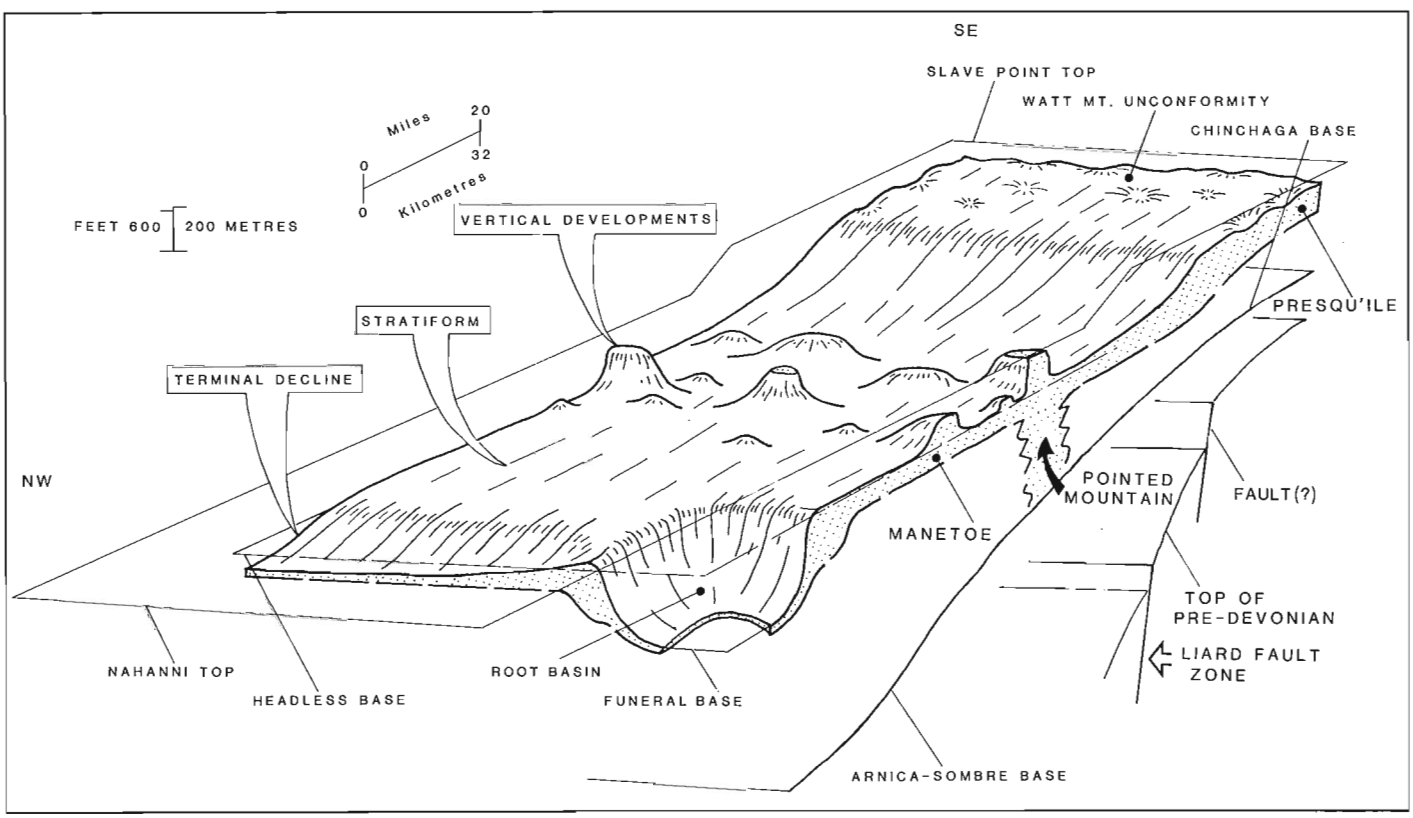

Figure 6. *Schematic three-dimensional reconstruction of the combined Manetoe and Presqu'île facies with respect to formation boundaries. The Manetoe is subdivided into three morphological regions: an area characterized by pronounced* ***vertical developments****; a central region where the Manetoe is largely* ***stratiform*** *beneath the Headless Formation; and a northwestern region of* ***terminal decline****, farthest away from the Presqu'île Barrier, where the Manetoe drops to lower stratigraphic levels in the Arnica Formation.*

influenced by the presence of a large intrashelf basin filled with the argillaceous sediments of the Funeral Formation. Northwest of this shale embayment the Manetoe is less than 50 m (150 ft) thick and tends to occur lower in the stratigraphic sequence – within the Arnica Formation or near the base of the Landry Formation, rather than in the Landry strata immediately beneath the Headless Formation (e.g., Sections 39 to 43 in Table 1). This is shown schematically in Figure 7 as the region of "terminal decline".

At certain localities along the south and east sides of the Funeral "shale embayment", the Manetoe Facies immediately adjacent to the depositional edge of the Funeral Formation (e.g., Sections 8 and 30 in Table 1) tends to be somewhat thicker and more continuous vertically than it is in the shelf sequence away from the Funeral edge (Fig. 4). The occurrence of a thick Manetoe Facies at these localities has been regarded as evidence of the existence of a "Manetoe Barrier Reef" rimming parts of this embayment (Brady and Wissner, 1961; Law, 1971). West of the Funeral shale limit the Manetoe is present within carbonate strata immediately beneath the Funeral Formation; for example, at the top of the Arnica Formation (Secs. 26, 27), at the top of the Grizzly Bear Formation (Sec. 38), and at the top of the Natla Formation (Sec. 38). The Manetoe is very thin beneath the Funeral Formation at these localities and in most places disappears only a short distance to the west (Fig. 6). Eastward, the Manetoe disappears after a progressive but gradual decrease in thickness (Williams, 1981b). The character of the easternmost part of the Manetoe Facies is less well known, because few cores were taken from wells along its eastern margin.

Relationship between the Manetoe and Presqu'île facies

As mentioned above, the dolomite of the Manetoe Facies extends southeastward without interruption into the stratigraphically slightly higher dolomite of the Presqu'île Facies, which lies beneath the Watt Mountain and Slave Point formations of the Elk Point Group (Law, 1971) (Figs. 3, 5). The Presqu'île Facies, originally identified and named as the Presqu'île Formation by Cameron (1922) but downgraded to the status of a facies by Skall (1975), is similar to the Manetoe Facies. The Presqu'île is a coarsely crystalline dolomite, the original fabric of which has been largely destroyed. It contains abundant solution collapse breccia and vugs cemented and occluded by white dolomite (Skall, op. cit.). Like the Manetoe Facies, the Presqu'île is a diagenetic facies that cuts across the bedding of the host formations (Skall, op. cit.).

The regional extent of the Presqu'île Facies is less well documented, but studies by Law (1955, 1971), Griffin (1967), Morrow (1970), Skall (1975), Morrow et al. (1978), and Kyle (1980), in various areas of Alberta, British Columbia and the Northwest Territories, indicate that it is developed within the Pine Point and Sulphur Point formations beneath the Watt Mountain Formation, across the entire Presqu'île Barrier Complex (Fig. 2).

Manetoe cavern fillings and associated dolomitization

The Manetoe Facies is particularly well exposed at Nahanni Butte (Sec. 1; Fig. 7), and at the type section of the former Manetoe Formation (Douglas and Norris, 1961) at First Canyon on South Nahanni River (Sec. 4; Fig. 8). From a distance, at both Nahanni Butte and First Canyon, the Manetoe Facies is mappable as a more or less continuous, white weathering unit at the top of the Arnica Formation and beneath the Nahanni and Headless formations.

At Nahanni Butte and along the Nahanni Range, large vertical developments of the Manetoe Facies extend upward through the Headless and Nahanni formations. These vertical developments are not readily visible at distances of more than a few hundred metres, and thus are not commonly discernible by aerial reconnaissance. One vertical development of Manetoe Facies, which extends about 45 m (150 ft) upward into the overlying Nahanni Formation at Little Doctor Lake on the north end of Nahanni Range, is perhaps the only previously documented occurrence of this phenomenon (Brady and Wissner, 1961). Dolomitization associated with the Manetoe Facies extends to the top of the Nahanni Formation at Nahanni Butte, analogous to dolomitization associated with the Manetoe Facies at Pointed Mountain gas field (Fig. 7, A).

The Manetoe Facies at Nahanni Butte comprises a zone of dolomite-cemented mosaic and rubble packbreccia (Morrow, 1982a) and floatbreccia, with large, somewhat tabular, subangular, dark fragments of host dolostone cemented by megacrystalline white dolomite (Fig. 7, B). It cannot be determined with certainty whether these fragments were originally dolostone from the Arnica Formation or limestone from the Landry Formation. The strata enclosing this part of the breccia zone have been included in the Arnica Formation (Morrow and Cook, 1987), but it is possible that part of this zone is developed within the Landry Formation, based on the occurrence of the Manetoe Facies in the Landry farther north along most of the Nahanni Range (e.g., Secs. 2, 3; and Douglas and Norris, 1977b).

Breccias of this zone extend upward into the Nahanni Formation and are visible in exposures along the south-facing cliff at Nahanni Butte as a vertically oriented breccia body about 15 m to 30 m (50 to 100 ft) wide. The original beds of Nahanni Formation limestone are dolomitized for various distances (ranging from a few feet to hundreds and even thousands of feet) away from the breccia body (Fig. 7, A). Along individual beds, the change from dolomite to limestone appears to be abrupt, although in detail it is in fact gradational over a distance of about 2.5 cm (one inch). Variations in

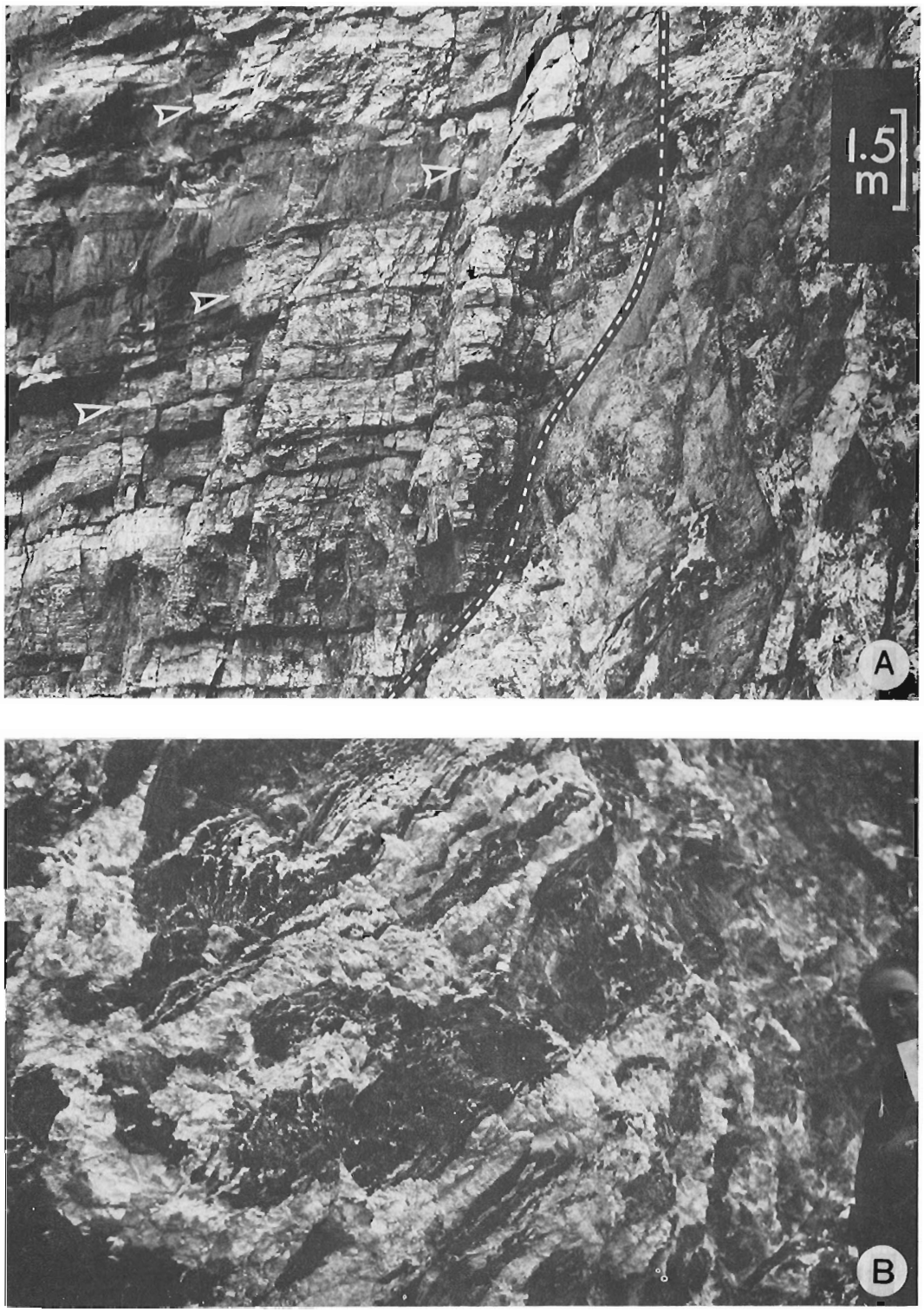

Figure 7. *Outcrop photographs of the Manetoe Facies at Nahanni Butte. (Section 1 in Table 1.)* ***A.*** *View of the west side of a vertical development of the Manetoe Facies that extends to the top of the Nahanni Formation. Dolomitization extends varying distances westward along Nahanni limestone beds, away from the central brecciated core of the Manetoe development. The limits of dolomitization in individual beds are marked by arrows.* ***B.*** *Coarse mosaic of breccia fragments of dark brownish grey dolostone of the Arnica Formation, cemented by coarsely crystalline white Manetoe dolomite. This exposure is in the lower part of the vertical Manetoe development shown in Figure 7A.*

porosity and permeability between individual beds apparently were the dominant factors that governed the extension of dolomitization from the edge of the breccia body. The large proportion of cavity-filling, white, dolomite cement in the Manetoe Facies indicates that dolomitization was preceded by an episode of cavernous porosity development at the stratigraphic level of the Landry Formation and the upper part of the Arnica Formation.

The Manetoe Facies at Section 4 includes a well exposed example of a cavern filling. At this section, the Manetoe Facies occurs in two parts: a lower part developed in the uppermost 90 m (290 ft) of the Arnica Formation, and an upper part developed throughout the Landry Formation (Fig. 5). The brownish grey dolostones of the lower and middle parts of the Arnica Formation pass upward to more resistant, very thick but discontinuously bedded, dark grey, medium crystalline dolostone containing abundant stromatactoid-shaped vugs that are filled with megacrystalline, white, sparry dolomite (Fig. 5). Near the top is a spectacular, 9 m (30 ft) thick, cavern deposit consisting primarily of white, megacrystalline, sparry dolomite and calcite (Figs. 5, 8). Some cleavage surfaces observed in this dolomite were more than 25 cm (10 inches) across.

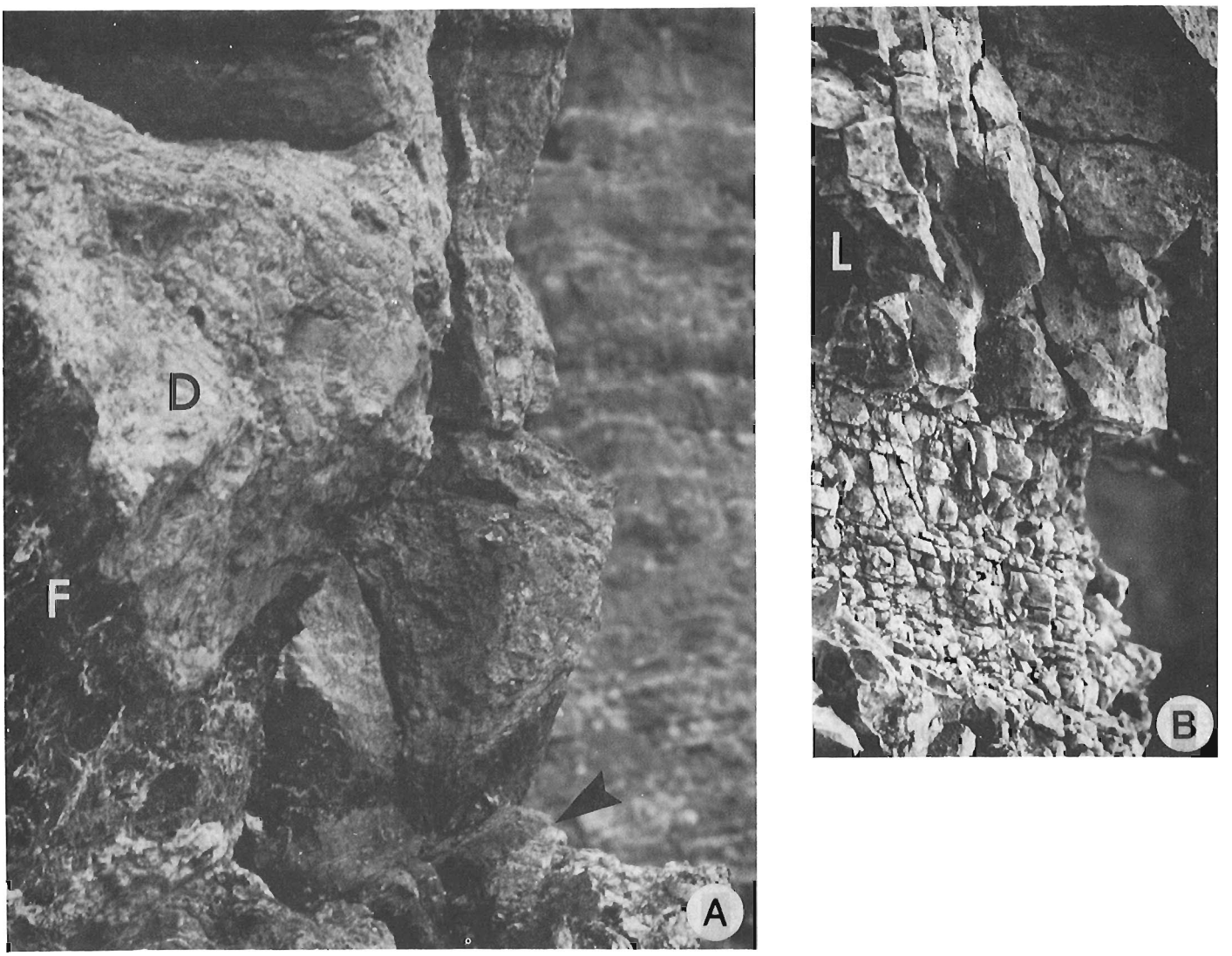

Figure 8. *Outcrop photographs of the Manetoe Facies at First Canyon. (Section 4 in Table 1.)* ***A.*** *Coarsely crystalline white Manetoe dolomite cement (D) in stromatactis-bearing, vuggy, dark grey dolostone (F) at the top of the Arnica Formation. The arrow points to the base of the white dolomite cement* ***B.*** *A remnant of tan coloured pelletal lime wackestone (L) of the Landry Formation, preserved within a mass of Manetoe replacement dolomite. (About 100 m above the base of the Landry Formation.)*

The Landry Formation above this cavern filling is medium bedded and comprises pelletal lime packstone interbedded with coarsely crystalline, white, sparry dolomite (Fig. 8, B). No breccia was observed in the Landry Formation at Section 4, but dolomite-cemented rubble packbreccias occur in Landry strata at many places. It seems likely that the dolomitized Landry beds at Section 4 are lateral extensions of dolomitized beds surrounding a breccia zone that becomes narrower upward, like that developed at Nahanni Butte.

Diagenetic sequence and petrography

Manetoe Facies dolomitization is only one of a series of diagenetic events that have affected this shelf carbonate sequence. Other events include: the emplacement of hydrocarbons and the subsequent formation of bitumen (pyrobitumen); silicification; the development of stylolites; and mineralization by galena, sphalerite, and pyrite (Fig. 9).

TABLE 2

Names and locations of wells from which Manetoe dolomite core has been sampled for fluid-inclusion, chemical, or isotopic analyses

Well name	Degrees north latitude	Degrees west longitude
Pan Am Beaver YT G-01	60.00694[1]	124.26333
Columbia Kotaneelee YT H-38	60.12110	124.10083
Pan Am A-3 Pointed Mountain G-62	60.35744	123.94633
Pan Am Pointed Mountain P-53	60.37933	123.90926
Amoco A-4 Pointed Mountain A-55	60.40139	123.91805
Pan Am B-1 Kotaneelee O-67	60.44183	124.19267
Amoco B-2 Pointed Mountain F-38	60.45533	123.86526
CPOG et al. Labiche F-08	60.62230	124.52031
Imperial Sun Netla Raven F-73	60.70694	122.73611
Horn River Amerada Hess Cli Lake M-05	61.91611	123.02972
Mobil Fort Simpson M-70	61.99930	122.46636
Chevron CS Ebbutt G-72	62.35694	122.47722
Chevron CS Berry F-71	62.50583	122.99083
Horn River et al. Willowlake G-47	62.60639	122.88666
FPC Tenneco Root River I-60	62.65895	123.40805

[1]Minutes expressed as a decimal fraction.

Galena and reddish brown sphalerite occur as small subvertical veinlets and final vug-fillings in the Manetoe Facies of the Pointed Mountain, Beaver River, and Kotaneelee gas fields. These veinlets appear to intersect all other fabrics (Fig. 10, A and B), and their development is interpreted as the final major diagenetic event to have affected this sequence. Mineralization is restricted to strata less than 60 m (200 ft) below the contact between the Devonian carbonates and the overlying Middle and Upper Devonian shales.

Stylolitization is another late event that clearly postdates the development of the breccias and dolomite of the Manetoe Facies (Fig. 10, C and D). In several places, stylolites were observed intersecting quartz- and bitumen-lined vugs (Fig. 10, A), which implies that the development of stylolites also largely postdated silicification and the emplacement of bitumen. These relationships were documented in core from the Pointed Mountain and Kotaneelee gas fields. Stylolitization and mineralization also were observed in outcrop.

Bitumen with an anthracitic, glassy lustre is common in all cores of the Manetoe Facies from the Pointed Mountain, Beaver River, and Kotaneelee gas fields. However, large masses of this type of bitumen were not observed in any outcrop sections of the Manetoe.

Silicification has affected a large part of the Manetoe Facies. It is represented mainly by final vug-fillings of medium crystalline quartz and coarsely crystalline "dogtooth" quartz in incompletely filled vugs. Most quartz vug-fillings are developed within the spaces that remained between breccia fragments after sparry dolomite cementation (Fig. 10, B), but some occur within incompletely occluded stromatactoid vugs and other nondescript vugs.

Quartz cementation is abundant in that part of the subsurface Manetoe Facies that hosts the upper parts of the gas fields, and in the Manetoe exposed at Nahanni Butte. Quartz cementation is much less common in the Manetoe exposed farther to the west in the Mackenzie Mountains and in the lower parts of the gas fields. It is noteworthy that there is a considerable amount of unoccluded porosity in the Manetoe Facies of the gas fields (e.g., Snowdon, 1977) and in the Manetoe at Nahanni Butte. Away from the areas in which it forms large vertical developments, the Manetoe Facies is more completely cemented by dolomite. This pervasive dolomite cement precluded extensive quartz cementation, although quartz, in small amounts, is present throughout the entire Manetoe Facies.

In addition to the pervasive quartz vug-fillings, the Nahanni Formation, adjacent to its upper contact, is silicified in several places by small masses (several inches thick) of chalcedonic chert. At Nahanni Butte, these replacement masses of chert and finely crystalline quartz are particularly

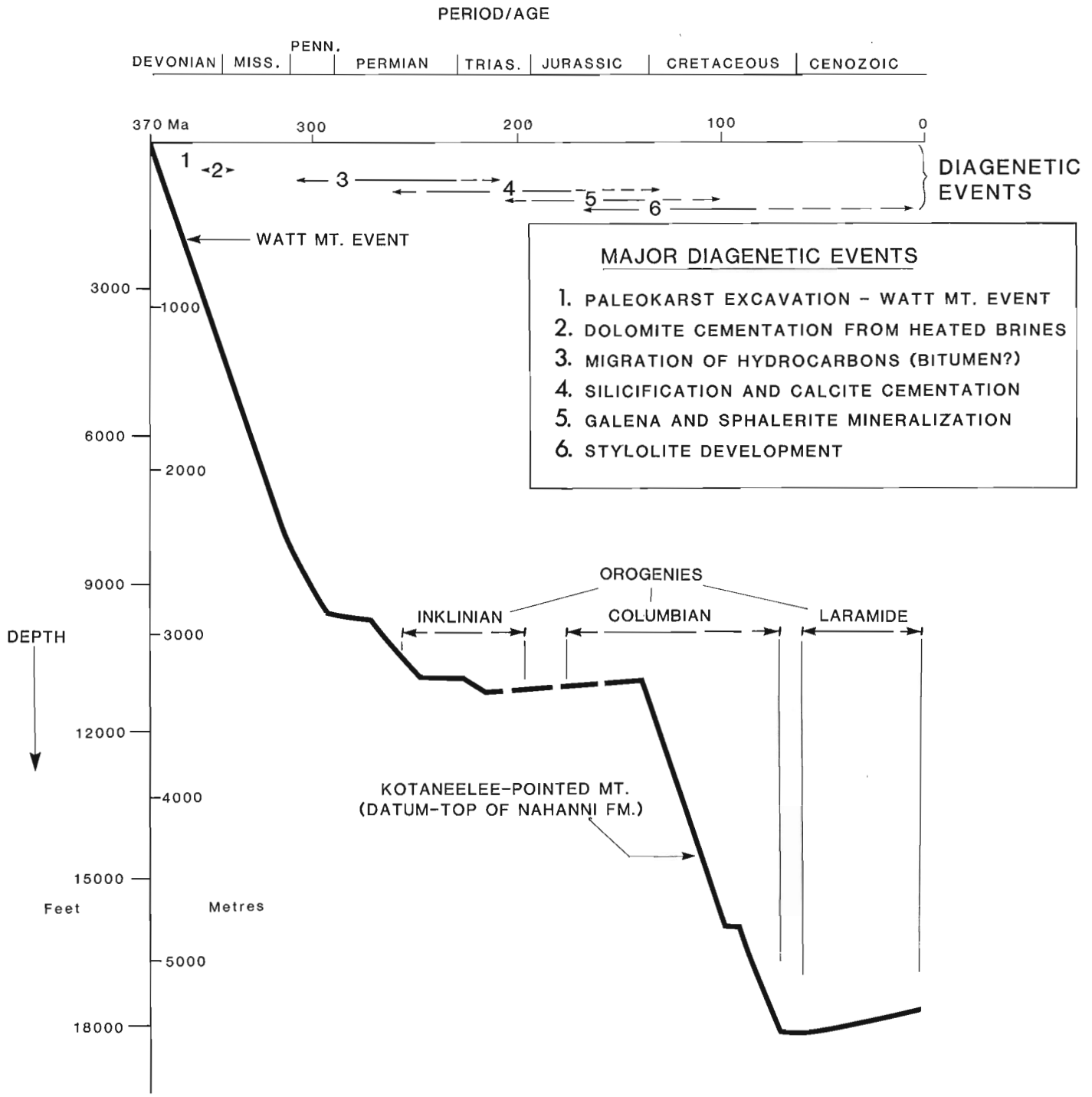

Figure 9. *Subsidence and diagenetic history of strata containing the Manetoe Facies in the vicinity of the Pointed Mountain and Kotaneelee gas reservoirs – probably representative of the burial history of the more deeply buried parts of the Manetoe. These strata were less deeply buried in the Interior Plains region east of the Mackenzie Mountains. This chart is approximate only and may be inaccurate, particularly for the intervals influenced by major orogenies.*

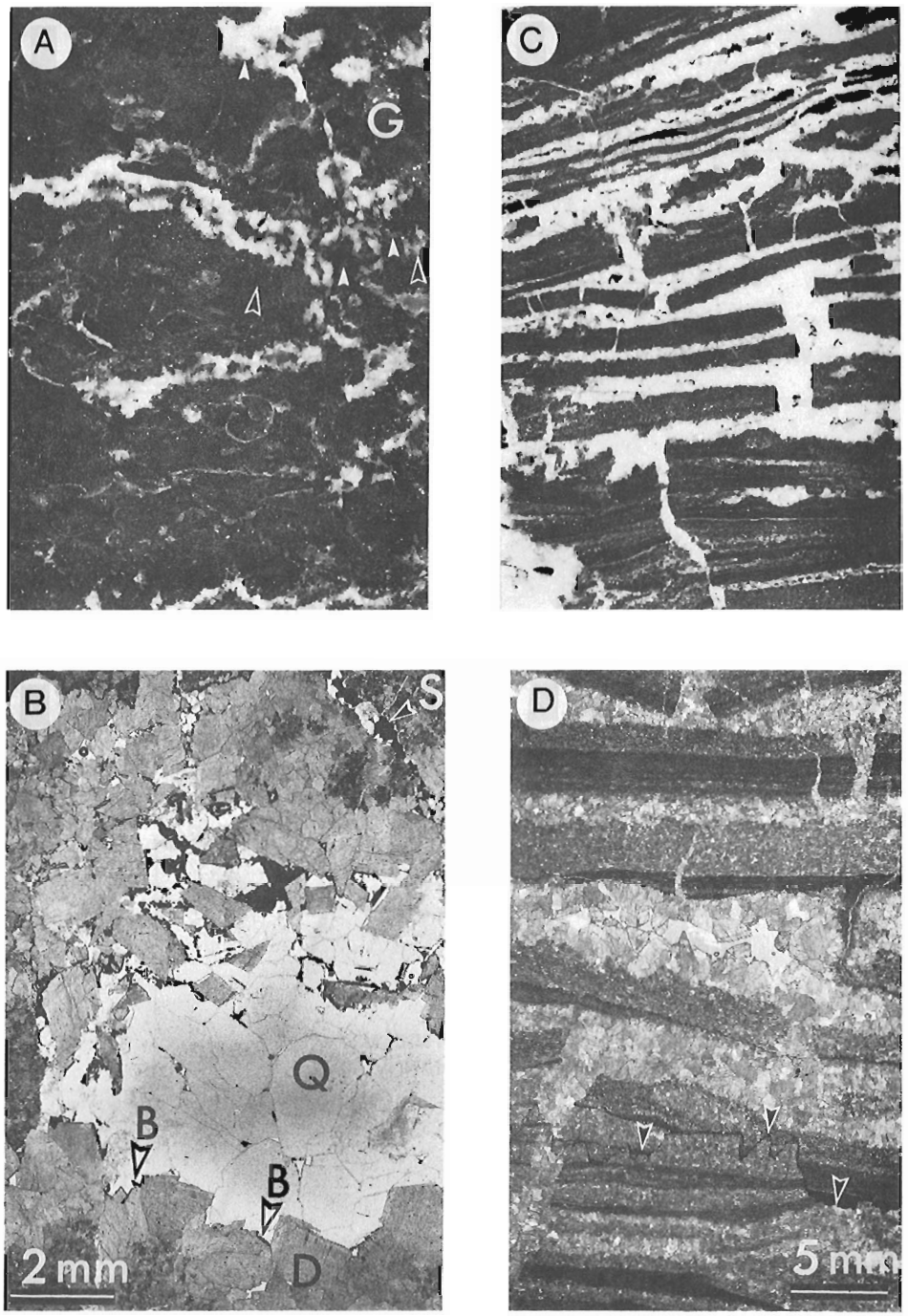

Figure 10. *Diagenetic textures of the Manetoe Facies in the Columbia et al. Kotaneelee YT H-38 well. (Lat. 60°07′16″N; long. 124°06′03″W.)* ***A.*** *Dolomitized Nahanni limestone from 22.5 m (74 ft) below the upper contact. Irregular cavities are filled with white sparry dolomite, then black bitumen and quartz. Arrows indicate stylolites that transect and displace these cavity fillings. A large, subvertical veinlet of galena (G) intersects a cavity filling. (3568.9 m/11 709 ft below KB, natural scale.)* ***B.*** *Photomicrograph of one of the cavity fillings shown in Figure 10A. Coarsely crystalline dolomite (D) lines the periphery of the vug. Bitumen (B) coats the faces of dolomite crystals that project inward. Quartz (Q) fills the centre of the vug, and dark reddish brown sphalerite (S) forms a crosscutting veinlet.* ***C.*** *Core sample of Manetoe Facies from the Nahanni Formation, from 131.7 m (432 ft) below its upper contact. Quartz and bitumen are absent from these deeper strata. Tabular style of brecciation may reflect an originally laminated fabric. (3678 m/12 067 ft below KB, natural scale.)* ***D.*** *Photomicrograph of part of the sample shown in Figure 10C. Arrows indicate the trace of a stylolite transecting Manetoe dolomite.*

large, up to 3 m in thickness and up to 20 m in breadth. This type of replacement has modified the Manetoe Facies immediately underlying the upper contact of the Nahanni Formation with the Devonian shales (Fig. 11). Veins of microcrystalline quartz, about 20 to 30 cm wide, extend downward from these silicified masses through the Manetoe Facies at Nahanni Butte. It seems possible that the source of silica for these chert masses, and for the crystalline vug-fillings at stratigraphically lower levels, may have been the immediately overlying shales.

In vug-filling cement sequences, bitumen commonly is present between the sparry dolomite that lines vug peripheries and the quartz that occludes the centres of the vugs (Fig. 10, A). Large masses of bitumen also occur in some vugs in which there is no quartz cement. These relationships imply that the emplacement of bitumen followed dolomitization in the gas fields of the deeper subsurface.

The megacrystalline, sparry dolomite characteristic of the Manetoe Facies represents the earliest well defined diagenetic phase. This white, medium crystalline to very coarsely crystalline, cavity-filling dolomite displays the curved crystal faces that typify the "saddle dolomite" of Radke and Mathis (1980). Bitumen tends to coat the dolomite crystal faces that project from the vug walls toward the interior (Fig. 10, B). No intracrystal bitumen or solid bitumen inclusions were observed in the dolomite in hand samples, core samples, or in thin sections, although other types of fluid inclusions are moderately abundant. Colloform textures, in which very fine crystalline dolomite is intergrown intimately with bitumen, as observed within the Presqu'île Facies at the Pine Point deposit (Macqueen and Powell, 1983), were not observed in the Manetoe Facies.

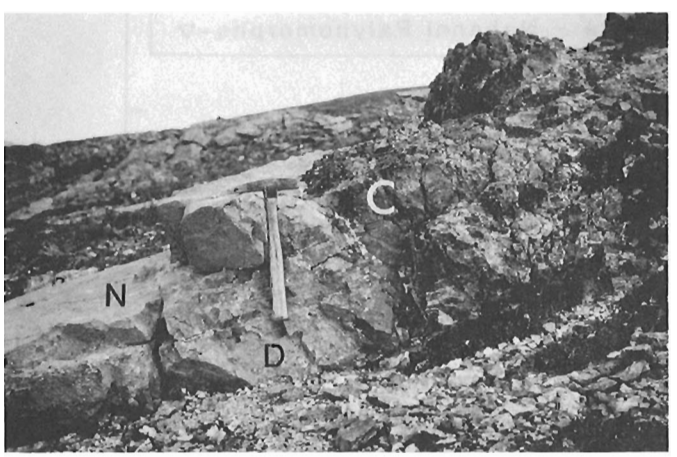

Figure 11. *A mass of dark grey microcrystalline quartz and chalcedony (C) at the top of the Nahanni Formation, exposed at Nahanni Butte (Section 1). This mass of chalcedonic quartz has replaced parts of the Manetoe Facies dolomite (D) and parts of the adjoining undolomitized Nahanni limestone (N).*

PALEONTOLOGICAL THERMAL MATURATION INDICATORS

Paleontological thermal maturation indicators provide a preliminary estimate of the maximum temperatures that

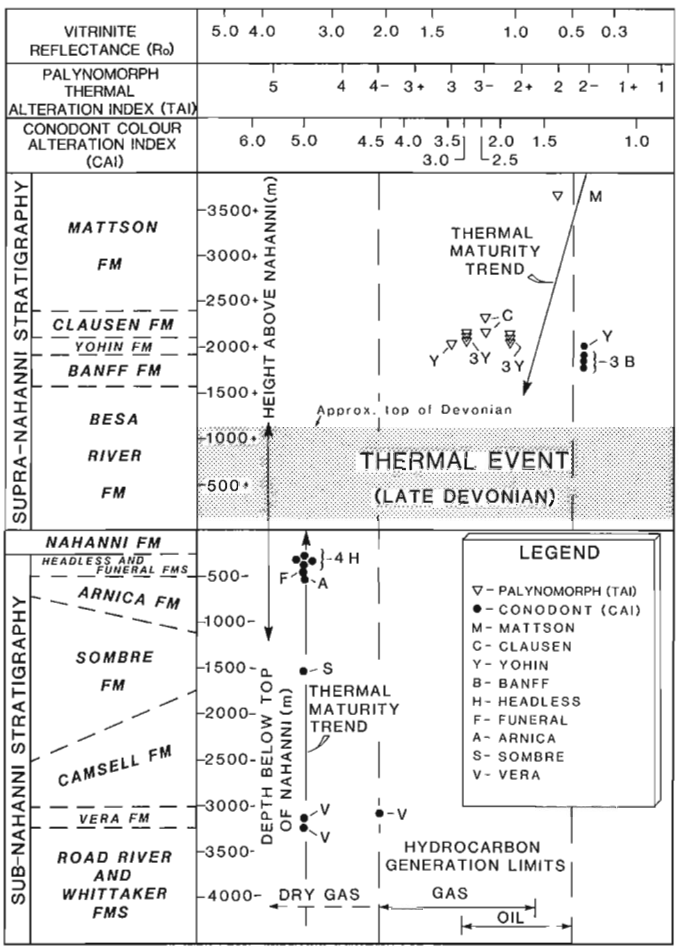

Figure 12. *Thermal maturation values plotted in terms of stratigraphic position. Results indicate uniformly high maturation values in Devonian strata below the Nahanni Formation. Above the Nahanni Formation the level of thermal maturation is much less. This abrupt decline in thermal maturity in Mississippian strata may be further evidence of a Late Devonian thermal event in northwestern Canada (Aulstead and Spencer, 1985; Morrow et al., 1986). The comparative thermal maturation scale calibrations for vitrinite reflectance (Ro), the palynomorph Thermal Alteration Index (TAI), and the conodont Colour Alteration Index (CAI), are derived from Utting (1987) and Utting et al. (1989).*

sedimentary sequences have undergone during their geological history.

Most commonly, thermal histories are related to the burial histories and the geothermal heat conduction gradients of the sedimentary sequences involved (e.g., Utting, 1987). Other sources of heat, such as local heat conduction near igneous intrusions, or the convective transfer of heat by the circulation of fluids in the subsurface, must also be considered in evaluating the thermal history of a particular sedimentary sequence.

The available data (Tables 3, 4) for thermal maturation indicators in the sedimentary sequence containing the Manetoe Facies, do not appear to conform to a normal burial thermal history dominated by the geothermal gradient. Conodont Colour Alteration Index data (CAI), derived from conodonts collected from a stratigraphic interval extending for 3300 m below the top of the Nahanni Formation, display a "flat" maturity trend with uniform values of 5.0 (Figs. 12, 13). At about 1900 m above the Nahanni, a closely spaced series of four conodont collections, from the Mississippian Yohin and Banff formations, have CAI values of 1.0 to 1.5. Palynomorph Thermal Alteration Index (TAI) values, derived from samples taken from the interval 2000 to 2300 m above the Nahanni, range from 2+ to 3. The one TAI value of 2 was determined from a sample collected from about 3700 m above the Nahanni. The thermal maturity of this palynomorph sample is slightly, but definitely, lower than the thermal maturity of the palynomorph samples from the underlying Yohin and Clausen formations. This may indicate that the thermal maturity of the sedimentary sequence above the Nahanni decreases progressively upward, in a manner consistent with a normal burial temperature regime dominated by a geothermal conduction gradient. Many more data are needed to validate this suggestion, but it is clear that there is an inflexion in the thermal maturation gradient, at the level representing uppermost Middle Devonian to Mississippian strata, that is consistent with a Late Devonian thermal event. Additionally, the flat thermal maturity trend for sub-Nahanni strata is consistent with the hypothesis that the Late Devonian thermal event involved the convective transfer of heat, from deep-seated crustal sources, by the circulation of basinal brines (see Aulstead and Spencer,

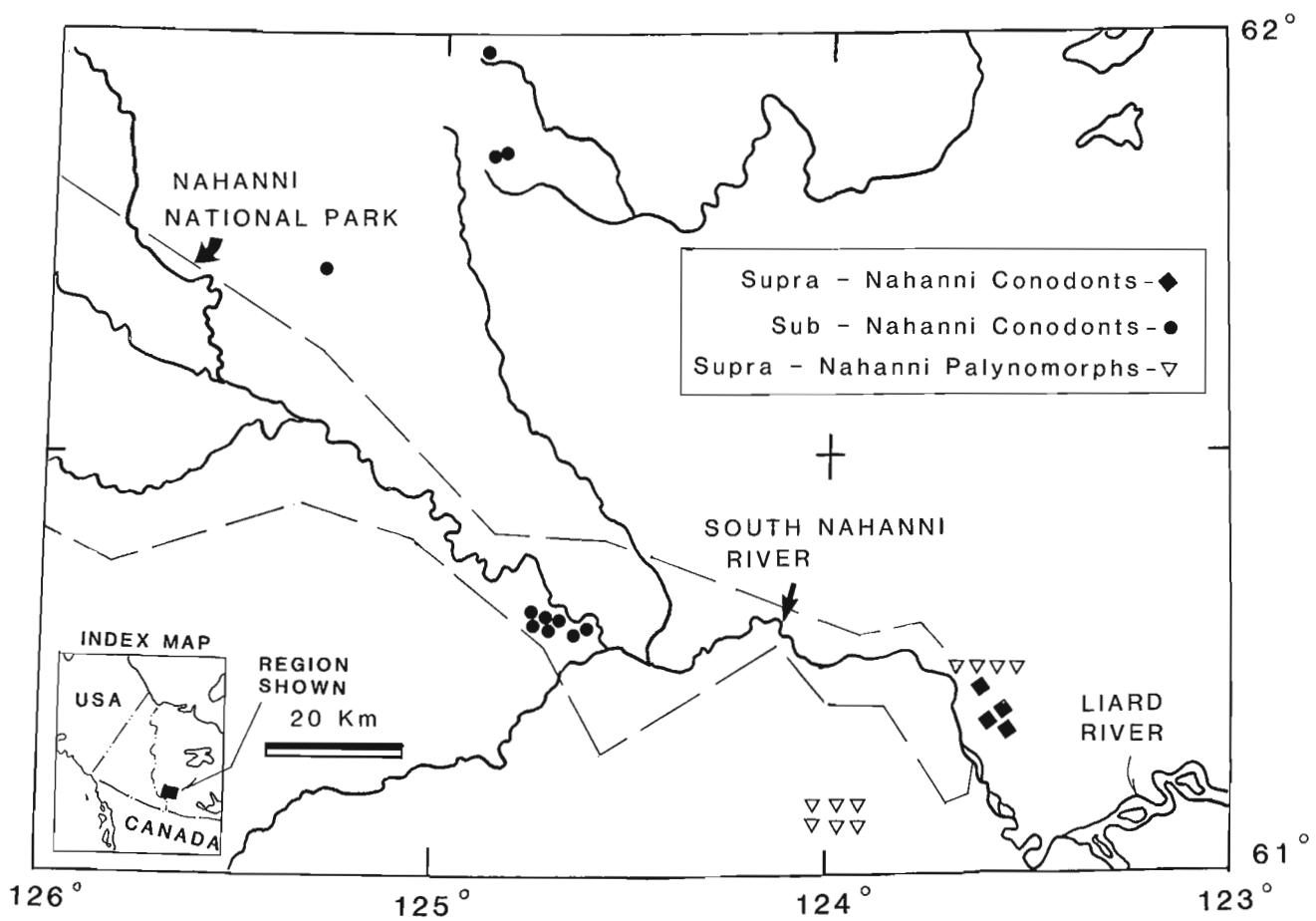

Figure 13. *Location map for conodont and palynomorph samples used to determine the thermal maturation levels plotted in Figure 12.*

TABLE 3

Paleontological thermal maturation data – conodont Colour Alteration Index (CAI)

Section – lat./long.	Formation – metres above base (below top)	GSC catalogue number	CAI	Metres above (below) Nahanni Fm
Bluefish Mountain[1]				
61°07′23″/123°29′13″	Banff (130 m)	C-47936	1-1.5	1884
	Banff (120 m)	C-58529	1-1.5	1894
	Banff (87 m)	C-52289	1-1.5	1927
Twisted Mountain[1]				
61°11′00″/123°37′38″	Yohin (129 m)	C-58994	1-1.5	2016
MTA-75-1				
61°52′00″/124°54′00″	Vera (top)	C-52606	4-5	(3090)
76-CW-80b				
61°55′15″/124°55′10″	Vera (base)	C-59499	5	(3200)
MTA-75-12				
61°18′00″/124°40′00″	Arnica 734 m	C-52837	5	(503)
	Headless 12 m	C-52844	5	(353)
MTA-75-20				
61°18′00″/124°42′00″	Arnica (27 m)	C-53029	5	(531)
	Funeral 29 m	C-53032	5	(475)
	Headless 1 m	C-53034	5	(344)
	Headless 8 m	C-53036	5	(337)
	Headless 25 m	C-53038	5	(320)
MTA-76-25				
61°43′00″/125°17′00″	Sombre 137 m	C-57792	5	(1528)
MTA-76-47				
61°53′00″/124°55′00″	Vera 36 m	C-60714	5	(3120)

[1]Samples supplied by B.C. Richards (Geological Survey of Canada).

TABLE 4

Paleontological thermal maturation data – palynomorph Thermal Alteration Index (TAI)[1]

Section – lat./long.	Formation – metres above base (below top)	GSC catalogue number	CAI	Metres above (below) Nahanni Fm
Twisted Mountain				
61°11′00″/123°27′38″	Yohin (50 m)	C-59008	2+ to 3–	2094
	Yohin (46 m)	C-59009	2+ to 3–	2098
	Yohin (6 m)	C-59014	2+ to 3–	2138
	Clausen 63 m	C-59021	3–	2206
Jackfish Gap				
61°05′54″/123°59′26″	Mattson 871 m	C-58810	2	3728
	Yohin (153 m)	C-58505	3	2028
	Yohin (64 m)	C-58503	3– to 3	2116
	Yohin (13 m)	C-58502	3– to 3	2167
	Yohin (1 m)	C-58501	3– to 3	2179
	Clausen 130 m	C-52180	3–	2310

[1]Samples supplied by B.C. Richards (Geological Survey of Canada).

1985). This type of heat dissipation would cause the development of a much "flatter" than normal geothermal gradient such that stratigraphically higher parts of the sequence would be heated to almost the same extent as lower parts of the sequence.

FLUID-INCLUSION DATA

Inclusions in dolomite

White, sparry dolomite cements contain two-phase aqueous liquid-vapour (LV) fluid inclusions that tend to be segregated into layers perpendicular to the growth directions of the crystals in the cement. In general, dolomite-cement crystals have clear, inclusion-free cores and cloudy rims with abundant inclusions (Aulstead, 1987). Typically, these inclusions are irregular to rectangular in outline, and are generally less than 20 μm in their longest dimension. These fluid inclusions contain normal shrinkage bubbles and thus may be considered to have preserved the original precipitational fluids. No hydrocarbons or daughter crystals were observed in dolomite fluid-inclusions.

Homogenization temperatures of inclusions in dolomite range from about 150°C to 220°C – based on 268 individual temperature measurements of Manetoe dolomite cements from five subsurface well cores and from one surface exposure near Ram Plateau (Fig. 14). The homogenization temperature distribution is the same for the Manetoe Facies at all these localities, regardless of its present depth of burial. This is also apparent in Figure 15, where the homogenization temperatures shown for inclusions in dolomite of the Manetoe Facies are the same at shallow depths in the subsurface of the Interior Plains (in the Berry F-71 and Ft. Simpson M-70 wells), and in the deeply buried Manetoe Facies in the mountain belt (in the Kotaneelee YT H-38 and Pointed Mountain A-55 wells).

Fluid inclusions in white, sparry dolomite show first or initial melting at temperatures between –58 and –53°C (Table 5). The temperature of first melting is an estimate of the eutectic temperature (Te) of a saline aqueous inclusion. The estimated eutectic temperature for Manetoe sparry dolomite indicates a complex solution composition, with dissolved NaCl, $MgCl_2$ and $CaCl_2$. The presence of a large proportion of dissolved $CaCl_2$ in these inclusions is indicated by a first melting temperature below –52.0°C (see Crawford, 1981).

Final melting temperatures (Tm), marking the disappearance of the solid phase, are deduced to have been between –14 and –29°C. The final melting temperature indicates the salinity of the fluid inclusion, and the salinity can be estimated from the relationship:

$$WS = 1.76958(*) - 4.2384 \times 10^2(*)^2 + 5.2778 \times 10^2(*)^3$$

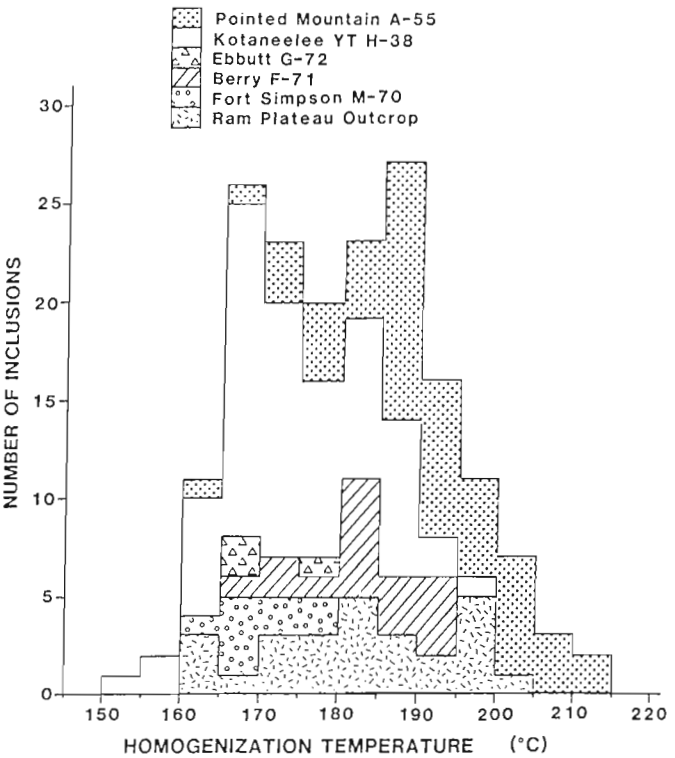

Figure 14. *Frequency plot of homogenization temperatures, based on two-phase, liquid-vapour, aqueous fluid inclusions in the Manetoe dolomite. Samples were obtained from six widely separated outcrop and subsurface localities (see Table 2). The temperature distribution is remarkably similar for Manetoe dolomite from all these localities. Well section depths (below KB) from which these data were obtained from the Manetoe Facies are as follows:*

Pointed Mountain A-55 well ..... 3114.4 m (10 218 ft); 3415.4 m (11 205.5 ft); and 3230.8 m (10 600 ft)
Kotaneelee YT H-38 well ..... 3571 m (11 715.9 ft) 3741 m (12 273.6 ft); and 3756 m (12 322.8 ft)
Fort Simpson M-70 well ..... 703.3 m (2307.5 ft)
Berry F-71 well ..... 706.2 m (2317 ft); 709.9 m (2329 ft); 710.8 m (2332 ft); and 720.5 m (2364 ft)
Ebbutt G-72 well ..... 786.1 m (2579 ft)

where:

WS = the equivalent weight per cent (eq. wt. %) NaCl
* = the freezing point depression in °C (Potter et al., 1978).

This indicates that the inclusion salinities ranged from about 15 to 29 eq. wt. % NaCl.

TABLE 5

Summary of freezing data for fluid inclusions in dolomite cements from the Manetoe Facies[1]

Locality, and sample location	{Number} and range of initial melting temperatures (°C)	{Number} and range of final melting temperatures (°C)
Kotaneelee YT H-38		
3739 m/12 267 ft[2]	{16} –58.0 to –53.4	{16} –28.8 to –19.3
3754 m/12 315 ft	{12} –58.9 to –55.4	{12} –29.4 to –26.5
Pointed Mountain A-55		
3231 m/10 600 ft	{12} –57.8 to –53.1	{12} –25.7 to –15.1
3415 m/11 205.5 ft	{14} –58.0 to –53.6	{14} –23.8 to –19.4
Berry F-71		
706.2 m/2 317 ft	{6} –58.3 to –56.1	{6} –23.3 to –19.9
710 m/2 329 ft	{10} –58.5 to –57.0	{10} –26.5 to –24.1
720.5 m/2 364 ft	{4} –58.1 to –56.3	{6} –19.1 to –18.3
710.8 m/2 332 ft	{7} –57.9 to –54.6	{7} –22.11 to –20.2
Ebbutt G-62		
786 m/2 579 ft	{3} –57.8 to –54.4	{3} –23.0 to –21.9
Ram Plateau outcrop		
R6a[3]-Headless Fm	{12} –58.0 to –55.3	{12} –22.3 to –20.7
R7b-Nahanni Fm	{10} –58.2 to –54.1	{6} –21.0 to –19.6
R7c-Nahanni Fm	{7} –58.3 to –54.5	{5} –15.7 to –14.2
R8b-Nahanni Fm	{6} –58.1 to –57.1	{6} –23.2 to –21.6

[1]Data from Aulstead (1987).
[2]Below KB.
[3]Field sample numbers (Aulstead).

TABLE 6

Summary of freezing data for fluid inclusions in calcite cements from the Manetoe Facies[1]

Locality, and sample location (m and ft below KB)	{Number} and range of initial melting temperatures (°C)	{Number} and range of final melting temperatures (°C)
Kotaneelee YT H-38		
3897.5 m/12 787 ft	{2} –57.9 to –55.6	{2} –11.5 to –9.8
Pointed Mountain A-55		
3154.5 m/10 349.5 ft	{10} –56.1 to –53.0	{10} –15.7 to –12.5
Fort Simpson M-70		
699.5 m/2 295 ft	{12} –57.6 to –54.5	{12} –17.0 to –10.0
700.1 m/2 297 ft	{8} –57.8 to –54.1	{8} –14.2 to –14.0
Berry F-71		
720.5 m/2 364 ft	{15} –58.1 to –54.5	{17} –16.2 to –10.5
Root River I-60		
1080 m/3 543 ft	{15} –57.9 to –53.9	{12} –14.5 to –11.7
Cli Lake M-05		
1483.3 m/4 866.5 ft	{12} –44.7 to –41.7	{12} –10.1 to –10.0
La Biche F-08		
1988.7 m/6 524.5 ft[2]	{8} –27.5 to –22.7	{6} –1.4 to –0.7
2046 m/6 713 ft	{11} –27.0 to –23.0	{11} –1.6 to –1.1
Beaver River YT G-01		
4176.4 m/13 702 ft	{24} –57.9 to –53.2	{24} –13.8 to –10.6
4395.5 m/14 421 ft	{10} –57.9 to –53.2	{10} –15.1 to –12.6

[1]Data from Aulstead (1987).
[2]Calcite cement in Nahanni Formation above Manetoe Facies.

Inclusions in calcite

Almost all Manetoe Facies calcite cements examined contain aqueous two-phase LV fluid inclusions with a normal shrinkage bubble. Inclusions in calcite are larger and more regularly shaped than those in dolomite. Homogenization temperatures for inclusions in calcite range from 110° to 190°C (Fig. 16). There is a definite segregation of homogenization temperatures with respect to location. Homogenization temperatures of inclusions from Manetoe Facies calcites in deeply buried sequences (as in the Pointed Mountain A-55, Kotaneelee YT H-38, and Beaver River YT G-01 wells) are much higher than homogenization temperatures from Manetoe calcites in the shallow subsurface (as in the Berry F-71, Ft. Simpson M-70, and Raven F-73 wells) east of the mountain front (Figs. 15, 16).

Analysis reveals that most fluid inclusions in calcite had first or initial melting temperatures between –58 and –52°C, and final melting temperatures between –10 and –17°C (Table 6). This indicates the presence of a complex salt mixture containing $CaCl_2$, with salinities of about 13 to 20 eq. wt. % NaCl. Some inclusions are markedly less saline, such as those in calcite from the La Biche F-08 well. A few multiphase inclusions, in calcite from the Manetoe Facies in the Ft. Simpson M-70 well, contain fluorescent hydrocarbons (see Aulstead, 1987).

Inclusions in quartz

Quartz cements in the Manetoe Facies contain complex multiphase inclusions, consisting of two or three liquids and solids as well as simple two-phase LV inclusions. Most inclusions are more than 50 μm in their longest dimension and are either irregularly shaped or are negative crystals. Most inclusions are primary, like the inclusions in the dolomite and calcite. Some secondary inclusions, which occur along healed intracrystal fractures, visible in cores from the Kotaneelee YT H-38 well, were also examined. Homogenization temperatures of two-phase inclusions range from 160 to 210°C for primary inclusions, and from 210 to 235°C for secondary inclusions, for a total temperature range of 160 to 235°C (Fig. 17). The more complex multiphase inclusions have homogenization temperatures within the range of primary inclusions. As in the case of the inclusions in calcite, homogenization temperatures for the inclusions in quartz are strongly dependent on present location and depth of burial. Inclusions in quartz from the deeply buried Manetoe Facies in the Kotaneelee YT H-38 well have much higher homogenization temperatures than inclusions in Manetoe quartz from the shallow subsurface in the Berry F-71 and Ft. Simpson M-70 wells (Figs. 15, 17).

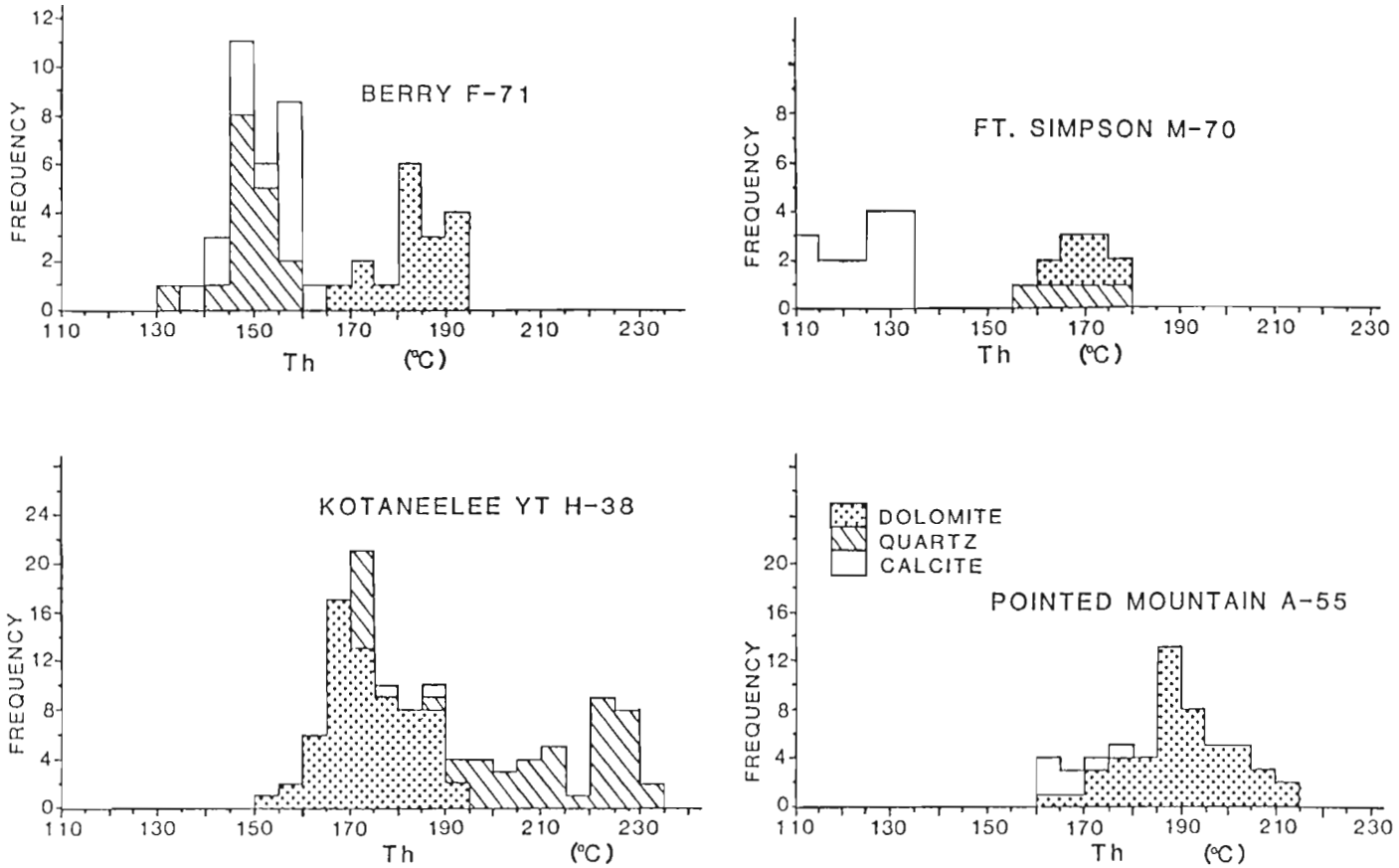

Figure 15. *A comparison of the fluid-inclusion homogenization temperatures for Manetoe dolomite, calcite, and quartz from four wells (see Table 2). Samples from two of these wells, Berry F-71 and Ft. Simpson M-70, are from the shallow subsurface in the Interior Plains east of the Mackenzie Mountains, where the Manetoe Facies is presently less than 1000 m below the surface, and was never deeply buried. In contrast, the Manetoe Facies is deeply buried, more than 3000 m below the surface, in the Kotaneelee and Pointed Mountain wells. Calcite and quartz homogenization temperatures are distinctly lower in the less deeply buried Manetoe. The present depths from which these analyzed samples were obtained, are cited in Figures 14, 16, and 17.*

The two-phase LV inclusions display first melting at -58.7 to –51.0°C and final melting between –18.6 and –1.0°C (Table 7). These characteristics indicate that they are complex saline-inclusion solutions, which include a significant proportion of $CaCl_2$. Salinities of these solutions vary widely from about 1.5 to 20 eq. wt. % NaCl. Inclusions in calcite and quartz, where these two minerals are intergrown, tend to be very similar in composition and salinity and tend to be more saline than is the case when these minerals occur separately (Aulstead, 1987). The multiphase inclusions have a more complex freezing behaviour. Final melting temperatures in the vicinity of 13°C indicate the probable presence of mixtures of CH_4 and CO_2 as clathrates, which melt at temperatures above 10°C (Aulstead, op. cit.).

TABLE 7

Summary of freezing data for fluid inclusions in quartz from the Manetoe Facies[1]

Locality, and sample location (m and ft below KB)	{Number} and range of initial melting temperatures (°C)	{Number} and range of final melting temperatures (°C)
Kotaneelee YT H-38		
3569 m/11 709 ft	{8} <–40.0	{8} –3.9 to –3.2
3569 m/11 709 ft[2]	{8} <–40.0	{8} –2.8 to –1.9
3739 m/12 267 ft	{6} <–40.0	{6} –6.6 to –7.0
3739 m/12 267 ft[2]	{8} <–40.0	{8} –2.6 to –1.0
Fort Simpson M-70		
697 m/2 287 ft	{8} –55.7 to –51.0	{9} –6.9 to –5.4
Berry F-71		
720.5 m/2 364 ft	{14} –58.7 to –55.4	{13} –18.6 to –15.1

[1]Data from Aulstead (1987).
[2]Secondary inclusions.

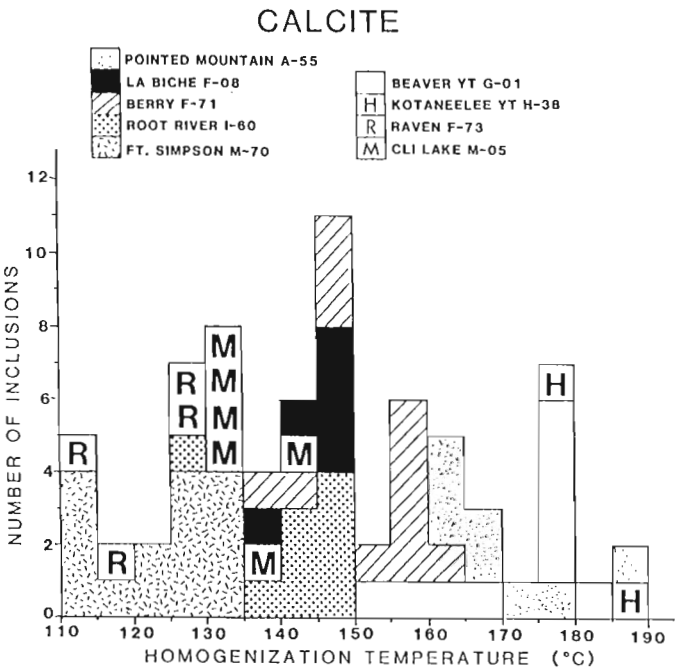

Figure 16. *Frequency plot of homogenization temperatures for fluid inclusions in calcite cements associated with the Manetoe Facies. Inclusions in samples from more deeply buried sections – as in the Pointed Mountain A-55 well – reveal much higher homogenization temperatures than those in samples from near surface sections that were never deeply buried – as in the Ft. Simpson M-70 well, located in the Interior Plains east of the Mackenzie Mountains. Depths (below KB) and wells from which these subsurface calcite samples were taken, are as follows:*

Pointed Mountain A-55 well.....3154.5 m (10 349.5 ft)
Fort Simpson M-70 well.....699.5 m (2295 ft); and 700 m (2297 ft)
Kotaneelee YT H-38 well.....3900 m (12 795 ft)
Berry F-71 well.....720.5 m (2364 ft)
Root River I-60 well.....1080 m (3543 ft)
Cli Lake M-05 well.....1483.3 m (4866.5 ft)
La Biche F-08 well.....1988.7 m (6524.5 ft); and 2046 m (6713 ft)
Beaver YT G-01 well.....4176.4 m (13 702 ft); and 4395.5 m (14 421 ft)

STABLE-ISOTOPE DATA AND CHEMISTRY

The oxygen isotope composition of Manetoe dolomite ranges from –17.33 to –6.25 with a mean value of –11.3 (Table 8; Appendices 1, 2, 4). These values are lower than almost all those previously reported for dolomite (including sparry dolomite) associated with sedimentary rocks (e.g., Land, 1980) (Fig. 19). Dolomites associated with high-temperature ore deposits can of course have $\delta^{18}O$ values that are much lower (Mattes and Mountjoy, 1980) than these. The carbon isotope composition ($\delta^{13}C$) of the Manetoe dolomite is less extreme and ranges from –5.05 to +1.10, with a mean value of –1.45 (Table 8; Appendices 1, 2, 4). This is within the range for carbon isotopes in published analyses of ancient dolomites (Land, 1980), but toward the lower end of that range.

White, sparry dolomite and grey, host dolomite have significantly different $\delta^{18}O$ and $\delta^{13}C$ contents, although there are insignificant differences between the mean values for all outcrop versus all subsurface dolomites, and between those of sparry dolomite from outcrop versus that from the subsurface, as determined by the application of the Student's "t" test (Table 8). White dolomite contains less of the heavier ^{18}O and ^{13}C isotopes in almost all pairs of analyses from individual samples (Appendices 1, 2). This is consistent with the interpretation that the white, cavity-filling dolomites received a greater contribution of carbon and oxygen isotopes from the dolomitizing solution.

A plot of carbon and oxygen isotope data shows that analyses from the Manetoe Facies fall along an approximately linear trend (Fig. 18). Previously published data for coarsely crystalline dolomites of the Presqu'île Facies (Fritz and Jackson, 1972) appear to show a continuation of this trend (Fig. 18). This is consistent with the physical continuity of these dolomites, and in itself implies that they had a common origin.

Isotope data for sparry calcites associated with the Manetoe Facies fall at the lighter end of the trend in isotopic compositions and display much more "scatter" than the same data for the dolomite. Some calcite cements are extremely depleted in both ^{18}O and ^{13}C (Fig. 18; Appendix 5). The few samples of limestone from the Landry and Nahanni formations that have been analyzed, reveal varied $\delta^{18}O$ and $\delta^{13}C$ values that do not fall along the dolomite trend.

If it is assumed that the Manetoe dolomite was precipitated from residual brines originating in Elk Point Basin strata, and derived from the evaporation of seawater (Morrow et al., 1986; Aulstead, 1987; Spencer, 1987), then it is possible to deduce the ^{18}O ‰ of these brines, if it is assumed that the ^{18}O ‰ value of Devonian seawater was several units per mil less than that of modern ocean water (Popp et al., 1986). Evaporation of seawater in modern evaporative sabkhas is enriched by +3 to +4 ‰ $\delta^{18}O$ relative to standard mean ocean water (SMOW) at 0 ‰ (Lloyd, 1966). This may be taken to indicate that the residual Elk Point brines that precipitated the Manetoe dolomites had an $\delta^{18}O$ ‰ value of about 0 ‰.

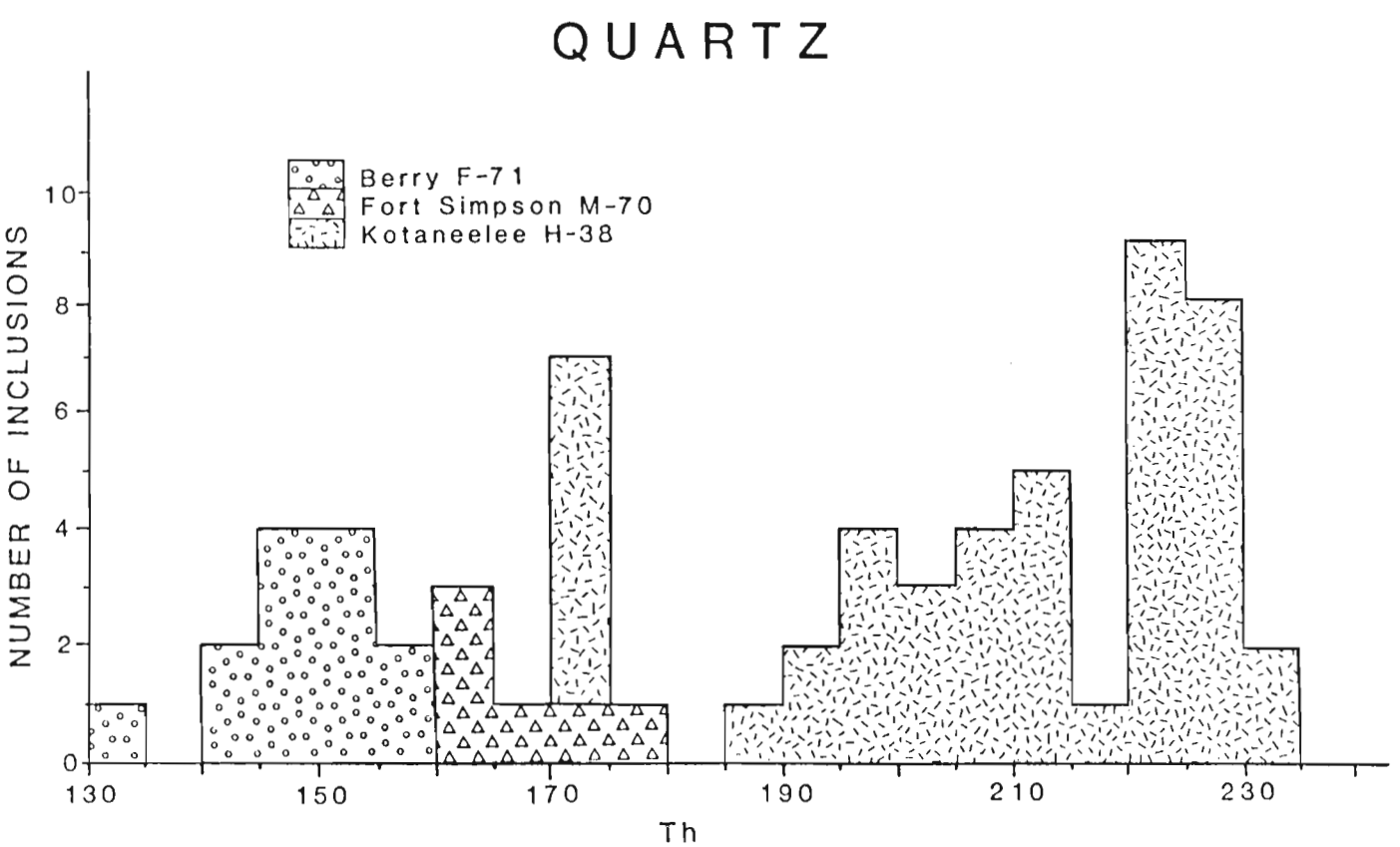

Figure 17. *Frequency plot of homogenization temperatures for fluid inclusions in quartz cements associated with the Manetoe Facies. As with the inclusions in calcite, there is a strong correlation between burial depth and homogenization temperature. Depths (below KB) and wells from which these subsurface quartz samples were taken, are as follows:*

Kotaneelee YT H-38 well ..... 3571 m (11 709 ft); and 3756 m (12 315 ft)
Ft. Simpson M-70 well ..... 698 m (2287 ft)
Berry F-71 well ..... 721 m (2364 ft)

TABLE 8

Summary and comparison of stable isotope data from white, void-filling dolomite and grey, replacement dolomite

Sample type[1]	Number of samples	Oxygen ($\delta^{18}O$)– mean (standard deviation)	Carbon ($\delta^{13}C$)– mean (standard deviation)
All samples	115	–11.308 (1.958)	–1.447 (0.960)
White dolomite (all)	51	–12.077 (1.524)	–1.825 (0.974)
Grey dolomite (all)	57	–10.712 (1.533)	–1.078 (0.749)
Outcrop dolomite (all)	33	–11.128 (2.366)	–0.964 (0.839)
Subsurface dolomite (all)	75	–11.457 (1.254)	–1.645 (0.915)
Outcrop white dolomite	15	–12.144 (2.236)	–1.342 (0.730)
Subsurface white dolomite	36	–12.049 (1.147)	–2.026 (0.993)

[1]All data are from Appendices 1 and 2.

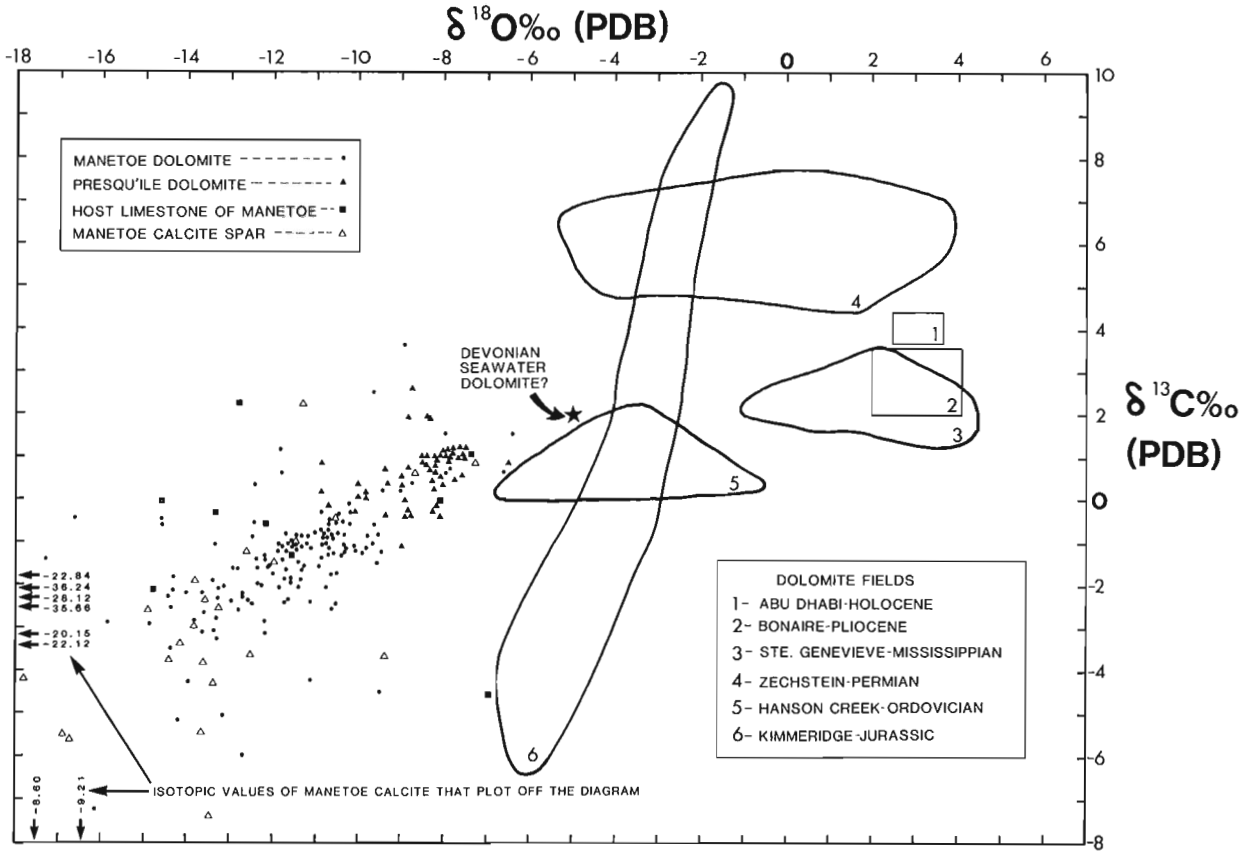

Figure 18. *Oxygen and carbon isotope data for dolomite and calcite of the Manetoe Facies (Appendices 1-3). Previously published data relating to isotopes in the Presqu'île dolomites (Fritz and Jackson, 1972) are also shown. The collinear and continuous trend of Manetoe and Presqu'île isotope data is consistent with the interpretation that these dolomites are in fact a single mass of diagenetic dolomite. For comparison, generalized fields are included, showing the distribution of isotope data from previously published studies of dolomite units inferred to have formed in low temperature, near surface environments at various periods (Patterson, 1972; Irwin et al., 1977; Choquette and Steinen, 1980; Clark, 1980; Dunham and Olson, 1980; Irwin, 1980). The Presqu'île and particularly the Manetoe dolomites display much lower ^{18}O contents than these low temperature dolomites. The plotted position of the inferred isotopic composition of dolomite in Devonian seawater is derived from James and Choquette (1983), based on the assumption that "Devonian seawater" dolomite would have an isotopic composition similar to that of unaltered Devonian marine calcite (see also Popp et al., 1986). The extremely 'light' ^{18}O ‰ values of many calcite cements may reflect an admixture of ^{18}O-depleted meteoric groundwater.*

Using the equation of Northrop and Clayton (1966) for oxygen isotopic fractionation between dolomite and aqueous solutions, it is possible to make an independent estimate of the temperature at which the Manetoe dolomites precipitated from solution (Fig. 19). The range of fluid-inclusion homogenization temperatures for Manetoe dolomite cements falls entirely within the temperature range (110° to 210°C) inferred from their oxygen isotope compositions (Fig. 19). Similarly, the published range of fluid-inclusion homogenization temperatures (Roedder, 1968) for Presqu'île dolomite cements from Pine Point, N.W.T., falls within the temperature range predicted from their isotopic composition (Fig. 19). Unfortunately, only three published homogenization temperatures for Presqu'île dolomites are available (Roedder, op. cit.). In spite of this limitation, however, it is possible to assert that the Presqu'île dolomites also were precipitated from residual Elk Point brines, on the basis of fluid-inclusion and isotopic evidence.

The average spacing of the d_{104} peak for all Manetoe dolomites is about 2.890 nm, indicating a mean content of 50 to 51 mole per cent $CaCO_3$ (Appendices 1, 2). This dolomite is very stoichiometric with respect to its $CaCO_3$ content compared to most dolomites (Lumsden and Chimahusky, 1980; Morrow, 1982b). The white, cavity-filling sparry dolomite has a slightly lower mean d_{104} spacing (2.889 nm) than the grey dolomite (2.891 nm), indicating that the former is slightly more stoichiometric. The mole per cent $CaCO_3$

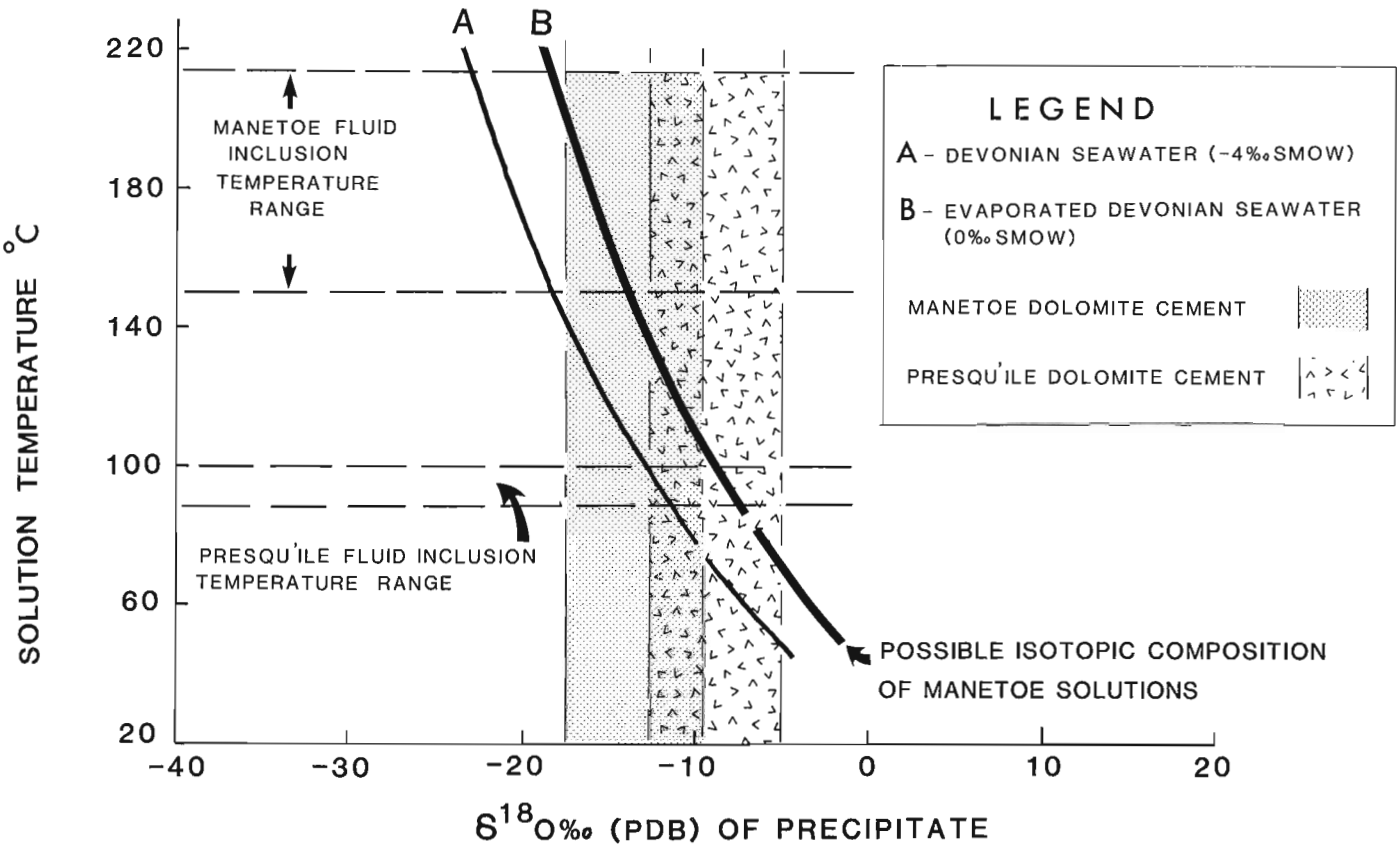

Figure 19. *Relationship between the temperature of precipitation of Manetoe dolomite and the $\delta^{18}O$ ‰ content of the precipitate. The analysis is based on the following equation from Northrop and Clayton (1966):*

$10^3 ln\alpha = 3.20(10^6 T^{-2}) - 1.50$

where 'α' is the oxygen isotopic fractionation factor between dolomite and aqueous solution.

Devonian seawater is assumed to have been depleted in ^{18}O with respect to standard mean ocean water (Popp et al., 1986). Curve 'A' illustrates the composition of dolomites that could be expected to have precipitated from unmodified Devonian seawater. Curve 'B' illustrates a case in which the ^{18}O content of Devonian seawater was increased by evaporation, as in the case of the brines generated during evaporation in the Elk Point Basin. There is a strong similarity between the isotopic compositions of the Manetoe and Presqu'île dolomite cements, their fluid-inclusion homogenization temperatures, and the inferred isotopic composition of the Elk Point residual brines from which these dolomites may have been precipitated.

content of Manetoe dolomites falls within the range of variation of the mole per cent $CaCO_3$ composition of Presqu'île dolomites, although the mean mole per cent $CaCO_3$ of Manetoe dolomite is somewhat less than that of Presqu'île dolomite (Fritz and Jackson, 1972). The degree of cation order in Manetoe dolomites, based on peak height ratios (0.40 to 0.55; Appendices 1, 2), is similar to that of many ancient dolomites, but is unlike dolomites forming in modern settings, as these are characterized by only a small degree of cation ordering as inferred from their peak ratios of less than 0.4 (e.g., Patterson, 1972).

The concentrations of minor and trace elements in Manetoe dolomite are very low (Appendix 3), a characteristic consistent with its high degree of major-element stoichiometry and its degree of cation order. Perhaps surprisingly, even the most abundant minor element, iron (Fe), is present in concentrations of less than 0.5 mole per cent (Table 9), and all other elements analyzed (Mn, Sr, Zn, Ca, Ba) are present in concentrations of less than a few hundred parts per million (Table 9). However, the bulk sample concentrations are well within the range of concentrations exhibited by ancient dolostones for elements such as Fe, Mn, and Sr (e.g., Mattes and Mountjoy,

TABLE 9

Iron, manganese, and strontium content (ppm) in Manetoe Facies dolomite – summary statistics

	Number of samples (n)	Mean ($\bar{x}$) (in ppm)	Standard deviation (σ) (in ppm)	
	39	415.4	488.2	All samples
Iron	16	227.3	225.2	White dolomite
(Fe)	23	543.5	579.0	Grey dolomite
	39	213.6	84.9	All samples
Manganese	16	237.4	99.6	White dolomite
(Mn)	23	197.0	70.6	Grey dolomite
	39	60.5	19.8	All samples
Strontium	16	63.2	27.6	White dolomite
(Sr)	23	55.6	16.9	Grey dolomite

1980). Radke and Mathis (1980) documented systematic intracrystal variations in the Ca^{2+}, Fe^{2+}, and Mn^{2+} concentrations, in the order of 1 to 6 mole per cent, across the curved crystal faces of white, sparry "saddle" dolomites from various localities. Systematic variations of this magnitude in Fe and Mn content are not possible within crystals of Manetoe dolomite, because of the low bulk concentrations of these elements, and are improbable for Ca as well because of the very uniform mole per cent $CaCO_3$ content of all Manetoe dolomites and their high degree of cation order. Some intracrystal variations in Fe and Mn content may be inferred for Manetoe dolomites, because of the presence of alternating luminescent and nonluminescent intracrystal growth bands in a single sample (e.g., Choquette and Steinen, 1980).

Only with respect to iron (Fe) is there a recognizable distinction between white and grey dolomite; white dolomite containing less iron than grey dolomite. Iron concentrations are extremely variable overall, however, whereas other elements (e.g., Mn, Sr) are much more constant in concentration (Table 9). More analyses are needed in order to develop statistically valid inferences concerning variations in element concentration within Manetoe dolomite. Compared to most dolomites, however, which contain many times more iron than manganese (e.g., Mattes and Mountjoy, 1980; Veizer et al., 1978), the manganese content of Manetoe dolomites is high relative to iron content.

STRONTIUM ISOTOPE DATA

Strontium isotope ($^{87}Sr/^{86}Sr$) contents were determined for 14 samples of Manetoe dolomite and associated carbonates (Table 10). The strontium isotope ratios for white, coarsely crystalline, dolomite cement samples of the Manetoe Facies range from 0.70906 to 0.71282. Samples of Manetoe replacement dolomite that had definitely replaced pre-existing limestone or dolomite have slightly lower strontium isotope ratios than the cavity-filling dolomite cements (Table 10; Fig. 20).

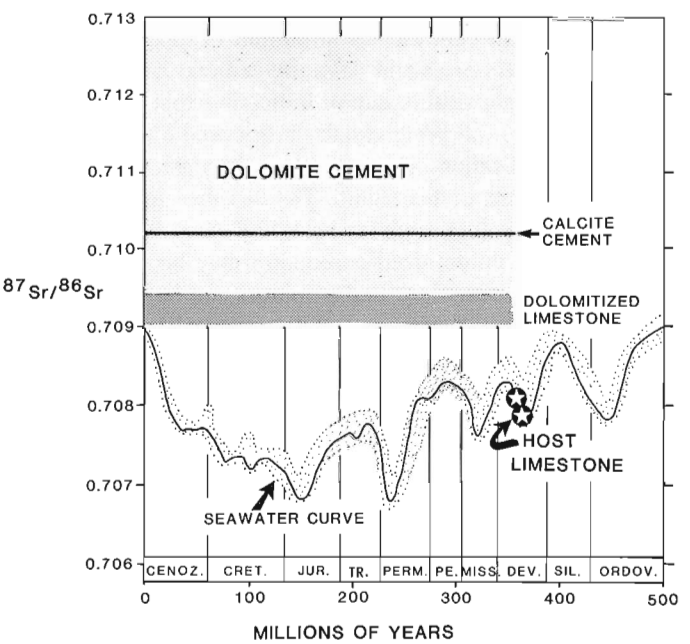

Figure 20. *The strontium isotope content of Manetoe dolomites, calcite cements associated with the Manetoe Facies, and unaltered limestones from the Nahanni and Landry formations (the main host units that contain the Manetoe Facies). Also shown is the seawater curve of Burke et al. (1982), which follows the secular variation of the $^{87}Sr/^{86}Sr$ ratio of marine carbonates throughout the Phanerozoic. Strontium isotope ratios from samples of undolomitized host limestones of the Manetoe Facies plot directly on this curve at a Devonian age of deposition. In contrast, the strontium isotope content of Manetoe dolomite cements and dolomite plot far above the seawater curve, indicating that radiogenic ^{87}Sr was preferentially introduced during diagenesis. This may have occurred following the albitization of feldspar minerals in basement crustal rocks during reactions with residual Elk Point brines (Spencer, 1987).*

Samples of host limestone from the Landry and Nahanni formations have much lower strontium isotope ratios than either the dolomite cements or the replacement dolomites. Calcite cements in two samples associated with the Manetoe Facies were found to have strontium isotope ratios similar to those of the dolomite cements (Fig. 20), but one of these samples had a strontium isotope ratio greater than any of the dolomite cement samples (Table 10).

Burke et al. (1982) plotted the variation of strontium isotopes for unaltered marine carbonates throughout the Phanerozoic, and derived a curve illustrating the secular variation of strontium isotope ratios. The strontium isotope ratios for limestone samples from the Lower and Middle Devonian Landry and Nahanni formations fall directly on this curve, indicating that these limestones retain the isotopic signature of Devonian seawater and have not been affected by later diagenesis (Fig. 20). In contrast, the strontium isotope ratios of the dolomitized carbonates and dolomite cements of the Manetoe Facies lie far above this curve, indicating that "radiogenic" strontium (^{87}Sr) was preferentially introduced into these rocks during dolomitization. The calcite cements are similar to the dolomite cements in this regard. The fact that, in the Manetoe Facies, the dolomite cements have higher strontium isotope ratios than the dolomitized carbonates may be related to the probability that strontium in the dolomitized host rock results from the mixing of strontium of the original limestone with the more "radiogenic" strontium of the dolomitizing fluids. In contrast, the dolomite cements contain only the ^{87}Sr-rich strontium from the dolomitizing solutions, so that this type of strontium is present in greater proportion.

Solutions with strontium isotope ratios in excess of 0.710 can develop through the interaction of subsurface fluids with shales or fine grained siliciclastic rocks. Typically, shales are characterized by strontium isotope ratios greater than 0.710 (Perry and Turekian, 1974) and are, therefore, likely to contribute radiogenic strontium to diagenetic fluids (Steuber et al., 1984). The deep sialic continental crust itself is characterized by high strontium isotope ratios, primarily because of the high original rubidium content of feldspar and micaceous minerals in these granitic, igneous, and metamorphic rocks. For example, waters in lakes and rivers draining the Canadian Precambrian Shield have strontium isotope ratios of 0.712 to 0.726 (Faure et al., 1963). Diagenetic solutions with these isotopic compositions could have precipitated dolomites with the elevated strontium isotope ratios that are characteristic of the Manetoe dolomite.

LEAD ISOTOPE DATA AND INTERPRETATION

As described above, lead-zinc mineralization, associated with that part of the Manetoe Facies developed in the uppermost part of the Nahanni Formation, is the final clearly defined diagenetic event that occurred in these strata. Lead isotope data were obtained for lead in galena samples from this mineralization, as well as from galena that occurs in a similar stratigraphic setting, but in regions beyond the area in which the Manetoe Facies is developed (Fig. 21; Table 11). Analyses of many of these galena samples have been reported previously (Kirker, 1982; Morrow and Cumming, 1982), but additional samples have been obtained and analyzed, and several of the earlier analyses have been repeated with improved precision. In addition, a slight bias in the remaining earlier measurements has been removed so that all data are directly comparable (Table 12).

It has been noted above that the isotopic compositions of lead samples from lower Paleozoic, post-Cambrian, carbonate-hosted, zinc-lead deposits in the northern Cordillera are radiogenic and fall far above the growth curve for common lead (Godwin et al., 1981, 1982; Morrow and Cumming, 1982) (Fig. 21). The data plot as nearly linear on lead/lead diagrams and these have been interpreted either as secondary isochrons, reflecting a simple two-stage lead evolution (Godwin et al., 1982), or as tertiary isochrons reflecting a more complex multistage lead evolution (Morrow and Cumming, 1982).

The improved data available for this study have permitted us to alter and refine our earlier interpretations. Previously, we hypothesized that the isotopic composition of these carbonate-hosted leads formed a set of four parallel linear arrays on lead/lead diagrams (Figure 4 of Morrow and Cumming, 1982). The more precise measurements and more comprehensive data of this study now suggest a different interpretation. Three of the sets of data from individual deposits (or groups of related deposits) define linear arrays that diverge slightly (Table 13, A; Fig. 21). The fourth data set has too little variation to define the slope without ambiguity. The three well defined linear arrays intersect the Stacey and Kramers (1975) growth curve between the 1800 and 2000 Ma points (Table 13; Fig. 21). The time of lead mobilization indicated is very close to that deduced by Godwin and Sinclair (1981) to account for the isotopic composition of shale-hosted lead-zinc deposits in this area. Our data for carbonate-hosted deposits indicate a similar mobilization event. Therefore, we constrained the linear regressions for our data so that the trend lines pass through the point on the Stacey and Kramers (op.cit.) growth curve corresponding to 1887 Ma, the time deduced by Godwin and Sinclair (op. cit.). This revision resulted in the slopes indicated in Table 13 (B) and shown in Figure 21.

The interpretation of these divergent linear arrays as a set of unrelated two-stage secondary isochrons appears to be precluded, as this implies that mineralization of isotopic group "d" from the Rusty Springs deposit (Tables 11, 13) occurred within only the past few million years – based on the upper intersection of the "d" group linear with the Stacey and

TABLE 10

Strontium isotope ($^{87}Sr/^{86}Sr$) content of selected samples of Manetoe dolomite and associated limestone

Well name or section and location[1]	GSC locality number	Sample description	$^{87}Sr/^{86}Sr$[2]
Root River I-60 864.3 m below KB	–	Host limestone, Nahanni Fm	0.70789
La Biche F-08 1389.2 m	–	White calcite cement, Nahanni Fm	0.72389
Berry F-71 710 m	–	Calcite cement, Manetoe Facies	0.71181
Berry F-71 710 m	–	Dolomite cement, Manetoe Facies	0.70960
Willowlake G-47 584.9 m	–	Dolomite cement, Manetoe Facies	0.71282
Kotaneelee YT H-38 3887.2 m	–	Dolomite cement, Manetoe Facies	0.71009
Kotaneelee YT H-38 3891 m	–	Replacement dolomite, Manetoe Facies	0.70907
Section 2 (322 m) above base	C-53019	Manetoe dolomite cement, Landry Fm	0.71038
Section 2 (379 m)	C-53022	Manetoe replacement dolomite, Landry Fm	0.70906
Section 6 (310 m)	C-52898	Pelletal lime mudstone, Landry Fm	0.70802
Section 6 (362 m)	C-52902	Manetoe replacement dolomite, Landry Fm	0.70918
Section 20 (1143 m)	C-59333	Manetoe dolomite cement, Sombre Fm	0.70952
Section 20 (532 m)	C-59319	Manetoe dolomite cement, Sombre Fm	0.70947
Section 26 (992 m)	C-59225	Manetoe dolomite cement, Arnica Fm	0.70945

[1]Well data from Aulstead (1987).
[2]Average precision is +/– $3*10^{-5}$.

TABLE 11

Zinc-lead deposits, host carbonates, and associated shales

Deposit (isotopic group)	Host carbonate formation and age	Associated shale formation and age
Mount McCusker (a)	Muncho-McConnell, Late Silurian to Early Devonian	Road River, Early Devonian
Mount Burden (a)	Stone, Early Devonian (Emsian)	Road River, Early Devonian
Poco Prospect (a)	Stone and lower Dunedin, Early Devonian (Emsian)	(?)Road River, Early Devonian
Richards Creek (a)	Stone and lower Dunedin, Early Devonian (Emsian)	(?)Road River, Early Devonian
Kotaneelee (b)	Upper Nahanni, Early Devonian (Eifelian)	Horn River, Middle Devonian
Robb Lake (c)	Upper Stone and lower Dunedin, Early Devonian (Eifelian, Emsian)	Besa River, Late Devonian (Frasnian)[1]
Rusty Springs (a)	Upper Ogilvie, Early Devonian (Emsian)	Hart River, Early Carboniferous

[1]GSC conodont collection (C-079362) – early Late Devonian, early Frasnian; Lower *dengleri* Subzone to Lower *asymmetricus* Zone, 18.6 m (61 ft) above the base of the Besa River Formation; fossil identifications by T.T. Uyeno (Geological Survey of Canada, ISPG, Calgary).

a = A group of small mineral showings in northeastern British Columbia.
b = Galena occurrences in the Manetoe Facies.
c = Robb Lake deposit.

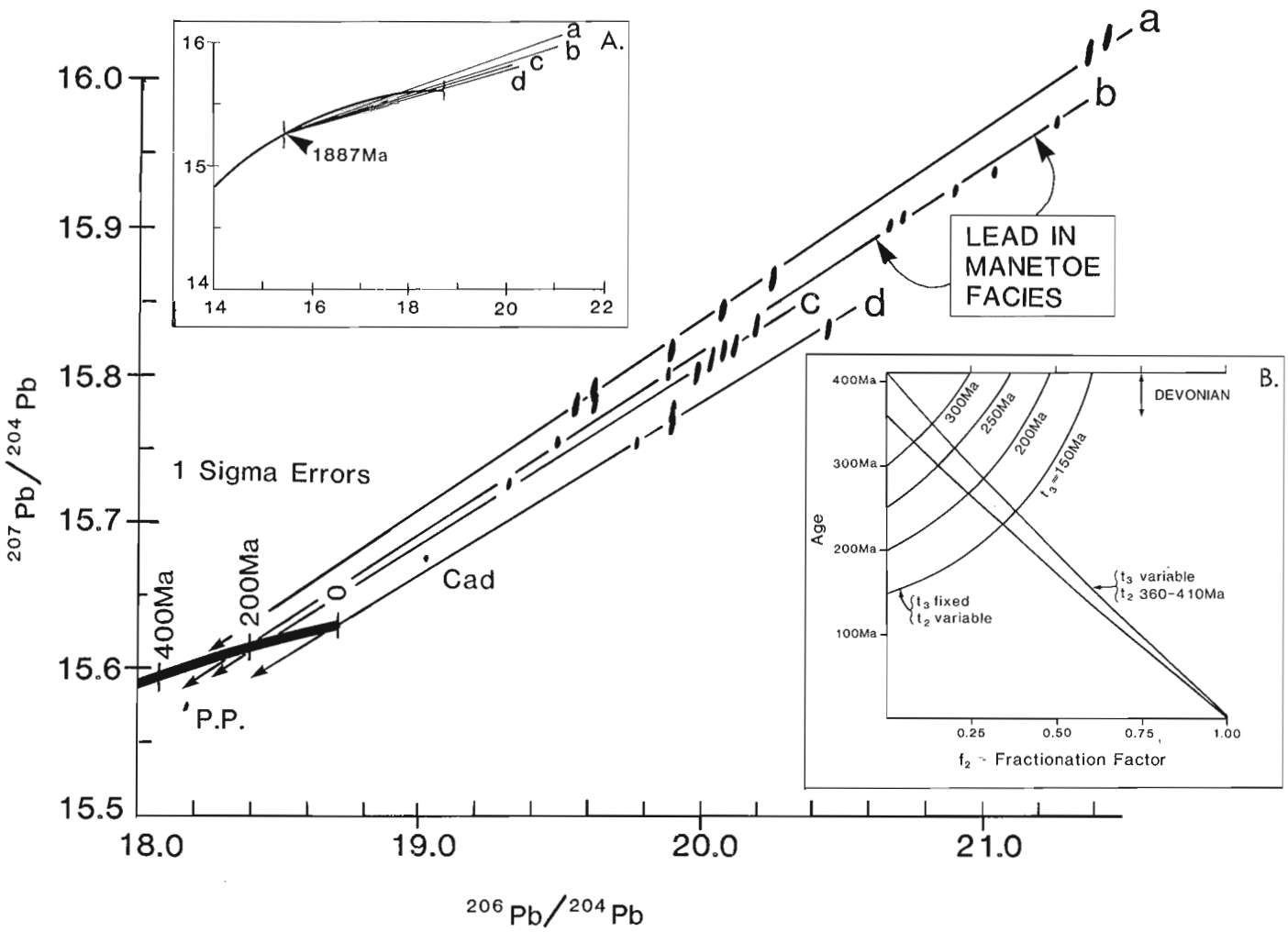

Figure 21. *Lead isotope data, derived from galena occurrences in the Manetoe Facies (isotope group 'b'), for the Robb Lake deposit (isotope group 'c'), for the Rusty Springs deposit (isotope group 'd'), and for a group of small mineral showings in northeastern British Columbia (isotope group 'a'; see Morrow and Cumming, 1982). These linear arrays are consistent with a three-stage evolution of lead leading to an early Mesozoic age of final mineralization (Macqueen and Thompson, 1978). Data from the Cadillac (Cad) lead-zinc-silver mine (see Morrow and Cumming, 1982), and from the Pine Point (P.P.) lead-zinc mine (R.P. Kyle, pers. comm., 1984) are also shown. Inset A shows the lower point of intersection of the linears with the growth curve of common lead at 1887 Ma. Inset B shows the relationship between the slope of the Tertiary isochron (0.11554 for the Rusty Springs deposit) and the possible combinations of the fractionation factor (f_2) and times of lead mobilization (t_2 and t_3) that can account for that slope. The age of shale deposition (t_2) is restricted to 410 Ma > t_2 > 360 Ma.*

Kramers (1975) growth curve (Table 13; Fig. 21). This time frame is unlikely, because fluid-inclusion data from the Rusty Springs deposit indicate that mineralization temperatures were 150 to 250°C (Kirker, 1982), and this in turn suggests a burial depth of between 5 and 10 km during mineralization, which is inconsistent with actual burial during the past several million years. Further, if the shale-dewatering mechanism proposed by Macqueen and Thompson (1978) has general validity in this area, then large variations in age of mineralization seem unlikely. We believe that a more complex multistage interpretation is indicated.

It is undoubtedly true that the actual geological situation is more complex than any mathematical model would suggest, but the relative simplicity of the data distribution has led us to examine simple models that may serve to place some useful constraints on the interpretation of the geological processes involved. We have examined our data, therefore, in the context of the work of Gale and Mussett (1973), who described the various three-stage models that can yield linear arrays of data.

The three-stage model that describes the history of a lead deposit is as follows:

1. A first stage, from t_0 to t_1, in which the lead exists in a U/Pb environment characterized by a "standard" value of $^{238}U/^{204}Pb = u_1$. In the model, this may change with time, but the details need not concern us here.

At t_1, a group of discrete systems with different values for the U/Pb ratio u_{2i} is generated. We may interpret this as resulting from the development of crustal rocks with local average values for u_{2i}. We characterize the change in U/Pb ratios by factors $f_{1i} = u_1/u_{2i}$, while the U/Pb ratio remains unchanged except for radioactive decay until time t_2.

2. At t_2, each subsystem then undergoes a further change in the U/Pb ratio to some new value, u_{3i}, and this new subsystem remains constant until t_3. The fractionation factor for this "event" is $f_2 = u_{2i}/u_{3i}$ and, in our context, we think of this event as the formation of the shale basins.

3. At t_3, lead is extracted from the shale and deposited as galena. No further changes in isotopic composition occur after this time.

Two situations can produce linear arrays on a lead/lead diagram. One is when f_1 is a constant that yields a series of parallel lines. The other is if f_2 is a constant yielding a family of lines diverging from a common point on the growth curve, corresponding to t_1. This is the situation for our data, and the relevant equation is:

$$m = \frac{1}{u} * \frac{[f_2((\exp\lambda' t_1 - \exp\lambda' t_2) + (\exp\lambda' t_2 - \exp\lambda' t_3))]}{[f_2((\exp\lambda t_1 - \exp\lambda t_2) + (\exp\lambda t_2 - \exp\lambda t_3))]}$$

(Equation A59 from Gale and Mussett, 1973.)

The parameters are:

m = slope of the tertiary isochron
u = $^{238}U/^{235}U = 137.88$
λ' = decay constant of ^{235}U
λ = decay constant of ^{238}U
t_1 = 1887 Ma, after Godwin et al. (1982)
t_2 = formation of shale basins
t_3 = time of mineralization

The diverging array of lines in Figure 21 is limited above by $f_2 = \infty$ and below the array by $f_2 = 0$. In the first case, the limiting slope depends only on $t_1$and t_2, while in the second case the limiting slope depends only on t_2 and t_3, and will be in the order of m = 0.06, much smaller than any observed slope. We are unable, therefore, to make any direct deduction regarding t_3. The steepest slope (i.e., group "a") provides a minimum value for t_2, since t_1 is already determined from the intersections of the array of lines with the growth curve. Solving equation 1 yields a minimum estimate of $t_2 \geq 359$ Ma.

TABLE 12

Lead isotope analyses of galena from carbonate-hosted zinc-lead deposits in the northern Cordillera

Deposit or showing and location	Lead isotope ratios		
	$^{206}Pb/^{204}Pb$	$^{207}Pb/^{204}Pb$	$^{208}Pb/^{204}Pb$
(1) Rusty Spring	20.455	15.833	40.429
66.5°N,			
140.33°W[1]	19.772	15.754	39.700
	19.897[2]	15.775	39.898
	19.899	15.767	39.820
	20.450	15.827	40.408
	19.893	15.766	39.839
(2) Columbia et al.	20.712	15.906	41.044
Kotaneelee			
YT-H38	20.670	15.900	40.991
60.12°N,			
124.10°W	21.037	15.936	41.276
	21.259	15.970	41.653
	20.899	15.923	41.192
(3) Columbia et al.	19.321	15.726	39.294
Kotaneelee			
YT-H48	19.883	15.801	40.003
60.12°N,			
124.12°W	19.491	15.755	39.508
(4) Richards Creek	21.439[3]	16.027	42.484
57.55°N,			
123.97°W	21.371	16.016	42.366
(5) Mount McCusker	20.259[3]	15.865	41.043
57.09°N,			
123.95°W			
(6) Robb Lake	19.987	15.801	40.726
56.93°N,			
123.75°W	20.037[3]	15.810	40.779
	20.081	15.816	40.865
	20.198	15.833	41.068
	20.122	15.819	40.885
(7) Mount Burden	19.620	15.790	40.355
56.22°N,			
123.46°W	19.557[3]	15.780	40.272
	19.894	15.816	40.764
(8) Poco Prospect	20.074[3]	15.843	41.027
("main showing")			
(Dunedin Fm)			
56.19°N,			
123.38°W			
(9) Poco Prospect	19.624	15.781	40.331
("stone showing")			
(Stone Fm)			
56.16°N,			
123.38°W			

[1]Minutes expressed as a decimal fraction.
[2]Analysis omitted from the regression shown in Figure 21.
[3]Average of two analyses.

TABLE 13

Regression analysis of isotopic groups

Isotope group	Slope of regression (R)	Mean square of weighted deviates (MSWD)	Upper intersection with growth curve (t_2)	Lower intersection with growth curve (t_1)
A. Unconstrained regression analysis				
(a)	0.13243+/–0.00344	0.31	271 Ma	1999 Ma
(b)	0.12293+/–0.001732	1.29	237 Ma	1879 Ma
(c)	0.1468+/–0.0379	0.06	–	–
(d)	0.11235+/–0.00521	0.39	53 Ma	1810 Ma
B. Regression analysis constrained by the point at 1887 Ma on the Stacey and Kramers (1975) growth curve				
(a)	0.12795+/–0.00054	0.56	359 Ma	1887 Ma
(b)	0.12327+/–0.00025	1.29	232 Ma	1887 Ma
(c)	0.12138+/–0.00067	0.18	179 Ma	1887 Ma
(d)	0.11554+/–0.00040	0.49	3 Ma	1887 Ma

a = A group of small mineral showings in northeastern British Columbia.
b = Galena occurrences in the Manetoe Facies.
c = Robb Lake deposit.
d = Rusty Springs deposit.

In fact, group "a" is a composite group and the two analyses from the Richards Creek samples place slightly above the line shown. If these points are joined to the t_1 point on the growth curve, a slightly steeper line, and hence a slightly older estimate of t_2, is obtained. This yields $t_2 \geq 386$ Ma, and approximates the age of the oldest Devonian shales that have been considered as the source of lead for these carbonate-hosted deposits (Macqueen and Thompson, 1978; Godwin et al., 1982). We considered the case, therefore, in which t_2 is "fixed" somewhere between 360 and 410 Ma, corresponding to the Devonian age of the shales, and investigated the permissible range of t_3 as a function of f_2 for the smallest slope so far observed. For the Rusty Springs deposit the slope is m = 0.11554 (Table 13, B). The linear arrays for other deposits have steeper slopes, and thus large values for f_2. Figure 21 illustrates the possibilities. The shaded region shows the various allowable combinations of t_3 and f_2, where t_2 varies from 410 to 360 Ma. For example, if t_3 = 200 Ma then f_2 has a lower limit of about 0.4 to 0.5. This implies that u in the third stage was never more than about twice its value in the second stage, which we suppose is a reasonable limit from a geochemical point of view. On the other hand, if the mineralization occurred at 360 Ma (latest Devonian), then $f_2 \geq 0.15$, which implies at least a sixfold increase in the U/Pb ratio between the second and third stages for some source rocks – this appears to be unlikely.

Another possible means by which such an array of lines could originate would be if t_3 were the same for all deposits and the age of the source rocks, t_2, varied from one deposit to another. The family of curves in Figure 21 shows the possibilities for various values of t_3, again calculated for the minimum observed slope of m = 0.11554. For example, if the time of mineralization t_3 = 250 Ma, then a Late Devonian (360 Ma) age for the source rocks requires that f_2 = 0.3. In general, Figure 21 illustrates the difficulty of modelling these deposits utilizing a three-stage system. If the time of mineralization is soon after the time of shale basin development, a large value for u_{3i} is required, and the later the mineralization the easier it becomes to generate the necessary radiogenic component (^{207}Pb) of the ores. Although this does not preclude a Paleozoic mineralization event, it seems to suggest relatively late mineralization, because of the modest changes that are required in the U/Pb ratio. This would then favour the suggestion by Macqueen and Thompson (1978) that mineralization at Robb Lake occurred in the early Mesozoic, and hence, by implication, at the same time in the other deposits.

A satisfactory solution to this problem requires another means for estimating t_3. This might be achieved by making detailed studies of the residual lead in the source rocks. Preliminary attempts to solve this problem have not been particularly successful, owing to the low lead content of the rocks that we have analyzed. We conclude that, although the present data are not completely convincing, they do favour a relatively late age for the mineralization.

ORIGIN OF THE MANETOE DOLOMITE

The field and petrographic evidence clearly demonstrate that the white sparry dolomite of the Manetoe Facies has filled a system of vugs and caverns containing solution-collapse breccia – similar to the paleokarst system associated with the

Presqu'île Facies dolomite at Pine Point. Like the Manetoe Facies, the Presqu'île Facies exhibits vertically oriented "chimney-like" breccia bodies cemented with white sparry dolomite, and containing laminated internal sediments of detrital dolomite (Rhodes et al., 1984). However, whereas the Presqu'île paleokarst system is intimately associated with the sub-Watt Mountain unconformity (Skall, 1975; Kyle, 1980; Rhodes et al., 1984) (Fig. 6), the "Manetoe cavern system" cannot be related closely, either geographically or stratigraphically, to any unconformity within the host strata of the Manetoe Facies. The base of the Headless Formation does become unconformable southeastward, where it merges with the disconformity at the base of the Upper Chinchaga (Law, 1971) (Fig. 6), but no large-scale paleokarst features have been documented beneath this unconformity (e.g., Griffin, 1967; Law, 1971). It is unlikely that this unconformity could have served as a recharge area for a Manetoe paleoaquifer. The vertical extent of the subsurface Manetoe breccia bodies, far above the stratigraphic level of the Headless Formation, is also a compelling argument against a sub-Headless recharge surface.

The probable lithostratigraphic continuity of the Manetoe and Presqu'île facies implies that the Presqu'île and Manetoe paleokarst systems were coextensive – as indicated also by a comparison of the oxygen and carbon isotope compositions of the Manetoe and Presqu'île dolomites. If this is true, then the sub-Watt Mountain unconformity, present today in Alberta and British Columbia, may have been the recharge area for an immense Middle Devonian paleoaquifer system that extended up to 128 km (80 miles) northwestward beneath the sea floor (Fig. 22). A modern analogue is the fresh and brackish water Floridan Aquifer, which extends eastward beneath the sea floor for up to 200 km from the Florida Peninsula (Manheim, 1967; Morrow, 1978).

The Watt Mountain and Gilwood formations of northern Alberta are thin siliciclastic units that overlie the Watt Mountain unconformity, and were themselves deposited under fresh to brackish water conditions (Rottenfusser and Oliver, 1977). The restriction of brecciation to strata beneath the shales of the Headless Formation, in the region where these shales are well developed, may be interpreted as indicating that the shales acted as an aquiclude, which confined circulation of meteoric water to sub-Headless strata (Fig. 22). The presence of the large, vertically oriented breccia bodies in the region close to the Presqu'île or Pine Point Barrier may indicate that, in this region, aquifer groundwaters were able to breach the relatively thin Headless shale and "stope" upward through the Nahanni Formation, forming solution-collapse breccias (Figs. 6, 22). The hydraulic head at any point within

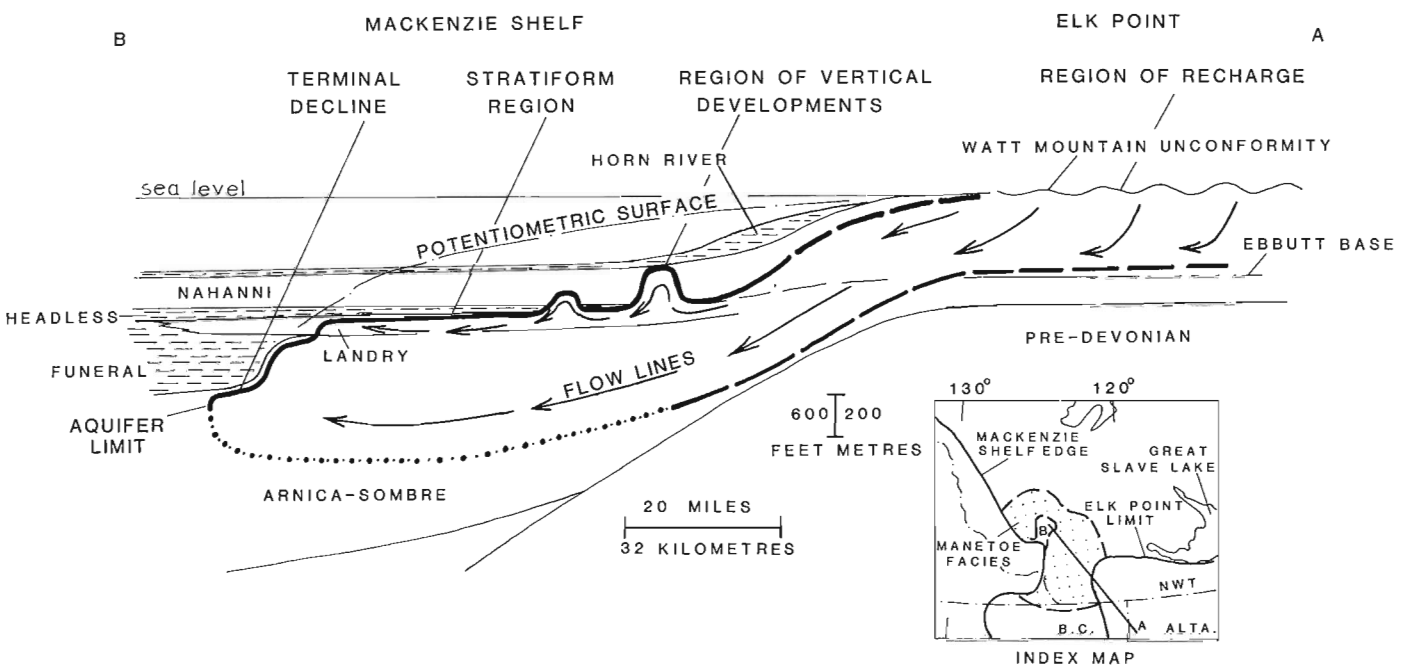

Figure 22. *Schematic reconstruction of a Middle Devonian paleoaquifer system in the Elk Point Basin and the southern part of the Mackenzie Shelf. This aquifer system originated as a result of subaerial exposure of the Elk Point Basin during deposition of the fluvial and deltaic Watt Mountain Formation. An extensive karst cavern system was developed in the Lower Devonian carbonates of the Mackenzie Shelf sequence immediately north of the Elk Point Basin. Dolomitizing solutions channelled through this cavern system produced the laterally extensive Manetoe and Presqu'île facies.*

such a vertically confined paleoaquifer is related to the elevation of its potentiometric surface. For example, the hydraulic head of the Floridan Aquifer is sufficient to cause artesian water to flow onto the decks of drillships after penetration of the aquifer during drilling (Manheim, 1967). The Floridan Aquifer occupies the Tertiary limestones and dolomitic limestones of Florida and adjoining states, and extends downward to 990 m below sea level. Extensive freshwater-filled caverns are developed throughout the aquifer and the main zone of cavern development is known as the "Boulder Zone" to drillers, because of the rough drilling conditions that are encountered during penetration of this zone (Kohout, 1965). The height of individual caverns in the Floridan Aquifer are estimated to be 1 to 28 m. This thickness is similar to that of the Manetoe Facies, particularly in northern areas (e.g., Sections 39 to 44 in Table 1).

Hydraulic fracturing, an alternative means of forming breccias in subsurface environments (Phillips, 1972), is far less attractive as a mechanism for the origin of Manetoe breccias than is a paleokarst solution-collapse mechanism. Certainly, during deposition and burial, considerable overpressures could have developed within the upper Paleozoic shales overlying the carbonate shelf sequence containing the Manetoe Facies (Fig. 9). It is possible that some fluids from these overpressured zones could have penetrated downward into the carbonate sequence, perhaps where the Manetoe Facies extends upward to the carbonate/shale contact. However, it is clearly impossible for these fluids to have created space by forcing strata apart along planes parallel to bedding in any strata beneath these shales. This is evident if one considers that the maximum fluid pressure attainable by pore fluids in a compacting shale sequence is equal to the combined pressure of the total hydraulic head plus the pressure of the lithostatic load for a given depth. This fluid pressure can never be large enough to force strata apart along bedding planes at a greater depth, because such pressures can never exceed or even equal the combined hydraulic head and lithostatic load at that depth.

Even if it is accepted that the caverns hosting the Manetoe Facies are the product of a paleokarst system, the time of karst development is still open to question. The early Mesozoic and the Cenozoic are the only times, other than the Middle Devonian, when groundwater of meteoric origin might have infiltrated the lower Paleozoic carbonate sequence during exposure of the overlying sequence (Fig. 9). However, the overall stratigraphic selectivity and geographic distribution of the Manetoe and Presqu'île paleokarst systems are less readily ascribed to these potential later periods of karst development. Later karstification could reasonably be expected to have affected strata along the entire length of the Mackenzie Mountains, not simply the southern part, and to have profoundly affected Nahanni and Slave Point limestones overlying Manetoe and Presqu'île breccias. Also, since the age deduced for lead mineralization of the Manetoe Facies in the Kotaneelee gas field is Mesozoic, and since mineralization followed dolomitization in the paragenetic sequence, the implication is that brecciation and dolomitization associated with the Manetoe Facies must have occurred earlier.

It is clear, therefore, from the geometry and stratigraphic relationships of the Manetoe Facies, that the original porosity network governing the lateral and vertical extent of the Manetoe was created during the Watt Mountain exposure event in the Middle Devonian. We may then speculate on the origin of the Manetoe dolomite itself. Three possible mechanisms of dolomitization at different times are shown in Figure 23.

Dolomitization may have accompanied aquifer development as the result of a mixed-water or brackish water chemistry conducive to calcite dissolution and dolomite precipitation – similar to that which occurred in the Floridan Aquifer (Hanshaw et al., 1971). A similar model for dolomitization has been applied previously to the Presqu'île Facies dolomite (Rhodes et al., 1984).

A slightly later period of dolomitization and dolomite cementation may have occurred, possibly during the Frasnian Stage of the Late Devonian. In this scenario, magnesium-enriched hypersaline brines, generated during deposition of the Elk Point evaporites, may have been recirculated from great depths through the Manetoe cavern system, precipitating dolomite cement in voids and dolomitizing parts of the enclosing host strata, during a Late Devonian thermal event of anomalously high heat flow. Aulstead and Spencer (1985) suggested a similar origin, during the Frasnian, for white sparry dolomite cements in the Keg River Formation of northern Alberta.

A much later period of dolomite cementation and dolomitization could have taken place during Cretaceous to early Tertiary uplift, associated with the Laramide Orogeny in the Cordillera. In this scenario, uplift would have caused the development of active groundwater flow, preferentially channelled through the Manetoe cavern system, updip toward the eastern margin of the foreland basin (Fig. 23) (see Garven and Freeze, 1982). Dolomitization would have occurred during this period of accelerated and large-scale groundwater flow. A similar mechanism has been suggested by Gregg (1985) to account for dolomitization of the Bonneterre Formation (the host for the Mississippi Valley lead-zinc deposits), involving large-scale groundwater flow through ancient basinal strata, with the flow induced by uplift and exposure.

All of the above scenarios satisfy the basic requirement for an active hydrology with continuous circulation, sufficient to transport the quantity of magnesium required for dolomitization and the volume of solution necessary to cause cementation of the Manetoe cavern system.

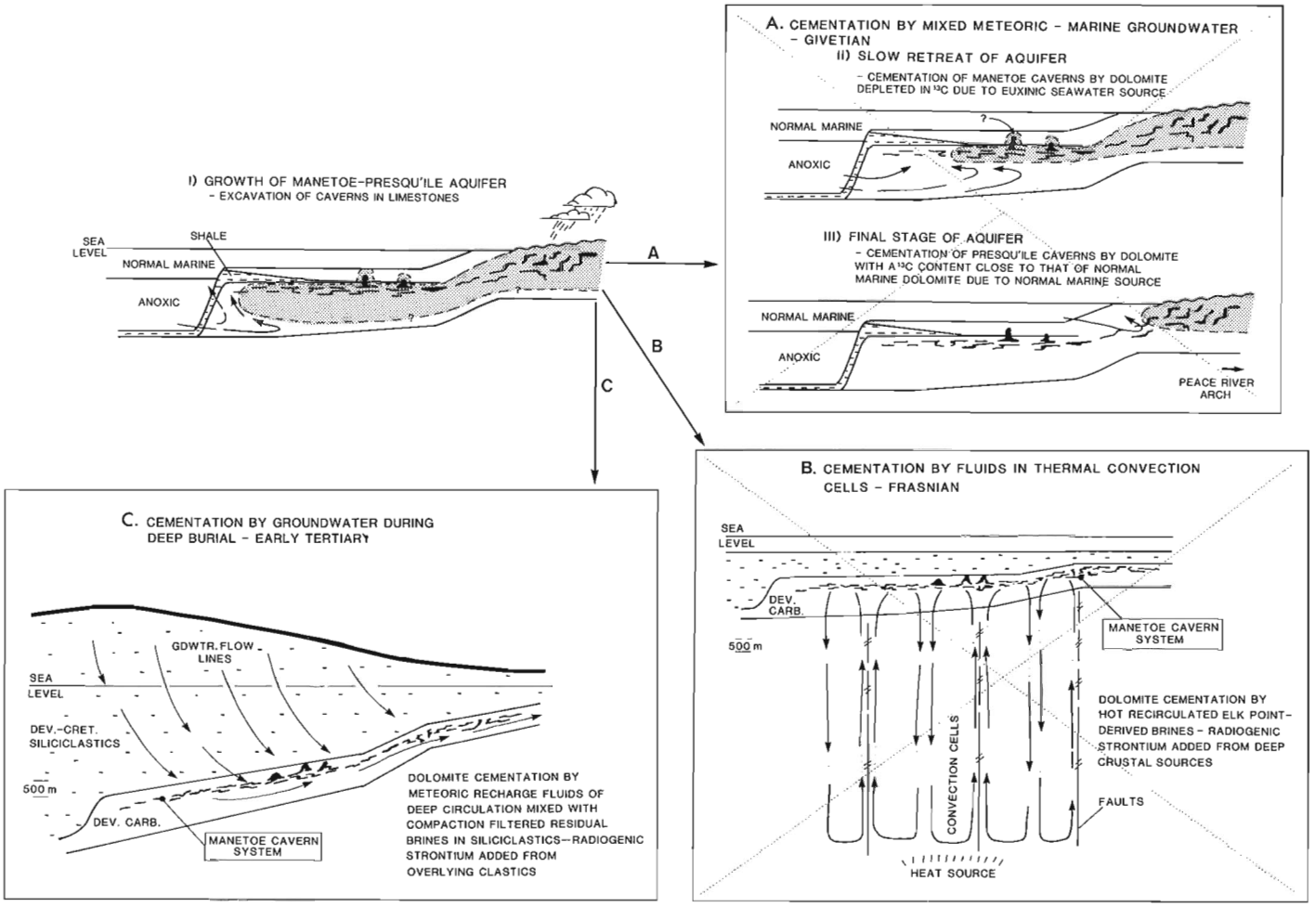

Figure 23. *Possible origins for Manetoe dolomite. Dolomite cementation of the Manetoe paleokarst system may have occurred during any of three possible episodes of enhanced fluid flow. Inset A indicates possible dolomitization in the Middle Devonian, resulting from the mixing of seawater with fresh aquifer waters during paleokarst development. Inset B indicates possible dolomitization resulting from circulation of heated residual Elk Point brines during Late Devonian shallow burial of the Manetoe paleokarst system. Inset C indicates possible dolomitization and cementation during early Tertiary circulation of modified meteoric groundwater through a deeply buried Manetoe paleokarst system. Evidence presented in this study favours scenario B.*

The evidence from this study, in part reported previously by Morrow et al. (1986) and Aulstead (1987), clearly supports the scenario involving shallow subsurface cementation by hot, recirculated, hypersaline brines derived from the Elk Point Basin (Fig. 23). Compelling evidence is provided by the fluid-inclusion data. Homogenization temperatures of primary inclusions in dolomite cluster around 180 to 200°C, and freezing temperatures indicate that these inclusions are NaCl-$MgCl_2$-$CaCl_2$ brines at a concentration of about 25 eq. wt. % NaCl. The composition of these inclusions is similar to that of subsurface connate brines that occur in Devonian strata throughout Western Canada. The latter have been interpreted as having originated as Devonian residual brines from the Elk Point Basin (Spencer, 1987). Dolomite homogenization temperatures for the Manetoe Facies are independent of location and depth of burial and are uniform across the facies, indicating that these homogenization temperatures reflect a uniform thermal event, rather than precipitation during burial under the influence of a normal geothermal gradient. Paleontological maturation indicators provide evidence that a thermal event of considerable magnitude occurred in Late Devonian to earliest Mississippian time. Interestingly, the sub-Nahanni sequence exhibits a uniform degree of thermal maturation over a stratigraphic range of more than 3000 m, within the limits of precision of the maturation indicators. This is consistent with the concept that, in the Late Devonian, thermally induced fluid movements transported heat upward, diminishing the slope of the geothermal gradient through the sub-Nahanni sequence.

A modern analogue for the residual-brine-solution/thermal-system inferred to have precipitated Manetoe dolomites occurs beneath the Salton Sea in southern California. A reservoir of deep hypersaline brines has accumulated over an area of 1000 km^2, at the base of the permeable sedimentary section, about 5 km beneath the Salton Sea and the Imperial Valley of southern California. These brines originated through the evaporation of saline Salton Sea lakewater and percolated downward into the deep subsurface (Rex, 1985). Increased heat flow and resultant heating, related to igneous intrusions at depth, caused these brines to become less dense and to rise buoyantly upward to depths of less than one kilometre below the surface of the Imperial Valley (McKibben et al., 1987). These brines have precipitated carbonate cements in fractures less than one kilometre below the surface of the Imperial Valley, at temperatures over 200°C (McKibben et al., 1987), in a manner similar to that inferred to have taken place in the geothermal system responsible for the precipitation of the dolomite cements of the Manetoe Facies.

The heating of the Salton Sea geothermal system is related to its location along the trend of the Gulf of California continental rift zone (McKibben et al., 1987). In a similar manner, the heating of the "Manetoe geothermal system" may have been related to tectonic activity along structural discontinuities. One of these, the Liard Fault Zone, has a trend that is approximately coextensive with the trend defined by the locations of the three Manetoe gas fields, where the Manetoe facies has its thickest development (Fig. 24). Since the fault zone displaces the top of the Nahanni Formation, a lower age limit is established, although the actual age of this post-Nahanni displacement is not known. It is possible that the faulting occurred in the Late Devonian and was accompanied by high heat flow. The Late Devonian was a time of enhanced tectonic activity throughout the Cordilleran region of Western Canada (Morrow and Geldsetzer, 1988), and probably caused the development of many geothermal heat flow anomalies. It seems possible that heated brines rose preferentially through permeable fault systems, such as the Liard Fault system, and spread laterally through the Manetoe cavern system to precipitate the Manetoe dolomite.

The strontium isotope evidence also is inconsistent with an early diagenetic origin for the Manetoe dolomite by

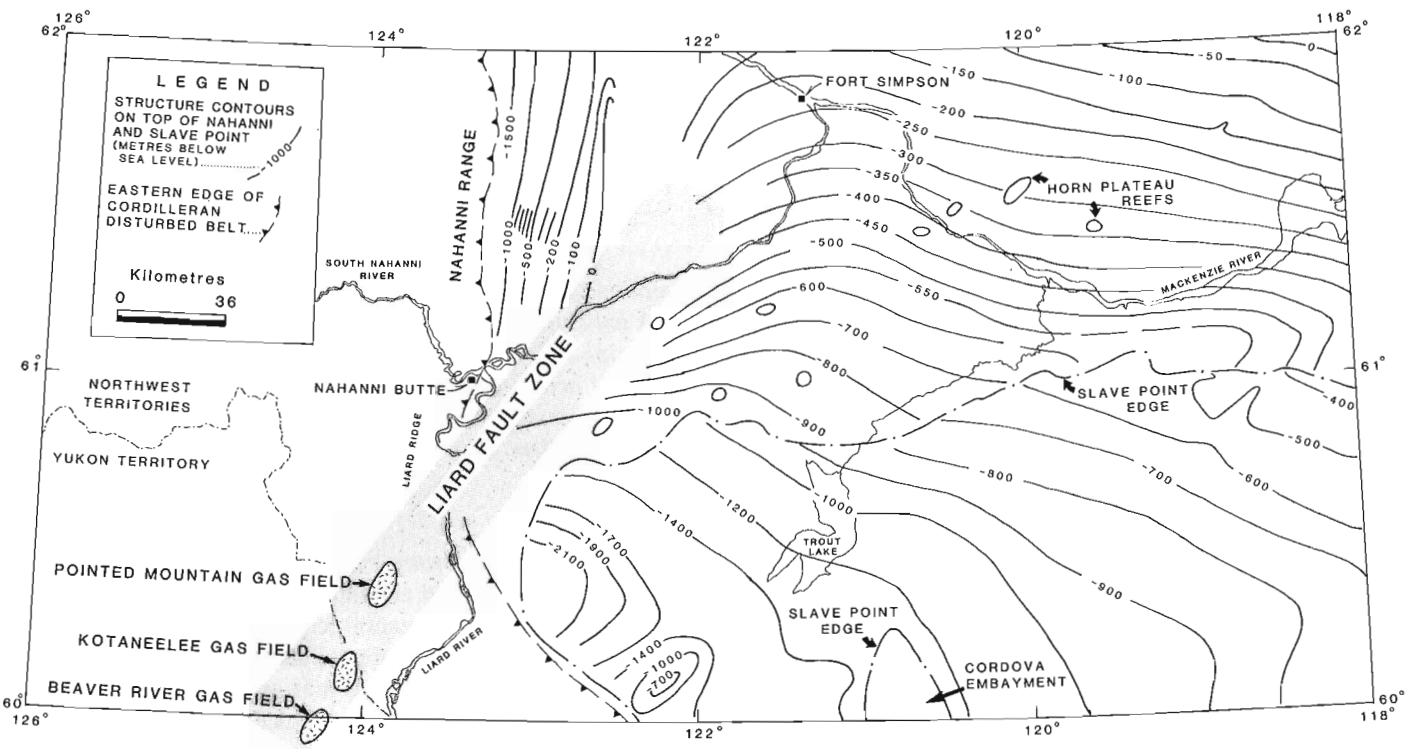

Figure 24. *Structure contour map, showing the displacement of the upper surface of the Nahanni Formation across the Liard Fault Zone. This fault zone has approximately the same orientation as, and may be collinear with, the trend defined by the positions of the three Manetoe gas fields west of the Liard River. Although the time or times of post-early Middle Devonian movement of this fault system are not known, it is possible that movement occurred during the Late Devonian, coincident with the development of Late Devonian uplifts throughout the North American Cordillera and in the Arctic regions of North America. (Adapted from Williams, 1981a.)*

freshwater/seawater mixing in the Manetoe paleoaquifer system. This type of dolomitization should cause the precipitation of dolomite with an isotopic signature very close to that indicated by the Devonian seawater curve of Burke et al. (1982), but the actual radiogenic strontium compositions of Manetoe dolomites are quite different. Spencer (1987) suggested that residual Elk Point brines circulated to great depths in the crust beneath the Elk Point Basin, and may have become calcium-enriched through the albitization of crustal feldspar minerals. Albitization of feldspars and the accompanying radioactive decay of rubidium would have enriched these brines in radiogenic strontium. Faure and Powell (1972, their Figure V.1) indicated that, by Devonian time, sialic continental crust would have had an average $^{87}Sr/^{86}Sr$ ratio of about 0.715. This ratio is slightly higher than that of the Manetoe dolomites, and is consistent with a Late Devonian episode of dolomitization resulting from geothermal activity and associated Elk Point brine recirculation.

Manetoe dolomites also could have acquired their elevated strontium isotope ratios during deep burial diagenesis in the early Tertiary (scenario 'C' in Figure 23), as diagenetic fluids might have leached radiogenic strontium from feldspars in the overlying siliciclastic sequence. However, the inferred early Mesozoic age for the associated lead mineralization, which postdates Manetoe dolomite formation, militates against this possibility.

It is not possible to assess the slope of the thermal maturation gradient of the supra-Nahanni sequence accurately from the available conodont and palynomorph maturation data. The palynomorph TAI data suggest a slightly higher level of maturation for these strata than the conodont CAI determinations. There is, however, some indication from the TAI values that the level of maturation of the Mattson Formation is measurably less than that of the underlying Clausen and Yohin formations. This is consistent with the normal burial type of thermal maturation gradient, shown schematically in Figure 12, for strata above the Nahanni and Besa River formations.

EMPLACEMENT OF HYDROCARBONS, AND POST-DOLOMITIZATION DIAGENESIS

The movement of hydrocarbons into Manetoe Facies gas reservoirs clearly postdates the emplacement of the Manetoe dolomite. No hydrocarbons were observed or inferred to be present in dolomite fluid inclusions, and the residual bitumen in vugs was emplaced after dolomite precipitation. The fact that some fluid inclusions in vug-filling quartz and calcite are inferred to contain methane and CO_2 may indicate that these phases, particularly quartz, were emplaced during the later, dry gas, stages of thermal maturation.

Studies of clay and organic diagenesis indicate that montmorillonitic or "swelling" clays, which are dominant in geologically young basinal sequences, undergo progressive dewatering and diagenesis, and that this process formed the illitic clays that are dominant in ancient siliciclastic sequences. This transformation is accompanied by a progressive loss of considerable amounts of silica from the clay minerals to the pore solution during burial and geothermal heating of the sequence. Foscolos (1984) suggested that this clay transformation process continues into burial depths and temperatures favourable for the generation of dry gas. This is in accord with the style of silicification observed in the Manetoe Facies at Nahanni Butte, and a deep burial phase of silica mobilization during compaction of the siliciclastic sequence overlying the Nahanni Formation is postulated. At Nahanni Butte, large masses of chert and microcrystalline quartz have replaced the Manetoe Facies along the contact between dolomitized Nahanni limestones and overlying Horn River Formation shales, and veins of finely crystalline quartz extend downward from the top of the Nahanni. In general, silicification of the Manetoe Facies appears to have proceeded downward from its top. The coarsely crystalline quartz that fills vugs in the Manetoe also may be related to this postulated deep burial phase of silica mobilization.

In addition to the silica mobilization, pore solutions in siliclastic sequences undergoing burial heating and organic maturation tend to be acidic and enriched in calcium bicarbonate ($Ca(HCO_3)_2$), as the result of the dissolution of calcite during organic maturation (Foscolos, 1984). Dissolved calcium would have been precipitated as calcite when these solutions infiltrated the underlying carbonate rocks of the Manetoe Facies and the Nahanni Formation.

This mode of origin for the calcite and quartz cements is supported by the approximate correlation between their inclusion homogenization temperatures and present depths of burial – unlike the dolomite cements whose inclusion temperatures do not correlate with burial depth. Also, the lower salinity of inclusions in the quartz and calcite cements is consistent with precipitation from solutions of moderate salinity, such as commonly occur in the subsurface of shale basins (Dickey et al., 1972).

Consequently, the time of initial hydrocarbon migration into Manetoe reservoirs is bracketed between the time of dolomitization and the later time or times of quartz and calcite cementation. If quartz and calcite cementation occurred at a burial depth somewhere between 2500 and 5000 m, as indicated by Foscolos (1984), then hydrocarbon migration may have been largely completed by the end of the Paleozoic (Fig. 9). The inferred early Mesozoic age for galena mineralization, postdating quartz and calcite cementation, supports this assessment.

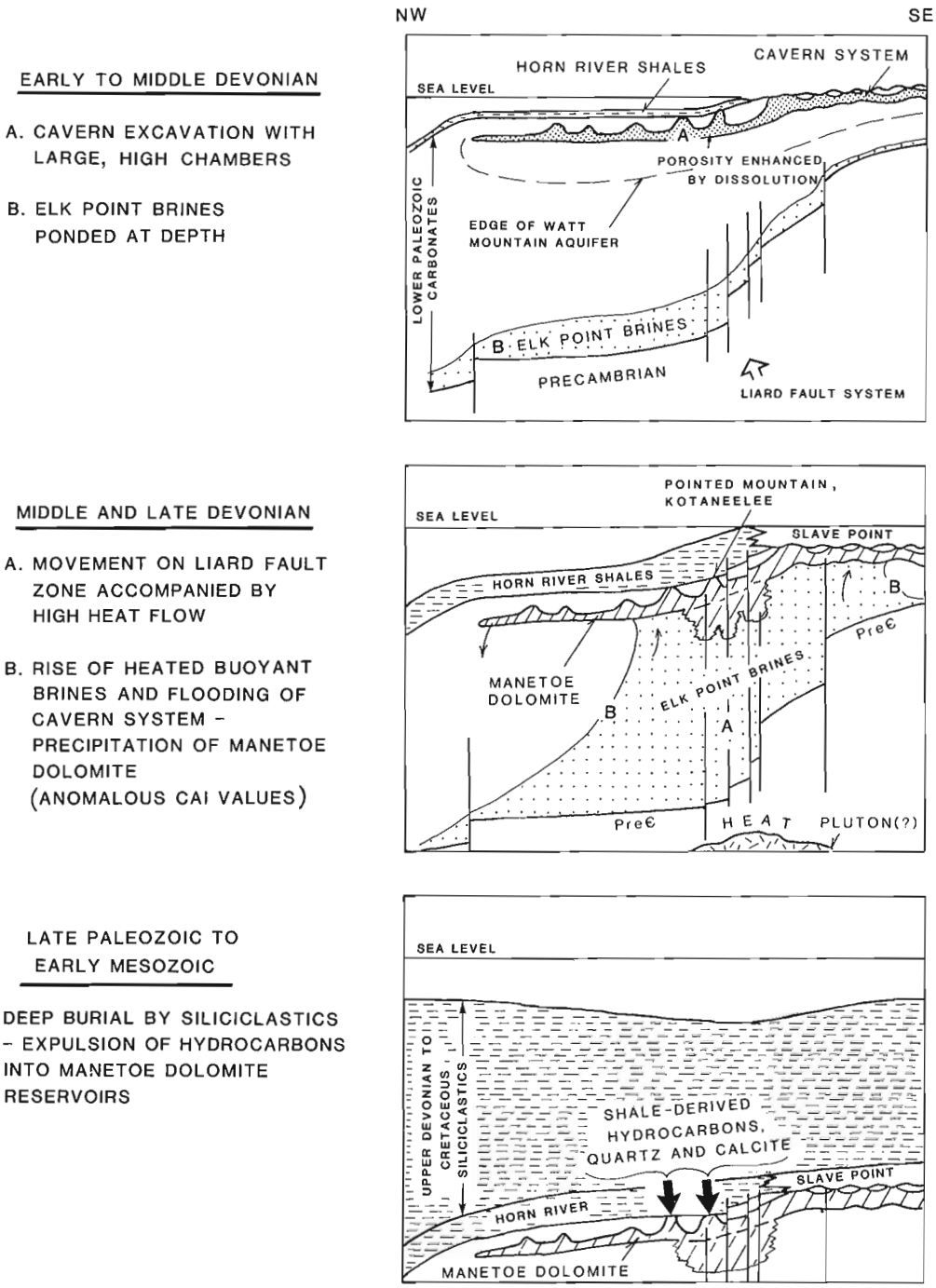

Figure 25. *Schematic summary of events leading to the emplacement of hydrocarbons in Manetoe reservoirs. Precipitation of dolomite cement, resulting from the circulation of geothermal brines through an extensive and not too deeply buried cavern system, formed the permeable Manetoe Facies dolomite in Late Devonian time. Siliciclastic rocks, containing organic material, subsequently accumulated above the Devonian carbonate rocks. Geothermal heating during burial caused maturation of the organic material to liquid hydrocarbons. Burial compaction caused the downward expulsion of these hydrocarbons from the siliciclastics into the Manetoe Facies, where the latter extended upward to the top of the Devonian carbonates, and locally enhanced the vertical permeability at the contact between the carbonates and the overlying siliciclastics. Quartz and calcite cementation may have coincided in part with the migration of hydrocarbons into Manetoe reservoirs in the late Paleozoic.*

SUMMARY AND CONCLUSIONS

Figure 25 schematically outlines the geological history of the stratigraphic sequence containing the Manetoe Facies. In the Early to early Middle Devonian, hypersaline brines, derived from the evaporation of seawater in the Elk Point Basin (see Bebout and Maiklem, 1973), filtered downward to the base of the more porous sedimentary rock above the impermeable Precambrian "basement". In the early Middle Devonian, a large freshwater aquifer system extended under the seafloor northward from the Elk Point Basin. Development of this aquifer system resulted in the excavation of a laterally continuous network of caverns, primarily in the more soluble limestones of the Landry Formation.

High geothermal heat flow, particularly along fault systems like the Liard Fault System, occurred in the Late Devonian as part of the generally intensified tectonic activity along the North American Cordillera at that time. Buoyant heated brines rose from the Precambrian surface and ascended preferentially through the zones of enhanced vertical permeability along faults (Fig. 25). The Manetoe dolomite was precipitated from these brines as they rose to the level of the cavern system and circulated through it. The entire sub-Nahanni sequence in this region was heated to an anomalous extent by these superheated brines.

Deep burial by an organic-rich, predominantly fine grained, siliciclastic sequence, throughout the late Paleozoic, was accompanied by the maturation and expulsion of hydrocarbons from the siliciclastics. These hydrocarbons migrated downward into the Manetoe Facies in regions, such as the Pointed Mountain and Kotaneelee gas fields, where the Manetoe Facies extends to the top of the Nahanni Formation (Fig. 25). The enhanced vertical permeability provided by the Manetoe dolomite at these localities facilitated the downward flow of hydrocarbons into these natural reservoirs. In a similar manner, solutions that precipitated calcite and quartz in the Manetoe were funneled preferentially downward into the Manetoe Facies at these same localities during slightly later and deeper burial and compaction. The entire area was, of course, intensely deformed during the Tertiary Laramide Orogeny, but it is conjectured from this study that the hydrocarbons in these reservoirs were generated and trapped largely, if not entirely, before the close of the Paleozoic Era.

The salient conclusions of this study are:

1. The Manetoe Facies developed as the result of two separate events in the Devonian. First, a laterally extensive cavern system was excavated, primarily in more soluble limestone strata of the Landry Formation and, to a lesser extent, in limestones of the Headless and Nahanni formations. Secondly, dolomite was precipitated from superheated hypersaline brines that circulated through the Manetoe cavern system during a thermal event of high heat flow.

2. Hydrocarbons were introduced into Manetoe gas reservoirs from overlying, organic-rich, fine grained, shaly, siliciclastic rocks during late Paleozoic burial and compaction, but only at those localities where the Manetoe Facies extends to the top of the Nahanni Formation immediately beneath the siliciclastics. This was followed by silicification and quartz and calcite cementation during later burial diagenesis of the overlying siliciclastic sequence.

REFERENCES

Aulstead, K.L.

1987: Origin and diagenesis of the Manetoe Facies, southern Yukon and Northwest Territories, Canada. Unpublished M.Sc. thesis, Department of Geology and Geophysics, University of Calgary, Calgary, Alberta, 143p.

Aulstead, K.L. and Spencer, R.J.

1985: Diagenesis of the Keg River Formation, northwestern Alberta: fluid inclusion evidence. Bulletin of Canadian Petroleum Geology, v. 33, no. 2, p. 167-183.

Bebout, D.G. and Maiklem, W.R.

1973: Ancient anhydrite facies and environments, Middle Devonian Elk Point Basin, Alberta. Bulletin of Canadian Petroleum Geology, v. 21, no. 3, p. 287-343.

Borshchevskiy, Yu.A., Borisova, N.A., and Popova, N.K.

1974: New method of extracting oxygen and carbon from carbonate and carbonate silicate minerals for isotope analysis. *In* Abstracts of 5th All Union Symposium on the Geochemistry of Stable Isotopes; Vernadsky Institute, Moscow, p. 207-209.

Borshchevskiy, Yu.A., Borisova, N.A., Popova, N.K., and Stepanova, N.A.

1980: New method for preparing CO_2 from bituminous carbonates for isotope analysis. *In* Abstracts of the 8th All Union Symposium on stable isotopes in geochemistry; Vernadsky Institute, Moscow, p. 273,274.

Brady, W.B. and Wissner, U.F.G.

1961: A stratigraphic reconnaissance of the western part of the District of Mackenzie, N.W.T., and bios-

tratigraphic correlation of Middle Devonian strata in the N.W.T. Technical Report 28-1-5-5, submitted by Union Oil Company of California to the Department of Indian Affairs and Northern Development, Canada.

Burke, W.H., Denison, R.E., Hetherington, E.A., Koepnick, R.B., Nelson, H.F., and Otto, J.B.
1982: Variation of seawater $^{87}Sr/^{86}Sr$ throughout Phanerozoic time. Geology, v. 10, no. 10, p. 516-519.

Cameron, A.E.
1922: Hay and Buffalo rivers, Great Slave Lake, and adjacent country. Geological Survey of Canada, Summary Report, 1921, Part B, p. 1B-44B.

Choquette, P.W. and Steinen, R.P.
1980: Mississippian non-supratidal dolomite, Ste. Genevieve Limestone, Illinois Basin: evidence for mixed-water dolomitization. *In* Concepts and Models of Dolomitization, D.H. Zenger, J.B. Dunham, and R.L. Ethington (eds.); Society of Economic Paleontologists and Mineralogists, Special Publication 28, p. 163-196.

Clark, D.N.
1980: The diagenesis of Zechstein carbonate sediments. Contributions to Sedimentology, v. 9, p. 167-203.

Correia, M.
1969: Contribution a la recherche de zones favorables a la genèse du pétrole par l'observation microscopique de la matière organique figurée. Revue de l'Institut Français du Pétrole, v. XXIV, no. 12, p. 1417-1454.

Crawford, M.L.
1981: Phase equilibria in aqueous fluid inclusions. *In* Fluid Inclusions: Applications to Petrology, L.S. Hollister and M.L. Crawford (eds.); Mineralogical Association of Canada, Annual Meeting, May 1981, Short Course Handbook, v. 6, chapter 4, p. 75-100.

de Wit, R., Gronberg, E.C., Richards, W.B., and Richmond, W.O.
1973: Tathlina area, District of Mackenzie. *In* The Future Petroleum Provinces of Canada – Their Geology and Potential, R.G. McCrossan (ed.); Canadian Society of Petroleum Geologists, Memoir 1, p. 187-212.

Dickey, P.A., Collins, A.G., and Ivan Fajardo, M.
1972: Chemical composition of deep formation waters in southwestern Louisiana. (Geological Note.) American Association of Petroleum Geologists, Bulletin, v. 56, no. 8, p. 1530-1533.

Douglas, R.J.W.
1974: Geology, Dahadinni River, District of Mackenzie. Geological Survey of Canada, Map 1374A. (Scale 1:250 000.)

Douglas, R.J.W. and Norris, D.K.
1960: Virginia Falls and Sibbeston Lake map-areas, Northwest Territories, 95 F and 95 G. Geological Survey of Canada, Paper 60-19, 26p.

1961: Camsell Bend and Root River map-areas, District of Mackenzie, Northwest Territories, 95 J,K. Geological Survey of Canada, Paper 61-13, 36p.

1977a: Geology, Root River, District of Mackenzie. Geological Survey of Canada, Map 1376A. (Scale 1:250 000.)

1977b: Geology, Sibbeston Lake, District of Mackenzie. Geological Survey of Canada, Map 1377A. (Scale1:250 000.)

1977c: Geology, Virginia Falls, District of Mackenzie. Geological Survey of Canada, Map 1378A. (Scale 1:250 000.)

Dunham, J.B. and Olson, E.R.
1980: Shallow subsurface dolomitization of subtidally deposited carbonate sediments in the Hanson Creek Formation (Ordovician-Silurian) of Central Nevada. *In* Concepts and Models of Dolomitization, D.H. Zenger, J.B. Dunham, and R.L. Ethington (eds.); Society of Economic Paleontologists and Mineralogists, Special Publication 28, p. 139-161.

Epstein, A.G., Epstein, J.B., and Harris, L.D.
1977: Conodont color alteration – an index to organic metamorphism. United States Department of the

Interior, Geological Survey Professional Paper 995, 27p.

Faure, G., Hurley, P.M., and Fairbairn, H.W.
1963: An estimate of the isotopic composition of strontium in rocks of the Precambrian Shield of North America. Journal of Geophysical Research, v. 68, no. 8, p. 2323-2329.

Faure, G. and Powell, J.L.
1972: Strontium Isotope Geology. New York, Springer-Verlag, 188p.

Foscolos, A.E.
1984: Diagenesis 7. Catagenesis of argillaceous sedimentary rocks. Geoscience Canada, v. 11, no. 2, p. 67-75.

Fritz, P. and Jackson, S.A.
1972: Geochemical and isotopic characteristics of Middle Devonian dolomites from Pine Point, northern Canada. *In* Section 6, Stratigraphy and Sedimentology; International Geological Congress, 24th Session, Montreal, 1972, p. 230-243.

Gabrielse, H., Blusson, S.L., and Roddick, J.A.
1973: Geology of Flat River, Glacier Lake, and Wrigley map-areas, District of Mackenzie and Yukon Territory. Geological Survey of Canada, Memoir 366, Pt.I:153p./Pt.II: 268p.

Gale, N.H. and Mussett, A.E.
1973: Episodic uranium-lead models and the interpretation of variations in the isotopic composition of lead in rocks. Reviews of Geophysics and Space Physics, v. 11, no.1, p. 37-86.

Garven, G. and Freeze, R.A.
1982: The role of regional groundwater flow in the formation of ore deposits in sedimentary basins: a quantitative analysis. *In* Proceedings of the Second National Hydrogeological Conference, G. Ozoray (ed.); International Association of Hydrogeologists, Canadian Chapter, p. 59-68.

Godwin, C.I. and Sinclair, A.J.
1981: Preliminary interpretations of lead isotopes in galena-lead from shale-hosted deposits in British Columbia and Yukon Territory. *In* Geological Fieldwork 1980; British Columbia, Ministry of Energy, Mines and Petroleum Resources, Paper 1981-1, p. 185-194.

Godwin, C.I., Sinclair, A.J., and Ryan B.D.
1982: Lead isotope models for the genesis of carbonate-hosted Zn-Pb, shale-hosted Ba-Zn-Pb, and silver-rich deposits in the northern Canadian Cordillera. Economic Geology, v. 77, no. 1, p. 82-94.

Godwin, C.I., Sinclair, A.J., Ryan, B.D., and Slawson, W.F.
1981: Lead isotope study of carbonate-hosted Pb-Zn deposits in and near Mackenzie Mountains, northern Canadian Cordillera. *In* Mineral Industry Report for 1977; Canada, Department of Indian Affairs and Northern Development, EGS 1979-1, p. 155-159.

Goldsmith, J.R. and Graf, D.L.
1958a: Structural and compositional variations in some natural dolomites. Journal of Geology, v. 66, no. 6, p. 678-693.

1958b: Relation between lattice constants and composition of the Ca-Mg carbonates. American Mineralogist, v. 43, p. 84-101.

Gregg, J.M.
1985: Regional epigenetic dolomitization in the Bonneterre Dolomite (Cambrian), southeastern Missouri. Geology, v. 13, no. 7, p. 503-506.

Griffin, D.L.
1967: Devonian of northeastern British Columbia. *In* International Symposium on the Devonian System, D.H. Oswald (ed.); Alberta Society of Petroleum Geologists, v. 1, p. 803-826.

Hanshaw, B.B., Back, W., and Deike, R.G.
1971: A geochemical hypothesis for dolomitization by ground water. Economic Geology, v. 66, no. 5, p. 710-724.

Heinrich, A.G. and Foscolos, A.E.
1984: Contributions to X-ray fluorescence spectroscopy. Part I – A comparison between theoretical and experimental corrections for interfering spectral lines from target elements in X-ray fluorescence spectroscopy; Part II – Comparison of X-ray tubes used for major and trace element analysis in X-ray fluorescence spectroscopy. Geological Survey of Canada, Paper 83-27, 18p.

Hunt, J.M.
1979: Petroleum Geochemistry and Geology. W.H. Freeman and Company, San Francisco, 617p.

Irwin, H.
1980: Early diagenetic carbonate precipitation and pore fluid migration in the Kimmeridge Clay of Dorset, England. Sedimentology, v. 27, no. 5, p. 577-591.

Irwin, H., Curtis, C., and Coleman, M.
1977: Isotopic evidence for source of diagenetic carbonates formed during burial of organic-rich sediments. Nature, v. 269, p. 209-213.

James, N.P. and Choquette, P.W.
1983: Diagenesis 6. Limestones – the sea floor diagenetic environment. Geoscience Canada, v. 10, no. 4, p. 162-179.

Kirker, J.
1982: Geology, geochemistry and origin of the Rusty Springs base-metal deposit, Yukon Territory. Unpublished M.Sc. thesis, University of Calgary, Calgary, Alberta, 158p.

Kohout, F.A.
1965: A hypothesis concerning cyclic flow of salt water related to geothermal heating in the Floridan Aquifer. Transactions of the New York Academy of Science, v. 28, no. 2, p. 249-271.

Kyle, J.R.
1980: Controls of lead-zinc mineralization, Pine Point district, Northwest Territories, Canada. Mining Engineering, v. 32, no. 11, p. 1617-1626.

Land, L.S.
1980: The isotopic and trace element geochemistry of dolomite: the state of the art. *In* Concepts and Models of Dolomitization, D.H. Zenger, J.B. Dunham, and R.L. Ethington (eds.); Society of Economic Paleontologists and Mineralogists, Special Publication 28, p. 87-110.

Law, J.
1955: Geology of northwestern Alberta and adjacent areas. American Association of Petroleum Geologists, Bulletin, v. 39, no. 10, p. 1927-1975.

1971: Regional Devonian geology and oil and gas possibilities, upper Mackenzie River area. Bulletin of Canadian Petroleum Geology, v. 19, no. 2, p. 437-484.

Lloyd, R.M.
1966: Oxygen isotope enrichment of sea water by evaporation. Geochimica et Cosmochimica Acta, v. 30, p. 801-814.

Lumsden, D.N. and Chimahusky, J.S.
1980: Relationship between dolomite nonstoichiometry and carbonate facies parameters. *In* Concepts and Models of Dolomitization, D.H. Zenger, J.B. Dunham, and R.L. Ethington (eds.); Society of Economic Paleontologists and Mineralogists, Special Publication 28, p. 123-137.

Manheim, F.T.
1967: Evidence for submarine discharge of water on the Atlantic Continental Slope of the southern United States, and suggestions for further search. Transactions of the New York Academy of Science, v. 29, no. 7, p. 839-853.

Macqueen, R.W. and Powell, T.G.
1983: Organic geochemistry of the Pine Point lead-zinc ore field and region, Northwest Territories, Canada. Economic Geology, v. 78, no. 1, p. 1-25.

Macqueen, R.W. and Thompson, R.I.
1978: Carbonate-hosted lead-zinc occurrences in northeastern British Columbia with emphasis on the Robb Lake deposit. Canadian Journal of Earth Sciences, v. 15, no. 11, p. 1737-1762.

McCrea, J.M.
1950: On the isotopic chemistry of carbonates and a

paleotemperature scale. Journal of Chemical Physics, v. 18, p. 849-857.

McKibben, M.A., Williams, A.E., Elders, W.A., and Eldridge, C.S.
1987: Saline brines and metallogenesis in a modern sediment-filled rift: the Salton Sea geothermal system, California, U.S.A. Applied Geochemistry, v. 2, nos. 5/6, p. 563-578.

Mattes, B.W. and Mountjoy, E.W.
1980: Burial dolomitization of the Upper Devonian Miette buildup, Jasper National Park, Alberta. *In* Concepts and Models of Dolomitization, D.H. Zenger, J.B. Dunham, and R.L. Ethington (eds.); Society of Economic Paleontologists and Mineralogists, Special Publication 28, p. 259-297.

Morrow, D.W.
1970: Stratigraphy and petrography of the Elk Point Group, northeast British Columbia. Unpublished M.A. thesis, University of Texas at Austin, Texas, 184p.

1978: Dolomitization of lower Paleozoic burrow-fillings. Journal of Sedimentary Petrology, v. 48, no. 1, p. 295-306

1982a: Descriptive field classification of sedimentary and diagenetic breccia fabrics in carbonate rocks. (Geological Note.) Bulletin of Canadian Petroleum Geology, v. 30, no. 3, p. 227-229.

1982b: Diagenesis 1. Dolomite – Part 1: The chemistry of dolomitization and dolomite precipitation. Geoscience Canada, v. 9, no. 1, p. 5-13.

Morrow, D.W. and Cook, D.G.
1987: The Prairie Creek Embayment and lower Paleozoic strata of the southern Mackenzie Mountains. Geological Survey of Canada, Memoir 412, 195p.

Morrow, D.W. and Cumming, G.L.
1982: Interpretation of lead isotope data from zinc-lead mineralization in the northern part of the western Canadian Cordillera. Canadian Journal of Earth Sciences, v. 19, no. 5, p. 1070-1078.

Morrow, D.W., Cumming, G.L., and Koepnick, R.B.
1986: The Manetoe Facies – a gas-bearing, megacrystalline, Devonian dolomite, Yukon and Northwest Territories, Canada. American Association of Petroleum Geologists Bulletin, v. 70, no. 6, p. 702-720.

Morrow, D.W. and Geldsetzer, H.H.J.
1988: Devonian of the eastern Canadian Cordillera. *In* Devonian of the World, Volume 1: Regional Syntheses, N.J. McMillan, A.F. Embry, and D.J. Glass (eds.); Proceedings of the Second International Symposium on the Devonian System, Calgary, Canada; Canadian Society of Petroleum Geologists, Memoir 14, v. 1, p. 85-121.

Morrow, D.W., Krouse, H.R., Ghent, E.D., Taylor, G.C., and Dawson, K.R.
1978: A hypothesis concerning the origin of barite in Devonian carbonate rocks of northeastern British Columbia. Canadian Journal of Earth Sciences, v. 15, no. 9, p. 1391-1406.

Noble, J.P.A. and Ferguson, R.D.
1971: Facies and faunal relations at edge of early mid-Devonian carbonate shelf south Nahanni River area, N.W.T. Bulletin of Canadian Petroleum Geology, v. 19, no. 3, p. 570-588.

Northrop, D.A. and Clayton, R.N.
1966: Oxygen-isotope fractionations in systems containing dolomite. Journal of Geology, v. 74, no. 2, p. 174-196.

Patterson, R.J.
1972: Hydrology and carbonate diagenesis of a coastal sabkha in the Persian Gulf. Unpublished Ph.D. thesis, Princeton University, Princeton, New Jersey, 498p.

Perry, E.A., Jr. and Turekian, K.K.
1974: The effects of diagenesis on the redistribution of strontium isotopes in shales. Geochimica et Cosmochimica Acta, v. 38, no. 6, p. 929-935.

Phillips, W.J.
1972: Hydraulic fracturing and mineralization. Journal

of the Geological Society of London, v. 128, pt. 4, p. 337-359.

Popp, B.N., Anderson, T.F., and Sandberg, P.A.
1986: Textural, elemental, and isotopic variations among constituents in Middle Devonian limestones, North America. Journal of Sedimentary Petrology, v. 56, no. 5, p. 715-727.

Potter, R.W. II, Clynne, M.A., and Brown, D.L.
1978: Freezing point depression of aqueous sodium chloride solutions. (Scientific Communication.) Economic Geology, v. 73, no. 2, p. 284,285.

Radke, B.M. and Mathis, R.L.
1980: On the formation and occurrence of saddle dolomite. Journal of Sedimentary Petrology, v. 50, no. 4, p. 1149-1168.

Rejebian, V.A., Harris, A.G., and Huebner, J.S.
1987: Conodont color and textural alteration: an index to regional metamorphism, contact metamorphism, and hydrothermal alteration. Geological Society of America, Bulletin, v. 99, no. 4, p. 471-479.

Rex, R.W.
1985: Temperature-chlorinity balance in the hypersaline brines of the Imperial Valley, California. *In* 1985 International Symposium on Geothermal Energy, C. Stone (ed.); Geothermal Resources Council, International Volume, p. 351-356.

Rhodes, D., Lantos, E.A., Lantos, J.A., Webb, R.J., and Owens, D.C.
1984: Pine Point orebodies and their relationship to the stratigraphy, structure, dolomitization, and karstification of the Middle Devonian Barrier Complex. Economic Geology, v. 79, no. 5, p. 991-1055.

Roedder, E.
1968: Temperature, salinity, and origin of the ore-forming fluids at Pine Point, Northwest Territories, Canada, from fluid inclusion studies. Economic Geology, v. 63, no. 5, p. 439-450.

1970: Application of an improved crushing microscope stage to studies of the gases in fluid inclusions. Schweizerische Mineralogische und Petrographische Mitteilungen, v. 50, no. 1, p. 41-58.

Rottenfusser, B.A. and Oliver, T.A.
1977: Depositional environments and petrology of the Gilwood Member north of the Peace River Arch. Bulletin of Canadian Petroleum Geology, v. 25, no. 5, p. 907-928.

Skall, H.
1975: The paleoenvironment of the Pine Point lead-zinc district. Economic Geology, v. 70, no. 1, p. 22-47.

Snowdon, D.M.
1977: Beaver River gas field: a fractured carbonate reservoir. *In* The Geology of Selected Carbonate Oil, Gas and Lead-zinc Reservoirs in Western Canada, I.A. McIlreath and R.D. Harrison (eds.); Canadian Society of Petroleum Geologists, 5th Core Conference, p. 1-18.

Spencer, R.J.
1987: Origin of Ca-Cl brines in Devonian formations, Western Canada Sedimentary Basin. Applied Geochemistry, v. 2, no. 4, p. 373-384.

Stacey, J.S. and Kramers, J.D.
1975: Approximation of terrestrial lead isotope evolution by a two-stage model. Earth and Planetary Science Letters, v. 26, p. 207-221.

Steuber, A.M., Pushkar, P., and Hetherington, E.A.
1984: A strontium isotopic study of Smackover brines and associated solids, southern Arkansas. Geochimica et Cosmochimica Acta, v. 48, p. 1637-1649.

Traill, R.J. and Lachance, G.R.
1965: A new approach to X-ray spectrochemical analysis. Geological Survey of Canada, Paper 64-57, 22p.

Utting, J.
1987: Palynology of the Lower Carboniferous Windsor Group and Windsor-Canso boundary beds of Nova

Scotia, and their equivalents in Quebec, New Brunswick and Newfoundland. Geological Survey of Canada, Bulletin 374, 93p.

Utting, J., Goodarzi, F., Dougherty, B.J., and Henderson C.M.

1989: Thermal maturity of Carboniferous and Permian rocks of the Sverdrup Basin, Canadian Arctic Achipelago. Geological Survey of Canada, Paper 89-19, 20p.

Veizer, J., Lemieux, J., Jones, B., Gibling, M.R., and Savelle, J.

1978: Paleosalinity and dolomitization of a lower Paleozoic carbonate sequence, Somerset and Prince of Wales islands, Arctic Canada. Canadian Journal of Earth Sciences, v. 15, no. 9, p. 1448-1461.

Williams, G.K.

1981a: Subsurface geological maps, southern Northwest Territories (NTS 85, 95). Geological Survey of Canada, Open File report 762, 11 maps. (Scale 1:500 000.)

1981b: Geological worksheets, subsurface and surface data, Lower and Middle Devonian strata, Slave-Redstone map areas, Yukon and Northwest Territories. Geological Survey of Canada, Open File report 793, 2 maps. (Scale 1:500 000.)

APPENDIX 1

ISOTOPIC AND MINERALOGICAL DATA – OUTCROP SECTIONS

GSC OUTCROP SECTION NUMBER	GSC SAMPLE LOCALITY NUMBER	DOLOMITE TYPE[3]	d, Å 10.4 peak	ORDER RATIO	$\delta^{18}O$	$\delta^{13}C$	I[4]	Q[5]	P[6]	C[7]	D[8]
	C-052856	1	2.893	0.46	-			1		tr	99
	C-052856	2	2.886	0.51	-10.81	-0.42		6			94
	C-052857[2]	1	2.889	TSTM	-	-		92	tr		7
	C-052858	1	2.888	0.49	-10.71	-0.75				tr	100
	C-052858	2	2.889	0.46	-10.70	-0.86				tr	100
	C-052861	1	2.899	0.46	-10.67	-0.82		1			99
	C-052861	2	2.893	0.40	-10.57	-0.82				tr	100
	C-052862	1	2.891	0.49	-11.45	-1.20	2			2	96
	C-052862	2	2.886	0.48	-10.78	-1.18				tr	100
	C-052863	1	2.895	0.47	-11.57	-1.17				2	98
1	C-052863	2	2.888	0.48	-11.65	-1.90					100
	C-052864[2]	1	2.893	TSTM	-	-	2			83	3
	C-052864[2]	2	2.888	0.43	-11.73	-1.84		tr		18	82
	C-052864[2]	3	2.896	0.41	-12.78	-2.09	1	1		15	83
	C-052866	1	2.896	TSTM				7		92	1
	C-052866	2	2.889	0.43						12	88
	C-052867	1	2.887	0.47				tr		6	94
	C-052867	2	2.899	0.47						5	95
	C-052868	1	-	TSTM				75		23	1
	C-052873[1]	1	2.890	TSTM	(-14.64)	(-0.05)		1		99	tr
	C-052875	1	2.894	0.47	(-11.44)	(-2.03)				2	98
	C-052875	2	2.888	0.45	(-13.28)	(-3.27)				1	99
	C-053009	1	2.888	0.45	-8.90	-0.49				1	99
	C-053009	2	2.889	0.45	-13.38	-1.07					100
	C-053016	1	2.889	0.51	-8.97	-0.52		1		tr	99
	C-053016	2	2.884	0.47	-9.55	-0.87					100
	C-053018	1	2.891	0.48	-9.00	-1.15					100
2	C-053018	2	2.890	0.51	-9.61	-0.59		1			99
	C-053019	1	2.888	0.46	-10.77	-0.79					100
	C-053019	2	2.888	0.51	(-11.82)	(-1.24)				tr	100
	C-053019				-12.49	-0.95					
	C-053020	1	2.891	0.46	-11.05	-0.78		tr		1	99
	C-053020	2	2.889	0.48	-11.88	-1.21				tr	100
	C-053021[2]	1	2.888	TSTM		-	tr	2		91	7
	C-053021				(-14.78)	(-2.68)					
	C-053022	2	2.900	0.43	-15.88	-2.97				2	98
	C-052695	1	2.888	0.49	-7.70	-0.05				tr	100
	C-052695[2]	2	2.888	0.38	-16.04	-3.88				41	59
	C-052696	1	2.892	0.52	-8.20	-0.41		8		1	91
	C-052696[2]	2	2.881	0.58?	-	-		91			9
	C-052697	1	2.894	0.48	-10.54	-1.76		2			98
4	C-052702	1	2.890	0.51	-9.69	-1.06					100
	C-052702[2]	2	2.889	0.42	-16.36	-3.86				30	70
	C-060987[2]	1	2.885	0.46	-11.93	-1.12	2	8		9	81
	C-060988	1	2.888	0.48	-8.91	-0.38				tr	100
	C-060988	2	2.886	0.44	-10.74	-0.97					100
	C-060989	1		TSTM	(-13.87)	(-2.94)		tr		100	
	C-060989				(-14.04)	(-3.43)					
	C-060990[2]	1	2.888	TSTM	(-13.52)	(-3.81)		1		97	2
	C-052895	1	2.890	0.40	(-14.91)	-2.99				2	98
	C-052895[2]	1	2.889	TSTM	(-13.34)	(-2.85)				99	1
	C-052895				(-12.15)	(-0.6)					
6	C-052901[2]	1	2.892	0.46	-13.96	+1.49		6		4	88
	C-052901	2	2.886	0.43	-12.79	-2.65					100
	C-052902	1	2.890	0.54	(-13.31)	(2.27)		8		1	91
	C-052902				-13.45	-1.97					
	C-052904	1	2.886	TSTM	-	-	tr	3		95	2
13	C-052842[2]	1	2.890	0.47	-10.40	-0.69		17		3	80
	C-059319	1	2.893	0.53	(-11.80)	(+1.60)					100
	C-059319				-10.65	+1.10					
	C-059319	2	2.886	0.49	(14.60)	(-2.86)					100
21	C-059319				-14.00	-2.21					
	C-059333	2	2.891	0.45	-17.33	-1.46				4	96
	C-059334[2]	1	2.893	-	-13.38	-0.44				89	11
	C-059335	1	2.891	0.43	-16.66	-0.47				4	96
	C-059225	1	2.887	0.49	(-7.74)	(+0.82)					100
26	C-059225				-8.80	+0.72					

[1]Values obtained by acid digestion technique (McCrea, 1950) are shown in parentheses
[2]Values not included in statistical compilations
[3]Type 1 dolomite is *in situ* replacement dolomite
Type 2 dolomite is cavity-filling, white sparry dolomite
Type 3 dolomite is a mixture of Types 1 and 2

[4]Illite%
[5]Quartz%
[6]Pyrite%
[7]Calcite%
[8]Dolomite%

TSTM = too small to measure
tr = trace

APPENDIX 2

ISOTOPIC AND MINERALOGICAL DATA – SUBSURFACE SECTIONS

SUBSURFACE SECTION NAME (lat.; long.)	SUBSEA ELEVATION (feet below K.B.)	DOLOMITE TYPE	d, Å 10.4 peak	Q	C	D	P	ORDER RATIO	$\delta^{18}O$	$\delta^{13}C$
	10298.25	1	2.890	1	1	98		.398	-10.48	-0.42
	10298.25	2	2.887		1	99		.479	-10.91	-0.72
	10308.0	1	2.889	1		99		.468	-9.75	-0.92
	10308.0	2	2.891	3		97		.494	-10.51	-0.55
	10600.25	2	2.893			100		.483	-14.32	-2.15
Amoco A-4	10612.0	1	2.889	1		99		.463	-10.23	-0.10
Pointed	10612.0	2	2.895	tr		100		.491	-11.80	-1.16
Mountain	10624.25	1	2.888	tr		100		.516	-10.66	-0.60
A-55	10624.25	2	2.895			100		.457	-13.21	-2.08
(60°24′05″;	10859.5	1	2.888	2		98		.481	-11.15	-0.84
123°54′39″)	10859.5	2	2.897			100		.508	-13.98	-4.34
	10863.0	1	2.890			100		.449	-11.47	-0.85
	10863.0	2	2.886	tr		100		.492	-12.94	-2.47
	11205.5	1	2.897			100		.437	-10.61	-2.88
	11205.5	2	2.886			100		.446	-13.11	-5.05
	12160.5	1	2.889	1		99		.465	-10.38	-1.27
	12160.5	2	2.897		tr	100		.483	-11.65	-1.65
Pan-Am.	8529.0	1	2.893	1	96	3			-8.14	-0.21
B-1	8566.0	1	2.899	2	59	39		.662		
Kotaneelee										
O-67										
(60°26′51″;										
124°11′56″)										
	13677.25	1	2.890	20		80		.457	-10.23	-0.63*
	13677.25	2	2.891	3		97		.475	-10.70	-1.13
	13927.75	1	2.891	tr		99		.468	-10.97	-1.63
Pan-Am.	13927.75	2	2.896			100		.452	-11.33	-1.91
Beaver	13932.75	1	2.893	1	1	98		.451	-11.32	-1.66
YT G-01	13932.75	2	2.891	25		75		.468	-11.66	-2.46*
(60°00′25″;	13940.5	1	2.888	1		99		.456	-10.42	-1.36
124°15′48″)	13940.5	2	2.895		11	89		.424	-12.13	-3.17*
	14414.5	1	2.893	tr		99		.454	-11.54	-1.97
	14414.5	2	2.891		tr	99		.450	-11.88	-1.06
	14429.0	1	2.891			100		.444	-10.54	-1.76
	14429.0	2	2.891		tr	99		.495	-11.67	-2.45
Pan-Am. A-3	13135.0	1	2.889	tr	tr	100		.459	-11.52	-1.16
Pointed	13135.0	2	2.888			100		.458	-11.72	-1.23
Mountain	13324.0	1	2.881	tr	tr	99		.471	-9.50	-1.25
G-62	13324.0	2	2.885	1	6	93		.407	-11.21	-1.03
(60°21′27″;	13875.0	1	2.886	tr	1	99		.460	-13.24	-2.31
123°56′47″)	13875.0	2	2.896			100		.428	-12.33	-1.62
Pan-Am. A-1	12855.0	1	2.889	1	tr	99		.468	-11.41	-0.81
Pointed	12855.0	2	2.886	tr		100		.442	-12.12	-1.46
Mountain	13066.0	1	2.889			100		.495	-11.56	-1.00
P-53	13066.0	2	2.893	1		99		.456	-11.48	-1.51
(60°22′46″;										
123°54′34″)										

APPENDIX 2 (cont'd)

Amoco B-2	14210.0	1	2.890	2	1	97		.443	-12.06	-1.64
Pointed	14210.0	2	2.885	1	1	98		.474	-13.63	-2.23
Mountain	14653.0	1	2.888			100		.419	-10.20	-0.37
F-38	14653.0	2	2.887		1	99		.469	-12.69	-2.27
(60°27'19";	14960.0	1	2.887	4	tr	96		.481	-11.71	-0.88
123°51'55")	14960.0	2	2.889	2	1	97		.450	-12.36	-2.00
	11698.5	1	2.890	31		66	3(S)	.481		
	11698.5	2	2.893	48		48	4(S)	.484		
	11707.0	1	2.898	18		92		.487		
	11707.0	2	2.884	16		82		.461		
	11709.0	1	2.893	73		27		.465		
	11709.0	2	2.895	19		81		.438		
	11713.0	1	2.893	42		53	5(G & S)	.439		
	11713.0	2	2.891	22		75	3(S)	.438		
	11740.0	1	2.891	36		64		.496		
	12042.0	1	2.892	tr		100		.468	-10.32	-1.06
	12042.0	2	2.886	3		97		.478	-11.71	-1.86
	12049.0	1	2.890	2		98		.469	-10.48	-0.78
	12049.0	2	2.885			100		.457	-10.55	-1.32
	12060.0	1	2.894	2		98		.474	-10.20	-0.61
	12060.0	2	2.890			100		.470	-12.32	-2.07
	12067.0	1	2.887	1		99		.456	-11.30	-1.63
	12067.0	2	2.886	tr	1	99		.465	-11.10	-2.47
Columbia	12284.0	1	2.891	1		99		.456	-11.13	-1.12
et. al.,	12284.0	2	2.890	3	1	96		.450	-13.59	-2.69
Kotaneelee	12315.0	1	2.887	2		98		.453	-11.32	-1.19
YT H-38	12315.0	2	2.891	1	27	72		.372		*
(60°07'16";	12452.5	1	2.893			100		.471	-10.86	-1.07
124°06'03")	12452.5	2	2.889		1	99		.465	-13.13	-2.07
	12457.75	1	2.890			100		.483	-13.61	-3.18
	12457.75	2	2.885		5	95		.436	-13.34	-3.07
	12468.5	1	2.888			100		.445	-11.49	-1.08
	12468.5	2	2.893		tr	100		.470	-13.76	-2.87
	12484.0	1	2.894	tr	tr	99		.473	-12.18	-1.45
	12484.0	2	2.888			100		.468	-10.02	-1.28
	12509.0	1	2.890			100		.455	-10.73	-2.13
	12509.0	2	2.889		tr	100		.482	-12.00	-1.77
	12717.5	1	2.893	1		94	3(I)	.456	-13.33	-2.81
	12717.5						2(P)			
	12717.5	2	2.889			100		.451	-10.62	-1.39
	12725.0	1	2.888	tr	tr	98	1(I)	.486	-10.37	-1.36
	12725.0	2	2.887	5	5	90		.522	-11.05	-4.24
	12735.5	1	2.894	2		97	1(P)	.474	-10.84	-1.45
	12735.5	2	2.889			100		.459	-12.77	-1.65
	12762.5	1	2.893			100		.456	-8.76	-0.98
	12762.5	2	2.889	1		99		.488	-12.23	-2.94
	12768.2	1	2.891			100		.463	-9.83	-1.18
	12768.2	2	2.888			100		.470	-10.03	-1.18
	12782.5	1	2.892			100		.475	-9.90	-1.76
	12782.5	2	2.886	60	10	30		.433		

*Values not included in statistical compilations

NOTE: See Appendix 1 for legend and explanations

S = Sphalerite
G = Galena
I = Illite
P = Pyrite

APPENDIX 3

MAJOR AND MINOR ELEMENT COMPOSITION – SURFACE SECTIONS

GSC OUTCROP SECTION NUMBER	GSC SAMPLE LOCALITY NUMBER	DOLOMITE TYPE[1]	SiO_2%	CaO%	MgO%	CO_2%	Al_2O_3%	Fe ppm	Mn ppm	Sr ppm	Zn ppm	Cu ppm	Ba ppm
	C-052856	1	0.58	30.51	21.38	47.24	-	1072	355	45	132	101	72
	C-052856	2						499	297	48	108	37	150
	C-052857	1	80.94	2.70	1.78	6.22	0.12	12276	645	9	960	31223	378*
	C-052858	1	0.11	30.55	21.60	47.56	-	545	343	42	87	326	121
	C-052858	2	0.09	30.77	21.32	47.65	-	503	407	47	180	70	80
	C-052861	1	1.27	29.91	21.23	47.15		1696	228	55	107	123	54
	C-052861	2	0.13	29.86	21.49	48.26		662	241	48	218	54	82
	C-052862	1	3.66	28.83	19.73	43.95	2.54	2113	253	68	59	177	75
	C-052862	2	0.22	30.73	21.74	47.20		247	194	56	56	31	59
Section 1	C-052863	1	0.59	30.94	20.85	46.72	0.36	1733	297	75	184	120	79
	C-052863	2	0.09	30.97	21.51	47.30		341	242	56	79	20	137
	C-052864	1	2.85	52.69	0.69	42.12	0.72	3292	107	211	45	35	104*
	C-052864	2	0.38	35.38	16.97	47.02		890	508	134	40	8	132*
	C-052864	3	2.77	31.74	16.28	46.67	1.47	2350	712	119	36	20	107*
	C-052866	1	4.76	51.85	0.64	41.63	0.51	1855	157	360	98	69	89-
	C-052867	1	0.45	31.70	19.86	47.48	0.18	740	215	75	221	12	68
	C-052867	2	0.05	32.87	20.08	47.00		154	229	72	120	9	106
	C-052868	1	65.31	14.34	0.56	13.83	0.43	4116	352	76	3519	27034	413-
	C-052873	1	1.19	54.49	0.63	43.13	0.26	751	17	280	28	45	106-
	C-052875	1	0.29	30.96	20.69	47.42	0.49	444	214	71	84	74	86
	C-052875	2	0.03	31.00	21.34	47.63		125	326	76	90	29	64
	C-053009	1	0.04	30.45	21.31	48.20		121	186	60	61	21	77
	C-053009	2	0.07	31.28	21.25	47.21	0.19	96	417	155	82	183	110
	C-053016	1	0.14	30.20	21.44	48.22		98	139	43	62	82	78
	C-053016	2	0.07	30.29	21.63	48.01		179	179	44	164	11	73
Section 2,	C-053018	1	0.18	31.00	21.25	47.57		142	166	44	21	94	77
Grainger	C-053018	2	1.53	30.28	20.81	46.71	0.48	607	284	44	37	182	81
River	C-053019	1	0.28	30.90	21.38	47.29		399	235	39	121	75	87
	C-053019	2	0.11	30.84	21.42	47.63		0	169	46	49	5	67
	C-053020	1	0.46	30.65	21.09	47.60		659	256	58	18	15	77
	C-053020	2	0.09	30.39	21.41	48.11		29	234	49	31	7	73
	C-053021	1	1.38	53.95	1.15	43.34	0.18	388	55	212	43	62	85*
	C-053022	1	0.58	30.45	19.92	48.67	0.25	356	149	61	26	41	66
	C-052695	1	0.12	31.22	21.12	47.54		87	118	59	50	0	76
	C-052695	2	0.08	43.40	11.12	45.40		174	178	329	183	0	59*
	C-052696	1	4.38	29.77	19.89	45.85		248	140	66	55	0	82
	C-052696	2	87.22	4.03	2.72	5.70		997	77	17	254	11	69*
Section 4,	C-052697	1	1.39	30.29	21.05	47.13		392	139	60	80	0	69
First	C-052702	1	0.30	30.43	21.12	47.92		374	173	54	144	0	71
Canyon	C-052702	2	0.18	39.85	13.77	46.05		450	243	242	271	5	95*
	C-052987	1	12.83	25.51	15.78	40.31	3.30	5582	264	61	208	250	150*
	C-060988	1	0.33	30.90	20.84	47.80	0.13	149	213	58	22	13	69
	C-060988	2	0.08	30.80	21.48	47.64		73	259	53	23	29	93
	C-060989	1	0.09	56.07	0.22	43.62		0	231	560	44	35	63
	C-060990	1	0.38	55.92	0.78	42.92		163	22	276	40	23	96*
	C-052895	1	0.36	30.31	20.99	48.01	0.15	569	157	81	16	15	65
Section 6,	C-052898	1	0.32	55.15	0.69	43.89		196	19	215	25	20	85*
Sundog	C-052901	1	6.05	31.46	16.51	44.89	0.60	646	181	102	390	32	93*
Creek	C-052901	2	0.03	29.79	21.65	48.53		0	197	60	444	212	88
	C-052902	1	7.73	28.55	19.23	44.37		312	238	71	20	12	69
	C-052904	1	1.44	54.06	0.84	43.14	0.31	846	49	908	47	84	93*
Section 3, Second Canyon 2	C-052842	1	9.67	28.32	18.39	43.51		1065	335	45	132	101	72*
Section 20,	C-059333	2	0.11	30.90	19.64	49.35		122	50	70	16	10	71
Manetoe	C-059334	1	0.09	53.53	1.54	44.46	0.38	0	109	96	63	146	80*
Range 2	C-059335	1	0.34	31.19	20.38	47.84	0.14	251	129	71	49	208	71
Section 21,	C-059319	1	0.07	31.05	21.29	47.59		0	151	50	49	13	86
Manetoe	C-059319	2		30.86	.21.49	47.65		0	73	87	37	10	65
Range 1													
Section 26, Arnica Ridge 1	C-059225	1	1.03	29.46	21.16	48.35		0	58	43	49	29	55

*Values not included in statistical compilations
[1]See Appendix 1 for definition

APPENDIX 4

CARBON AND OXYGEN ISOTOPE CONTENT OF SELECTED DOLOMITE SAMPLES FROM THE MANETOE FACIES[1]

		$\delta^{13}C$ ‰	$\delta^{18}O$ ‰
HOST DOLOMITE			
Ram Plateau	R5a[2]	–2.48	–14.30
	R6a	–0.45	–14.57
(clast)	R6d	+1.56	– 7.94
	R7b	–1.49	–12.32
(clast)	R7b	–2.43	–12.40
	R7c	+0.74	– 7.88
	R8a	+1.53	– 6.28
	R8b	+0.58	– 7.92
First Canyon	(Arnica Fm)	+0.51	– 6.25
Kotaneelee YT H-38	3571 m[3]	–6.05	–12.74
	3756 m	–1.45	–11.71
Pointed Mountain A-55	3418 m	–2.57	–10.41
WHITE DOLOMITE CEMENTS			
Kotaneelee YT H-38	3571 m	–0.60	–10.35
	3714 m	–2.33	–12.56
	3756 m	–0.23	–10.31
Pointed Mountain A-55	3418 m	–7.35	–16.04
Berry F-71	706.7 m	–5.14	–14.10
	708.3 m	–2.08	–11.80
	711.3 m	+0.16	– 8.98
	721.0 m	–1.96	–14.27
Ebbutt G-72	786.6 m	+0.73	–11.77
Ram Plateau	R5a	–4.55	– 9.34
	R6a	–0.67	–14.68
	R7a	–2.18	–14.43
	R7b	–1.77	–12.96
	R7c	–0.61	–12.29
	R8a	–1.54	– 9.54
	R8b	+3.53	– 8.96
	R8f	–0.64	–10.66
First Canyon	(Arnica Fm)	+0.29	–12.35
	DZ C1N	+0.12	– 9.28
	DZ C1O	+0.36	– 8.70
	DZ A	+2.51	– 9.61
Arrowhead I-46 (Presqu'île Facies)	2112.4 m	–3.18	–14.19

[1]Data from Aulstead (1987).
[2]Field sample numbers.
[3]Below KB.

APPENDIX 5

CARBON AND OXYGEN ISOTOPE CONTENT OF SELECTED LIMESTONES AND CALCITE CEMENTS ASSOCIATED WITH THE MANETOE FACIES[1]

Section or well	Formation or type	Depth below KB, or field sample number	$\delta^{13}C$ ‰	$\delta^{18}O$ ‰
LIMESTONES				
Root River I-60	(Nahanni Fm)	846.7 m	+1.02	– 7.66
La Biche F-08	(Nahanni Fm)	1995.6 m	–4.16	– 6.77
Nahanni Butte	(Landry Fm)	3a	–2.08	–14.77
	(Nahanni Fm)	0a	–1.19	–11.78
Ram Plateau	(Headless Fm)	6e	+2.25	–12.84
CALCITE CEMENTS				
La Biche F-08	(Nahanni Fm)	1990.0 m	–2.08	–36.24
		2047.5 m	–2.40	–35.66
Netla Raven	(White)	2373.0 m	–1.95	–13.86
	(Pink)	2373.0 m	–1.15	–12.56
Cli Lake M-05		1483.4 m	–3.27	–22.12
		1488.9 m	–2.47	–13.10
Beaver G-01		4179.0 m	–7.44	–13.44
		4398.0 m	–9.21	–16.52
Grainger N-42		1051.3 m	–1.01	–11.73
		1053.2 m	–3.78	– 9.37
Berry F-71		721.0 m	–2.33	–13.61
Fort Simpson M-70		700.6 m	+0.66	– 8.75
		700.0 m	+2.15	–11.21
		703.8 m	+0.98	– 7.13
Pointed Mountain A-55		3157.0 m	–3.84	–14.43
Kotaneelee YT H-38		3899.0 m	–5.43	–13.63
Root River I-60		1080.6 m	–3.19	–20.15
Ram Plateau		R7c	–8.60	–15.61
	(white)	R6b	–1.88	–22.84
	(brown)	R6b	–5.57	–16.78
	(scalenohedral)	R6c	–5.70	–16.54
First Canyon	(white)		–0.45	–10.48
(Arnica Fm)	(brown)		–4.09	–17.73
	(Detrital Zone)	C1C	–2.75	–14.91
		C1N	–4.36	–13.23
Nahanni Butte		1a	–1.60	–12.02
	(brown)	1g	–2.38	–28.12
		3a	–3.71	–12.40

[1]Data from Aulstead (1987).